THESIS APPROVAL

GRADUATE SCHOOL, KASETSART UNIVERSITY

Doctor of Engineering (Water Resources Engineering)

DEGREE

Water Resources Engineering	Water Resources Engineering
FIELD	**DEPARTMENT**

TITLE: Applications of Rain Gauge and Radar Rainfall to A Hydrologic Model for Flood Estimation

NAME: Mrs. Punpim Puttaraksa Mapiam

THIS THESIS HAS BEEN ACCEPTED BY

_____ **THESIS ADVISOR**

(Associate Professor Nutchanart Sriwongsitanon, Ph.D.)

_____ **COMMITTEE MEMBER**

(Associate Professor Ashish Sharma, Ph.D.)

_____ **COMMITTEE MEMBER**

(Mrs. Siriluk Chumchean, Ph.D.)

_____ **COMMITTEE MEMBER**

(Associate Professor Kobkiat Pongput, Ph.D.)

_____ **DEPARTMENT HEAD**

(Assistant Professor Surachai Lipiwattanakarn, M.ASc.)

APPROVED BY THE GRADUATE SCHOOL ON _____

_____ **DEAN**

(Associate Professor Gunjana Theeragool, D.Agr.)

THESIS

APPLICATIONS OF RAIN GAUGE AND RADAR RAINFALL TO A HYDROLOGIC MODEL FOR FLOOD ESTIMATION

PUNPIM PUTTARAKSA MAPIAM

A Thesis Submitted in Partial Fulfillment of
the Requirements for the Degree of
Doctor of Engineering (Water Resources Engineering)
Graduate School, Kasetsart University
2009

Punpim Puttaraksa Mapiam 2009: Applications of Rain Gauge and Radar Rainfall to A Hydrologic Model for Flood Estimation. Doctor of Engineering (Water Resources Engineering), Major Field: Water Resources Engineering, Department of Water Resources Engineering. Thesis Advisor: Associate Professor Nutchanart Sriwongsitanon, Ph.D. 173 pages.

Radar rainfall was proved in this study to be an effective input data for improving the accuracy of flood estimates compared to the gage rainfall in the upper Ping river basin. The URBS (rainfall-runoff model) was first chosen for flood estimation at the stations P.20, P.4A, P.28, P.21, and P.71 using daily gauge rainfall (DGR) as the input data. The NAM model – one of the most reliable commercial models – was also applied at these 5 stations. Results of flood hydrograph obtained from these models are very close. However, the URBS model requires only 4 parameters whereas the NAM requires 6 in the calibration, the URBS model was therefore chosen for further analysis. The URBS model was then applied at other 6 stations in the study basin. The ungauged relationships between the URBS model parameters and catchment characteristics were also formulated to be used for the ungauged catchments in the study area. Thereafter, the radar reflectivity data (Z), obtained from the Omkoi radar, and the corresponding rainfall data (R) were used to formulate the most suitable relationship; $Z=74R^{1.6}$, which can be used to estimate daily radar rainfall (DRR) and hourly radar rainfall (HRR) in the upper Ping river basin. To be able to possibly improve the accuracy in runoff estimate, the scaling transformation equation was generated (using reflectivity and corresponding continuous rain gauge data from Bangkok, and Sydney and Brisbane, Australia) to be used as the logic to prepare the hourly radar rainfall (HRRS). Four types of rainfall data (DGR, DRR, HRR, and HRRS) were finally used as the input data for the URBS model to estimate the flood hydrographs at the stations P.21, P.71, P.77, P.24A, P.73, and P.14. The accuracy of overall hydrograph and peak flow estimated using all radar rainfall data are generally higher than that of estimated using the DGR, respectively. The use of HRR however cannot produce better results of runoff hydrograph than the use of DRR. On the other hand, the HRRS has shown its ability to improve the accuracy of runoff estimates, especially the overall hydrographs. The scaling logic is therefore necessary to be applied to prepare the HRRS for the situation like in the upper Ping river basin, where daily Z-R relationship is only available.

/ /

Student's signature Thesis Advisor's signature

ACKNOWLEDGMENTS

I would like to express my gratitude to my advisor, Assoc. Prof. Dr. Nutchanart Sriwongsitanon, for her valuable suggestions, encouragement and understanding through my graduate experience. I would like to thank the other members of my committee, Assoc. Prof. Dr. Ashish Sharma, Dr. Siriluk Chumchean, and Assoc. Prof. Dr. Kobkiat Pongput for the assistance they provided at all levels of the research. Finally, I would like to thank Assoc. Prof. Dr. Chavalit Chaleeraktrakoon from Graduate School for his valuable comments and suggestions to improve my thesis writing.

I wish to thank Mr. Terry Malone (Australian Bureau of Meteorology, Queensland, Australia) and Dr. Alan Seed (Australian Bureau of Meteorology, Melbourne, Australia) for their many helpful suggestions.

I gratefully acknowledge the Thailand Research Fund through the Royal Golden Jubilee Ph.D. program (Grant No. PHD/0118/2547) and Kasetsart University Research and Development Institute (KURDI) for financially supporting this research.

I am especially appreciated my mother and my sisters for their loving supports and continuing encouragements.

I am deeply appreciated to my husband, Mr. Monthep, for his love, supports, encouragement, and understanding. Finally, this thesis is dedicated to my son, Master Supanat, who has greatly inspired me to fulfill my research study.

Punpim Puttaraksa Mapiam

March 2009

TABLE OF CONTENTS

Page

LIST OF TABLES

LIST OF TABLES (Continued)

LIST OF FIGURES

LIST OF FIGURES (Continued)

LIST OF FIGURES (Continued)

APPLICATIONS OF RAIN GAUGE AND RADAR RAINFALL TO A HYDROLOGIC MODEL FOR FLOOD ESTIMATION

INTRODUCTION

Flood forecasting is a non-structural measure that is a very useful tool to mitigate flood hazard which causes economic and social damage, especially with regard to human life. To be able to estimate flooding correctly, a hydrologic model is a very crucial tool (Singh *et al*., 2002). Conventional hydrologic models were developed based on the hydrologic cycle imitation. However, there are many components involved in the cycle such as interception, infiltration, depression storage, evaporation, subsurface flow, groundwater flow, overland flow, and channel flow (Wilson, 1983; Chow *et al*., 1988). As a result, various computer software packages have been developed for runoff estimation by the considerations only some significant hydrologic cycle components. Examples of well known runoff estimation models are the TANK model (Sugawara, 1974), TOPMODEL model (Beven *et al*., 1979; Beven *et al*., 1984; Beven, 1997), NAM model (DHI, 1990), HEC-HMS model (HEC, 2000), SWAT model (Neitsch *et al*., 2002), and URBS model (Carroll, 2004).

In this study, the most suitable hydrologic model according to proposed criteria will be chosen for flood estimation that will be carried out at the upper Ping river basin, which has been facing serious flooding problems during the last decade. To be able to confirm an effectiveness of the chosen model for flood estimation in the study area, the NAM model - a sub-module of the MIKE 11 model package, which has been accepted and generally applied for many basins world wide but it is quite expensive model – will also be applied at the same runoff stations and the results of the flood hydrographs gained from these two models will be compared to identify their effectiveness. In the model application, rain gauge rainfall will be used as the input data for these two hydrologic models. Rain gauge rainfall is therefore one of the most significant data influences the results of estimated flood hydrograph. Unfortunately, the distribution of rainfall usually varies significantly in both space and time (Seed and Austin, 1990); therefore, the limited number of rainfall stations in

the catchment can have a significant impact on the accuracy of flood estimations (Wilson, 1979; Bevan and Hornberger, 1982; Hamlin, 1983). This problem also occurs in Thailand basins including the upper Ping river basin. This study aims to improve the accuracy of flood hydrograph prediction in the study area by proposing spatial rainfall estimation method using weather radar. This is because the weather radar, which is a widely used basis for rainfall estimation at fine spatial and temporal resolutions (Collinge and Kirby, 1987; Sun *et al*., 2000; Uijlenhoet, 2001; Vieux, 2003), can better capture the spatial variation of rainfall fields than rain gauge rainfall data in areas where rain gauges are distributed sparsely (Yang *et al*., 2004; Segond *et al*., 2007). Moreover, there are number of papers shown the improvements in flood estimation and flood forecasting using radar rainfall data as the input data to hydrological models (Wyss *et al*., 1990; Pessoa *et al*., 1993; Borga *et al*., 2000; Sun *et al*., 2000).

In this study, the relationship between radar reflectivity data (Z) - obtained from the Omkoi radar - and corresponding rain gauge rainfall data (R) at the upper Ping river basin will be investigated to be used for temporal and spatial rainfall estimation. Rain gauge rainfall and radar rainfall will later be applied as the input data for the selected hydrologic model at particular runoff stations in the study area. Results of flood hydrograph estimated by these two sets of rainfall data will be compared for their accuracy and effectiveness.

OBJECTIVES

1. To study the theory and concept of the well known hydrologic public domains or low cost models. A suitable hydrologic model for rain gauge and radar rainfall data will be chosen for flood estimation in the upper Ping river basin.

2. To setup the selected hydrologic model using rain gauge rainfall as the input data for different runoff stations in the upper Ping river basin.

3. To calibrate the relationship between the radar reflectivity factors (Z) and rainfall rates (R) using radar reflectivity data and corresponding rain gauges data available within the upper Ping river basin.

4. To propose a generic scaling rule that can be used to estimate radar rainfall at fine temporal resolution for the cases where only daily rain gauge rainfall data are available for use in the Z-R calibration.

5. To setup the selected hydrologic model using rain gauge and radar rainfall as the input data for different runoff stations in the upper Ping river basin. The results gained from different input datasets will be compared for their reliability and effectiveness for flood estimation in the upper Ping river basin.

Scopes

1. The comparison between the well known hydrologic models will be carried out and the suitable model will be chosen to suit the upper Ping river basin.

2. To setup the selected hydrologic model for different runoff stations in the upper Ping river basin by using gauge rainfall as the input data. The performance comparison between the selected model and the NAM model will be verified at some runoff stations in the upper Ping river basin.

3. The recorded instantaneous reflectivity data and ground truth rainfall data for different flood events will be used to evaluate of the parameters A and b in Z-R relationship for the upper Ping river basin. This relationship will be used to estimate the initial radar rainfall for a specific flood event in the upper Ping river basin.

4. To study the impact of gauge rainfall temporal resolution on the specification of a Z-R relationship. Climatological Z-R relationships will be calibrated using rainfall aggregated over 1 to 24 hours to investigate the evidence of temporal scaling in the Z-R calibrated parameters using the data collected from Sydney and Brisbane, Australia, and Bangkok, Thailand. A simple scaling hypothesis will thereafter be proposed to develop transformation equations that could scale the A parameter in the Z-R relation across a range of temporal resolutions.

5. To estimate daily and hourly radar rainfall using the Z-R relationship of Omkoi radar and the scaling transformation equation.

6. The selected hydrologic model will be set up for flood hydrograph estimation at the appropriate runoff stations located within the radar radius of the Omkoi radar using rain gauge and radar rainfall as the input data. Results of flood hydrograph can be used to show the suitability of applying radar rainfall to replace the conventional data of rain gauge rainfall.

LITERATURE REVIEW

1. Study area description

The Ping river basin is situated in Northern Thailand and has an area of around 34,856 km^2 across five provinces: Chiang Mai, Lamphun, Kamphaeng Phet, Tak, and Nakhon Sawan Provinces. The Ping river - the main river of the Ping River Basin - has a 740 km length and originates in Chiang Dao District in the north of Chiang Mai. The Ping flows downstream to the south and joins the Wang and Nan Rivers at Tak and Nakhon Sawan Provinces, respectively, to become the Chao Phraya River which has a catchment that covers the area of around one third of the country. There are 3 large reservoirs situated in the Ping river basin: the Bhumiphol, Mae Kuang, and Mae Ngat Reservoirs with the capacity of approximately 13,462, 263, and 265 mcm, respectively. The Bhumiphol Dam, located in Doi Tao District in Chiang Mai Province, separates the Ping river basin into two parts called the upper Ping and the lower Ping river basins.

The upper Ping river basin, which is chosen as the study area, has a catchment area of approximately 25,370 km^2 in Lam Phun and Chiang Mai Provinces. The basin is located between latitude 17° 14′ 30″ and 19° 47′ 52″ north, and between longitude 98° 4′ 30″and 99° 22′ 30″ east. The terrain of the basin is undulating and rolling. The upper Ping river basin can be separated into 14 sub-basins (Figure 1) consisting of the following sub-basins: 1) the upper Ping river, 2) Nam Mae Ngat, 3) Nam Mae Taeng, 4) the Ping river section 2, 5) Nam Mae Rim, 6) Nam Mae Kuang, 7) Nam Mae Ngan, 8) Nam Mae Li, 9) Nam Mae Klang, 10) the Ping river Section 3, 11) upper Mae Jam, 12) Lower Mae Jam, 13) Nam Mae Hat, and 14) Nam Mae Tun. The average annual runoff and rainfall are around 6,815 mcm and 1,174.1 mm, respectively.

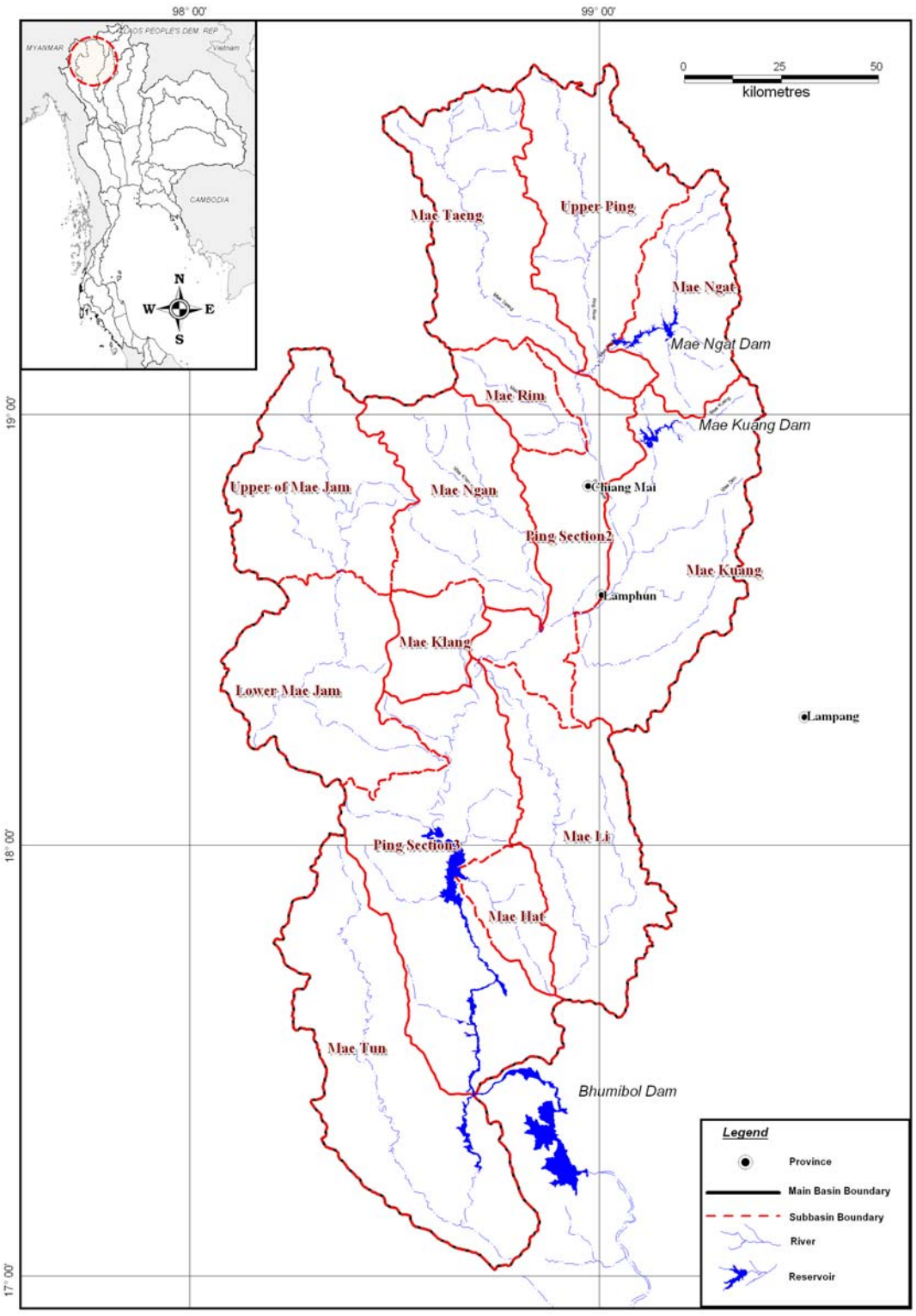

Figure 1 Location of the upper Ping river basin and its sub-basins.

Source: Department of Water Resources (2003)

2. Hydrologic Model

Hydrologic model is a very crucial tool for flood estimation. Conventional hydrologic models were developed based on the hydrologic cycle imitation. However, there are many components involved in the cycle such as interception, infiltration, depression storage, evaporation, subsurface flow, groundwater flow, overland flow, and channel flow (Wilson, 1983; Chow *et al*., 1988). Most parameters for these processes cannot be measured directly. Many researchers have developed different techniques to estimate unmeasured hydrological components. Horton (1919, 1933, 1935, 1939) suggested the empirical formulas to estimate interception, infiltration, channel flow, and overland flow, respectively. Lowdermilk (1934); Hursh (1936); and Hursh and Brater (1944) concluded that subsurface water is a significant hydrological component in flood hydrographs by observation in humid regions. Keulegan (1944) introduced the kinematic wave approach for overland flow. Soil Conservation service (1956) developed the SCS curve number approach to evaluate rainfall loss rate. Various computer software packages have been developed for runoff estimation by the considerations only some significant hydrologic cycle components. More complicated models normally require more input data and are difficult to apply, especially for catchments with limited or no hydrologic data. In this study, model ability of 4 hydrologic models namely NAM, HEC-HMS, URBS, and SWAT models will be compared, and the most suitable model will later be chosen for flood estimation in the upper Ping river basin. The theory and concept of the four models can be described below.

2.1 NAM Model

NAM model is an acronym for Nedbor-Afstromings Model that means precipitation-runoff model. It was developed by Hydrological Section of the Institute of Hydrodynamics and Hydraulics Engineering, Technical University of Denmark (Nielsen and Hansen, 1973). The model is based on physical structures and semi-empirical equations to imitate the behavior of the land phase of the hydrologic cycle. Catchments are represented by four storage layers including snow, surface, lower

zone, and groundwater as shown in the Figure 2. However, only three storages excluding the snow storage were consider in Thailand river basin including this study.

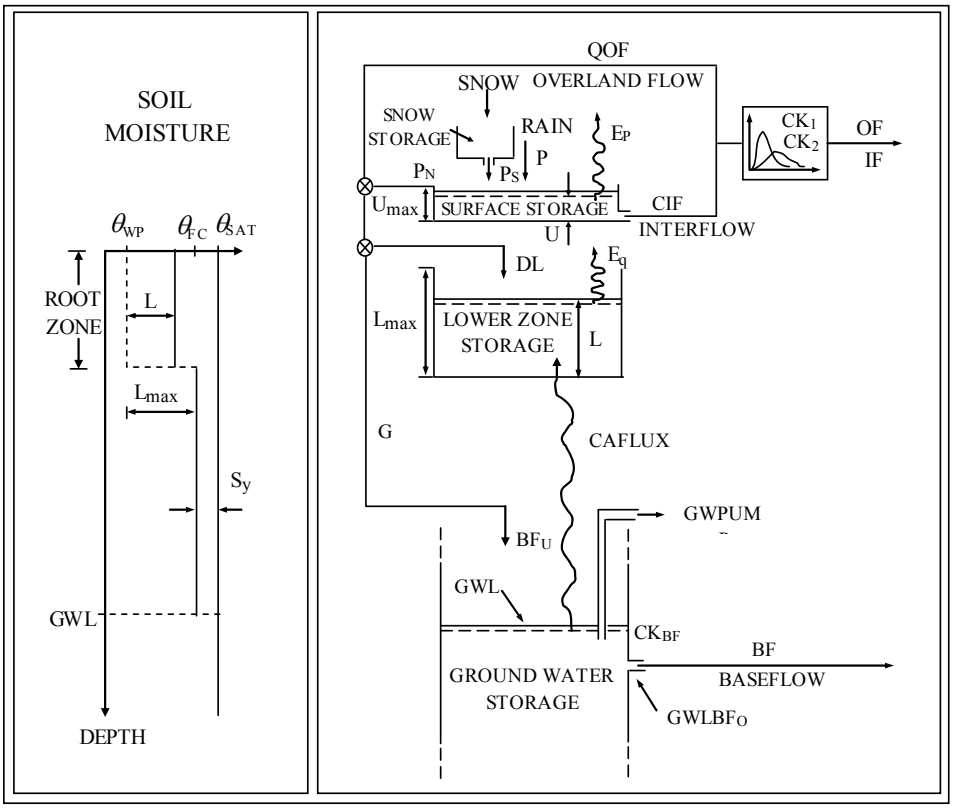

Figure 2 NAM Model structure.
Source: Danish Hydraulic Institute (1990)

Flow storage approximations are provided in the NAM model manual prepared by the Danish Hydraulic Institute (NAM Documentation and User's Guide, 1990) and also briefly presented in this thesis as follows.

a. Surface storage

The upper limit of the amount of water in the surface storage is denoted as U_{max}. The amount of water, U, in the surface storage is continuously diminished by evaporative consumption as well as by horizontal leakage (interflow). When there is maximum surface storage, some of the excess water, P_N, will enter the

streams as overland flow, whereas the remainder is diverted as infiltration into the lower zone and groundwater storage. The overland flow (*QOF*) equation can be shown below.

$$\begin{aligned} QOF &= CQOF\,\frac{L/L_{\max} - TOF}{1 - TOF}\,P_N \qquad for\ L/L_{\max} > TOF \\ &= 0 \qquad\qquad\qquad\qquad\qquad\qquad for\ L/L_{\max} \le TOF \end{aligned} \tag{1}$$

where *CQOF* is overland flow runoff coefficient ($O \le CQOF \le 1$), *TOF* is threshold value for overland flow ($O \le TOF \le 1$), and L/L_{max} = relative soil moisture content

b. Lower zone storage

The soil moisture in the root zone, a soil layer below the surface from which the vegetation can draw water for transpiration, is represented as lower zone storage. L_{max} denotes the upper limit of the amount of water in this storage. Moisture in the lower zone storage is subject to consumptive loss from transpiration. The moisture content controls the amount of water that enters the groundwater storage as recharge and the interflow and overland flow components. The amount of infiltrating water G recharging the groundwater storage depends on the soil moisture content in the root zone as presented in the equation below.

$$\begin{aligned} G &= \left(P_n - QOF\right)\frac{L/L_{\max} - TG}{1 - TG} \qquad for\ L/L_{\max} > TG \\ &= 0 \qquad\qquad\qquad\qquad\qquad\qquad for\ L/L_{\max} \le TG \end{aligned} \tag{2}$$

where, TG = the root zone threshold value for groundwater recharge ($O \le TG \le 1$)

The amount of water remained in the lower zone storage (DL) are calculated using the following equation.

$$DL = \left(P_n - QOF\right) - G \tag{3}$$

The interflow contribution (QIF) is assumed to be proportional to U and to vary linearly with the relative moisture content of the lower zone storage.

$$\begin{aligned} QIF &= CKIF \frac{L/L_{\max} - TIF}{1 - TIF} U \qquad for\ L/L_{\max} > TIF \\ &= 0 \qquad\qquad\qquad\qquad\qquad\quad for\ L/L_{\max} \le TIF \end{aligned} \tag{4}$$

where, CKIF = time constant for interflow, and TIF = root zone threshold value for interflow (O ≤ TIF ≤ 1)

Evapotranspiration which is an important process for the calculation in surface and lower zone storage can be calculated using the following equation.

$$E_a = E_p\left(L/L_{\max}\right) \tag{5}$$

where E_p is potential evapotranspiration.

c. Groundwater storage

The water percolated from the lower zone storage will be retained in groundwater storage. Groundwater level (*GWL*) represents the groundwater table depth measured from ground level. There are 4 essential parameters needed for groundwater level calculation which are a recharge G, capillary flux CAFLUX, net groundwater abstraction GWPUMP, and baseflow BF. The baseflow can be calculated as follows.

$$\begin{aligned} BF &= (GWLBF_0 - GWL) S_Y (CK_{BF})^{-1} \qquad for\ GWL \le GWLBF_0 \\ &= 0 \qquad\qquad\qquad\qquad\qquad\qquad for\ GWL > GWLBF_0 \end{aligned} \tag{6}$$

where, $GWLBF_0$ = maximum groundwater table depth, S_y = specific yield of groundwater reservoir.

The Capillary Flux is calculated using the equation below.

$$CAFLUX = \left(1 - \frac{L}{L_{\max}}\right)^{1/2} \left(\frac{GWL}{GWLFL_1}\right)^{-\alpha}$$
$$\alpha = 1.5 + 0.45\, GWLFL_1 \tag{7}$$

where, $GWLFL_1$ is groundwater table depth at which capillary flux

2.2 HEC-HMS Model

HEC-HMS is an acronym for Hydrologic Modeling System, which was developed by the Hydrologic Engineering Center (HEC) of U.S. Army Corps of Engineering since March 1998. It can be used to simulate the processes of precipitation-runoff and runoff routing for both natural and controlled channel system. The model is a modified version of the HEC-1 Model by improving the capability of HEC-1 and provides capabilities for distributed modeling and continuous simulation. There are 4 sub-models provided by the HEC-HMS for precipitation-runoff-routing simulation which are: 1) Runoff-Volume models, 2) Direct-Runoff models, 3) Baseflow models, and 4) Channel flow models. However, this study has objective to study the rainfall-runoff process for flood estimation in the upper Ping river basin, only 3 categories excluding the channel flow models were considered in this study. Details of the three models are presented as follows.

2.2.1 Runoff-Volume Models

The runoff-volume models or rainfall loss models contain several techniques for excess rainfall estimation. The HEC-HMS computes runoff volume by computing the volume of water that is intercepted, infiltrated, stored, evaporated, or transpired and subtracting it from the precipitation. Interception and surface storage are intended to represent the surface storage of water by trees or grass, local depressions in the ground surface, cracks and crevices in parking lots or roofs, or a surface area where water is not free to move as overland flow. Infiltration represents the movement of water to areas beneath the land surface. Interception, infiltration, storage, evaporation, and transpiration collectively are referred to in the HEC-HMS program and documentation as losses. Gross rainfall subtracted by the mentioned rainfall losses will become the excess rainfall. There are 6 sub-models provided by the HEC-HMS for rainfall losses estimation. Details of theory and concept of those loss models are presented as follows.

a. The initial and constant-rate model

The underlying concept of the initial and constant-rate loss model is that the maximum potential rate of precipitation loss (f_c) is constant throughout an event. If p_t is mean areal rainfall during a time interval t to $t + \Delta t$, the excess rainfall (pe_t) during the interval is therefore given by:

$$pe_t = \begin{cases} p_t - f_c & if \ \ p_t > f_c \\ 0 & if \ \ p_t \le f_c \end{cases} \qquad (8)$$

If the initial loss (I_a) is added to the model to represent the loss caused by interception and depression storage, the excess rainfall equation above is then changed by the following:

$$pe_t = \begin{cases} 0 & if \sum p_i < I_a \\ p_t - f_c & if \sum p_i > I_a \quad and \quad p_t > f_c \\ 0 & if \sum p_i > I_a \quad and \quad p_t < f_c \end{cases} \tag{9}$$

b. The Deficit and Constant-Rate Model

This model is a quasi-continuous model of precipitation losses. It is similar to the initial and constant-rate loss model, but the initial loss can be recovered after no rainfall for a long period.

c. The SCS Curve Number Loss Model

The Soil Conservation Service (SCS) Curve Number (CN) estimates rainfall excess as a function of cumulative rainfall, soil cover, land use, and antecedent moisture, using the following equation:

$$P_e = \frac{(P - I_a)^2}{P - I_a + S} \tag{10}$$

where P_e is accumulated precipitation excess at time t, P is accumulated rainfall depth at time t, I_a is the initial abstraction (initial loss), and S is potential maximum retention. From the study of runoff estimation in many small watersheds in USA, the SCS developed an empirical relationship of I_a and S:

$$I_a = 0.2S \tag{11}$$

Therefore, the cumulative rainfall excess at time t is:

$$P_e = \frac{(P - 0.2S)^2}{P + 0.8S} \tag{12}$$

The relationship between the potential maximum retention and the CN parameter can be shown as the follows.

$$S = \begin{cases} \dfrac{1000 - 10CN}{CN} & (foot - pound \quad system \\ \dfrac{25400 - 254CN}{CN} & (SI) \end{cases} \tag{13}$$

The CN which is represented a watershed characteristic can be estimated as a function of land use, soil type, and antecedent watershed moisture using the SCS tables (SCS, 1971, 1986). However, the CN derived from the tables represent only one soil type and land use, the several soil types and land used can be estimated by using a composite CN as follows.

$$CN_{composite} = \frac{\sum A_i CN_i}{\sum A_i} \tag{14}$$

where $CN_{composite}$ is the composite CN, i is an index of subdivided watersheds, A_i is subdivided catchment area.

d. Gridded SCS model

This model is another sub-model of the HEC-HMS model using for the CN estimation. For the model application, a basin will be divided as grid cells, and each cell has only one CN represented a watershed characteristic. The description of each cell composes of the location of the cell, the travel distance from the watershed outlet, the cell size, and the cell CN. The HEC-HMS computes precipitation excess for each cell independently using Eq (12), the excess rainfall will thereafter routed to the outlet of the watershed using the ModClark method.

e. Green and Ampt loss model

This model is a conceptual model of precipitation infiltration. The model computes the precipitation loss on the pervious area using the equation below.

$$f_t = K\left[\frac{1+(\phi-\theta_i)S_f}{F_i}\right] \quad (15)$$

where, f = loss during period t, K = saturated hydraulic conductivity, $\phi-\theta_t$ = volume moisture deficit, S_f = wetting front suction, F_t = cumulative loss at time t

f. Continuous Soil-Moisture Accouting Model (SMA)

Since most of concepts of the models described earlier are event models that simulate hydrological behavior during a precipitation event, whereas the SMA model is a continuous model that simulates both wet and dry weather behavior. The model simulates the watershed with a series of storage layers as illustrated by the following figure.

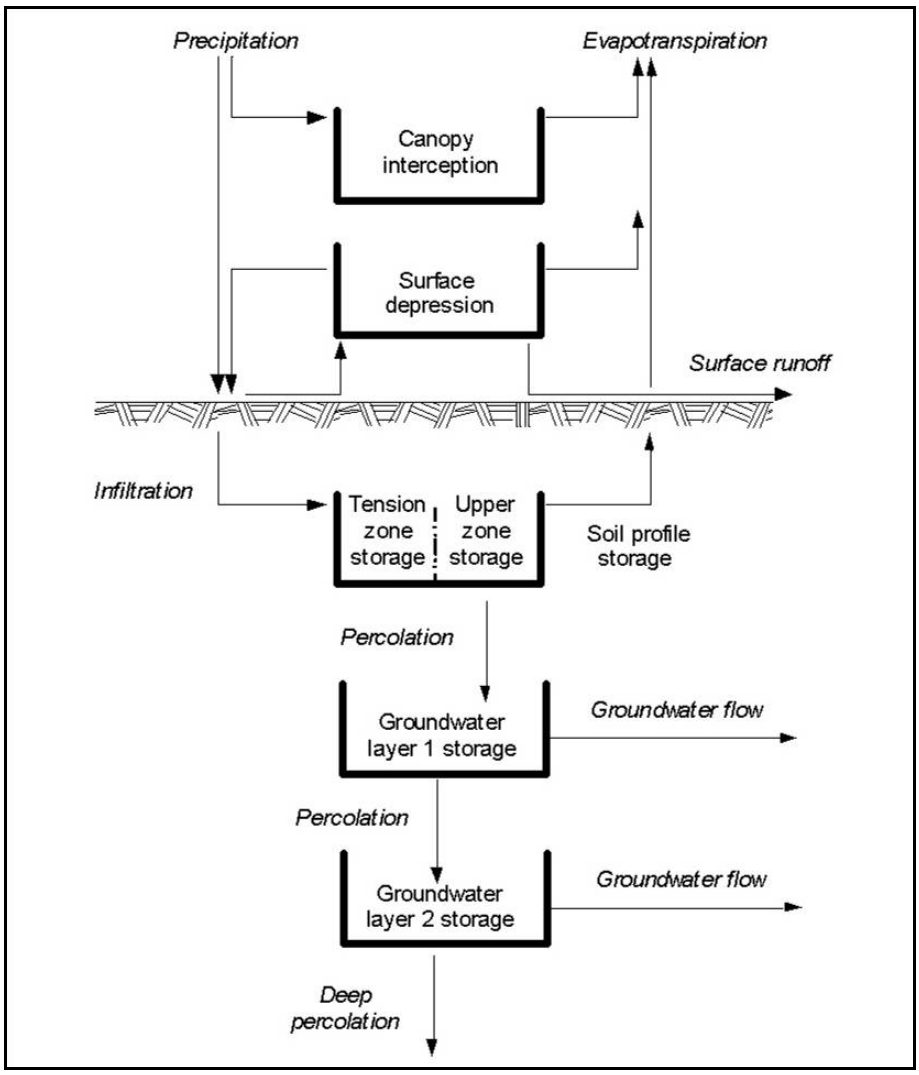

Figure 3 Conceptual schematic of the contimuous soil moisture accouting algorithm. **Source:** Bennett (1998)

2.2.2 Direct Runoff Models

There are 6 sub-models in the direct runoff models. All models excepted kinematic-wave model are unit hydrograph (UH) models, whereas kinematic-wave model is a conceptual model. Details of each sub-model can be presented below.

a. User-Specified Unit Hydrograph

HEC-HMS model directly allows user to specify a UH by entering all ordinates of the UH via the user interface.

b. Snyder's Unit Hydrograph Model

For this technique, Snyder selected the lag, peak flow, and total time base as the critical characteristics of a UH. He defined a standard UH as one whose rainfall duration, t_r, is related to the basin lag, t_p, by:

$$t_p = 5.5t_r \tag{16}$$

The UH lag and peak per unit of excess precipitation per unit area of the watershed were related by:

$$\frac{U_p}{A} = C\frac{C_p}{t_p} \tag{17}$$

where U_P is peak of UH, A is catchment area, C_P is UH peaking coefficient, and C is conversion constant (2.75 for SI or 640 for English unit).

In case of the other rainfall durations, the relationship in Eq. (16) and Eq.(17) will be changed as the following equation.

$$t_{pR} = t_p - \frac{t_r - t_R}{4} \tag{18}$$

$$\frac{U_{pR}}{A} = C\frac{C_p}{t_{pR}} \tag{19}$$

where t_R is duration of desired UH, t_{pR} is lag of desired UH, and U_P is peak of desired UH.

c. SCS Unit Hydrograph Model

There are 2 important parameters in SCS model. The first is unit hydrograph peak discharge (U_P), and another one is time to unit hydrograph peak (T_P). These parameters will be applied to the dimensionless unit hydrograph as shown in Figure 4 to produce unit hydrograph. SCS research suggests that the unit hydrograph peak and time of unit hydrograph peak are related by the following equations:

$$U_P = C\frac{A}{T_P} \tag{20}$$

where A is catchment area, C is conversion constant (2.08 for SI or 484 for English unit). The time of peak (T_P) is related to the duration of the unit of excess precipitation as:

$$T_P = \frac{\Delta t}{2} + t_{lag} \tag{21}$$

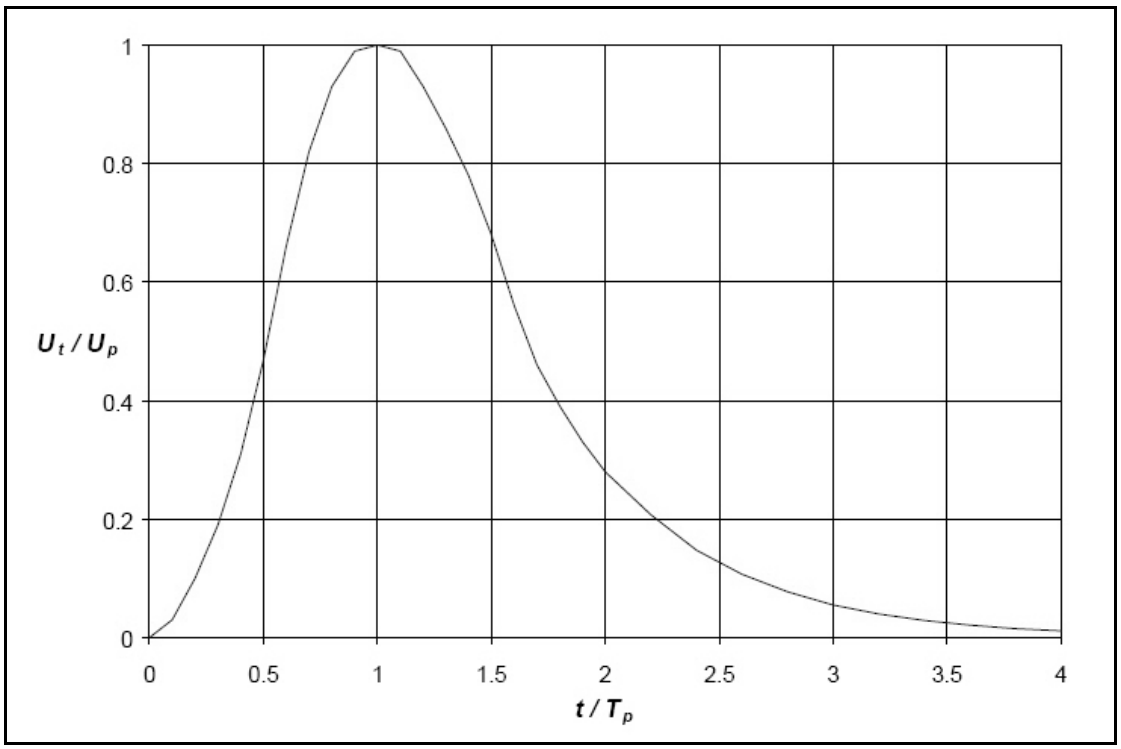

Figure 4 SCS Unit Hydrograph.
Soruce: USACE (2000)

where Δt is the excess precipitation duration, and t_{lag} is the Basin Lag.

d. Clark's Unit Hydrograph Model

Clak's UH model has an assumption that the storages in the whole catchment including soil, surface and channel storages are important to rainfall-runoff process. Linear reservoir can represent the effect of these storages. The basic equations of linear reservoir are presented as:

$$\frac{dS}{dt} = \overline{I_t} - \overline{O_t} \tag{22}$$

where, dS/dt is time rate of change of water in storage at time t, I_t is average inflow to storage at time t and $\overline{O}_t$ is average outflow from storage at time t. The relationship between storage at time t and the outflow of the linear reservoir model can be shown as:

$$S_t = RO_t \tag{23}$$

where, R is a constant linear reservoir parameter, and O_t is outflow from storage at time t. These two above equations will be combined, and the simple finite difference approximation is then used for solving the equations. The modified equation is performed as:

$$O_t = C_A \bar{I}_t + C_B O_{t-1} \tag{24}$$

where, C_A, C_B are routing coefficients which are calculated from:

$$C_A = \frac{\Delta t}{R + 0.5\Delta t} \tag{25}$$

$$C_B = 1 - C_A \tag{26}$$

The average outflow during period t is

$$\overline{O}_t = \frac{O_{t-1} + O_t}{2} \tag{27}$$

e. ModClark Model

The concept of ModClark (modified Clark) model based on quasi-distributed approach (Peters and Easton, 1996) are similar to Clak's UH model, but in model application the watershed will be divided as grid cells representing sub-

catchment. Distance from each grid to watershed outlet will be specified by user, while translation time to outlet can be calculated using the following equation.

$$t_{cell} = t_c \frac{d_{cell}}{d_{\max}} \tag{28}$$

where t_{cell} is time of travel for a cell, t_c is time of concentration for the watershed, d_{cell} is travel distance from a cell to the outlet, and $d_{\max}$ is travel distance for the cell that is most distant from the outlet.

f. Kinematic-wave model

Kinematic-wave model is a conceptual model for open channel flow simulation. This model represents a watershed as an open channel (a very wide, open channel), with inflow to the channel equal to the excess precipitation. Then it solves the equations that simulate unsteady shallow water flow in an open channel to compute the watershed runoff hydrograph. Momentum and continuity equation are fundamental equations of the kinematic-wave model. In one dimension, the momentum equation is:

$$S_f = S_0 - \frac{\partial y}{\partial x} - \frac{V}{g}\frac{\partial y}{\partial x} - \frac{1}{g}\frac{\partial V}{\partial t} \tag{29}$$

where S_f is energy slope, S_0 is bottom slope, V is velocity, y is hydraulic depth, x is distance along channel, t is time, g is gravity acceleration, $\frac{\partial y}{\partial x}$ is pressure gradient, $\frac{V}{g}\frac{\partial V}{\partial x}$ is convective acceleration, and $\frac{1}{g}\frac{\partial V}{\partial t}$ is local acceleration (Chow, 1959; Chaudhry, 1993). The energy gradient can be estimated using the Manning's equation written as:

$$Q = \frac{CR^{2/3}S_f^{1/2}}{N}A \tag{30}$$

where Q is flow, R is hydraulic radius, A is cross-section area, and N is a resistance factor depending on planes covering. For shallow flow, bottom slope and the energy gradient are approximately equal and acceleration effects are negligible. Thus the momentum equation is simplified to:

$$S_f = S_0 \tag{31}$$

The Manning's equation can be transformed to:

$$Q = \alpha A^m \tag{32}$$

where α and m are parameters related to flow geometry and surface roughness. For the continuity equation can be show as:

$$\frac{\partial A}{\partial t} + \frac{\partial Q}{\partial x} = q \tag{33}$$

where q is lateral inflow per unit length of channel. The continuity equation can be changed by substitution of equation (32) into (33) shown as:

$$\frac{\partial A}{\partial t} + \alpha m A^{(m-1)}\frac{\partial A}{\partial x} = q \tag{34}$$

2.2.3 Baseflow Models

There are 3 sub-models in baseflow models.

a. Constant, Monthly-varying Baseflow

This is the simplest baseflow model in HEC-HMS. It represents baseflow as a constant flow; this may vary monthly. This user-specified flow is added to the direct runoff computed from rainfall for each time step of the simulation.

b. Exponential Recession Model

The HEC-HMS includes a exponential recession model to represent watershed baseflow (Chow *et al*., 1988). The recession model has been used often to explain the drainage from natural storage in a watershed (Linsley *et al*., 1982). The relationship between the constant baseflow at time t (Q_t) and initial baseflow at time zero (Q_0) can be presented as follows:

$$Q_t = Q_0 k^t \tag{35}$$

where k is an exponential decay constant. From mentioned equation above, the computed baseflow can be shown as a figure below.

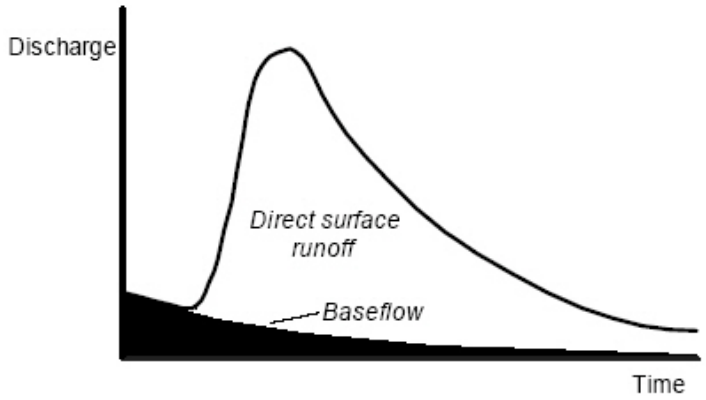

Figure 5 Initial baseflow recession.
Source: Hydrologic Engineering Center (2000)

The baseflow model is applied both at the start of simulation of a storm event, and later in the event as the delayed subsurface flow reaches the watershed channels, as illustrated in Figure 6. The threshold flow value will be specified by user as Q_0 to define the starting time as presented in equation (35).

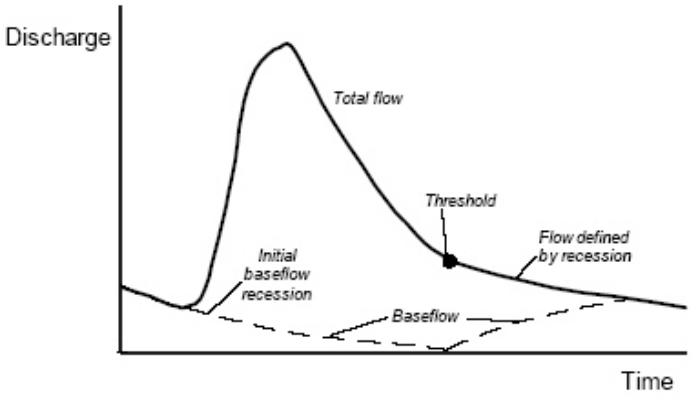

Figure 6 Base flow model illustration.
Source: Hydrologic Engineering Center (2000)

c. Linear Reservoir Model

The linear-reservoir baseflow model is used in conjunction with the continuous soil-moisture accounting (SMA) model. This baseflow model simulates the storage and movement of subsurface flow as storage and movement of water through reservoirs. The reservoirs are linear: the outflow at each time step of the simulation is a linear function of the average storage during the time step. Mathematically, this is identical to the manner in which Clark's UH model represents watershed runoff. The outflow from groundwater layer 1 of the SMA is inflow to one linear reservoir, and the outflow from groundwater layer 2 of the SMA is inflow to another. The outflow from the two linear reservoirs is combined to compute the total baseflow for the watershed.

2.3 URBS Model

URBS model is a distributed non-linear rainfall runoff routing model which can account for the spatial and temporal variation of rainfall (Malone, 2000). This model is based on the technical approach developed by Laurenson and Mein and later as the WT42 model by Shallcross (Carroll, 2004). Model development focuses for flood forecasting that requires good data management and be able to interface with external inputs and outputs.

There area many features in the URBS model consisting of 1) accessing to hydrological data, 2) results will be interpreted in the form of text and graphics, 3) water levels will be calculated as well as discharges, 4) output from third party water balance model can be integrated easily, 5) output files that can be readily imported into commercial spreadsheets, 6) DHI software (Mike 11) and HEC-RAS V.3 software can directly read output file, 7) AR&R design storms can be generated automatically for any zone, 8) automatic collation of design storm results for various ARIs and durations, 9) Monte-Carlo design storm results can be integrated to management routines, 10) rainfall-runoff loss model has the ability for event and continuous modelling, 11) there are several method to simulate hydrological

behaviour comprising splitting the catchment and channel routing components, introducing more sophisticated event loss models, development of Recovering Initial Loss Model, splitting of loss model into pervious and impervious components, and better accounting for the effects of urbanization and de-forestation, 12) sediment wash off and deposition modelling, 13) traffic disruption costs due to flooding, 14) on-site detention analysis, 15) assessment of the impacts of roofwater retention, 16) detention basin design routines, 17) allowance for channel transmission losses, 18) incorporation of simple Dam operating rules, 19) batch processing to minimise runtime and maximize review time and 20) hotstart capabilities for flood forecasting operations.

2.3.1 Runoff Routing Models

URBS is a runoff-routing networked model of sub-catchments. There are two runoff routing models to describe catchment and channel storage routing behaviour. These are the URBS Basic and Split routing model. Details of both sub-models are described as follows.

a. Basic Model

The Basic model is similar to a simple RORB model (Laurenson and Mein, 1990). The assumption of the both models is that the catchment and channel storage for each sub-catchment are lumped together as a single non-linear reservoir. The storage-discharge (S-Q) relationship of conceptual non-linear reservoir can show by the following.

$$S = k_c^1 Q^m \tag{36}$$

where, k_c^1 is the non-linear routing constant for a single reservoir. It is a function of the sub-catchment and channel storage characteristics. When k_c^1 is replaced with these characteristics, the Basic model will be change by the following.

$$S = \left\{ \frac{\alpha f L n (1+F)^2}{\sqrt{S_c}(1+U)^2} \right\} Q^m \tag{37}$$

where, S = catchment and channel storage (m^3 h/s), α = storage lag parameter, f = reach length factor, L = length of reach (km), U = fraction urbanization of sub-catchment, F = fraction of sub-catchment forested, n = channel roughness or Manning's n, S_c = channel slope (m/m), Q = outflow (m^3/s), and m = catchment non-linearity parameter.

The instability of calculation can be checked by using the sub-catchment lag divide by the chosen time interval. The result should close to zero. The criterion of calculation instability can show by the following.

$$\frac{k_c^1}{\delta T} \leq 0.01 \tag{38}$$

However, when instability occurs, the sizes of sub-catchment should be increased or the time step δT should be reduced.

b. Split Model

The Split model is a runoff routing model as well as the Basic model, but the catchment and channel routing for each sub-catchment will be separated individually. When the rain fall on a sub-catchment, it is then routed through the catchment storage located at the centroid of the catchment to the channel using the catchment routing component. After that, the outflow of catchment storage

which is the inflow of channel storage will be routed along a reach using a non-linear Muskingum method to the next catchment. The catchment and channel routing component can be estimate using the following criteria.

1) Catchment Routing

For catchment routing criteria, the catchment storage represents a non-linear reservoir. Once the rain fall on the ground, it is routed through the non-linear reservoir using the storage-discharge relationship as shown by follows.

$$S_{catch} = \left\{ \frac{\beta \sqrt{A}(1+F)^2}{(1+U)^2} \right\} Q^m \tag{39}$$

where, S_{catch} = catchment storage (m^3h/s), β = catchment lag parameter, A = area of sub-catchment (km^2), U = fraction urbanization of sub-catchment, F = fraction of sub-catchment forested, and m = catchment non-linearity parameter.

2) Channel Routing

Routing criteria for the channel routing is based on the non-linear Muskingum model as shown below:

$$S_{chnl} = \alpha f \frac{nL}{\sqrt{S_c}} \left(xQ_u + (1-x)Q_d \right)^n \tag{40}$$

where, S_{chnl} = channel storage (m^3h/s), α = channel lag parameter, f = reach length factor, L = length of reach (km), S_c = channel slope (m/m), Q_u = inflow at upstream end of reach (includes catchment inflow), Q_d = outflow at downstream end of the channel reach (m^3/s), z x = Muskingum translation parameter, n = Muskingum non-linearity parameter (exponent), n = Manning's n or channel roughness.

2.3.2 Rainfall Runoff–Loss Models

There are two rainfall loss approaches consisting of event based and continuous modeling in URBS model. Details of the two approaches are follows.

a. Event Base Rainfall Loss Modelling

This model requires the user to specify the initial loss, which is rainfall loss on the catchment before surface runoff occurrence. There are several loss models provided by the URBS that can be used for rainfall loss estimation. Details of each model are presented as:

1) Impervious Loss Model

The default of URBS model is that there is no initial loss for impervious area, total rainfall therefore become runoff with 100%. Recent research seems to suggest an initial loss of approximately 1 to 2 mm and a runoff proportion between 90% and 100% to be more appropriate. Boyd *et al*. (1993) adopt an effective fraction impervious to represent the directly connected impervious components of the catchment. A value between 0.7 and 0.9 is often used.

2) Pervious Loss Models

There are three types of pervious loss model composing of:

- Continuing Loss Model

This model assumes that there is an initial loss of il (mm) before any rainfall becomes effective. After this, a continuing loss rate of cl (mm) per hour is applied to the rainfall.

- Proportional Runoff Model

This model assumes that there is an initial loss of il (mm) before any rainfall becomes effective. After this, a proportional amount of runoff (pr , mm) is applied to the rainfall.

- Manley-Phillips Loss Model

The model assumes a loss rate based on a equation proposed by Manley (1974) as:

$$f_i = \frac{1}{2}(2kP)^{1/2} t^{-1/2} + k \tag{41}$$

where, f_t = loss rate after time t (mm/h), t = time (h), P = capillary suction head (mm), k = saturated loss rate (mm/h).

3) Including Spatial Variability Effects in Loss Model parameters

This model has an objective to account the spatial variability of soil loss model parameter by using a statistical distribution approach. The assumption is that when the rainfall infiltrate into the pervious areas that has reach x mm, it can expect that y fraction of the catchment is contributing to runoff. The model assumes a loss rate based on the following equation:

$$f_{eff} = f_u + \frac{F_t}{F_{\max}}, \quad Max(f_{ect}) = 1 \tag{42}$$

where f_{eff} = the fraction of the effective impervious area, f_u is the fraction of the existing impervious area, F_t is the cumulative infiltration into the pervious area (mm)

after time t, and $F_{\max}$ is the maximum infiltration capacity of the catchment. The URBS catchment infiltration model based on effective impervious areas can be shown as the figure below.

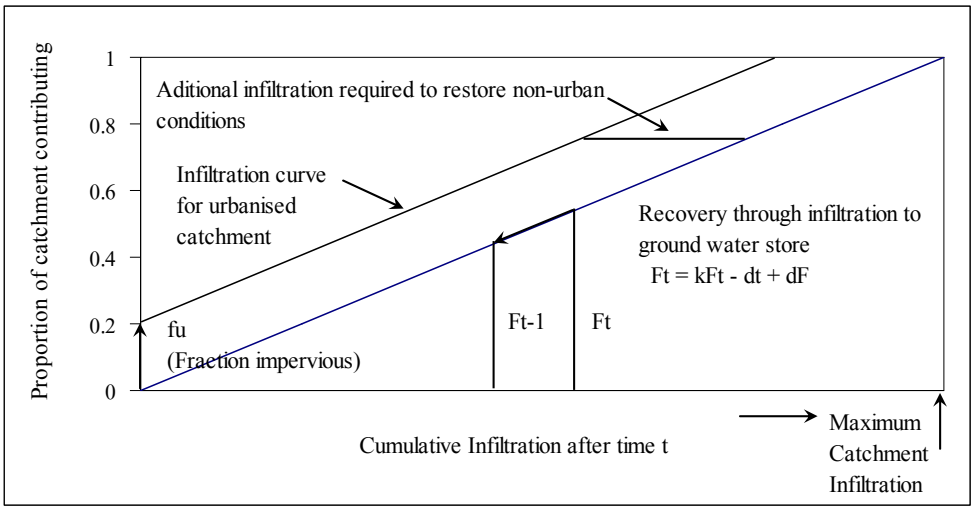

Figure 7 URBS spatial infiltration model based on effective impervious areas.
Source: Carroll (2004)

$$R_i = f_{eff} C_{imp} R_i^{tot} + (1 - f_{eff}) R_i^{per} \tag{43}$$

where R_i^{tot} is total rainfall depth, C_{imp} is the impervious runoff coefficient and R_i^{per} is the pervious excess rainfall depth.

$$F_t = k_{\delta T} F_{tl}, k_{\delta T} = k_{\frac{\delta T}{24}} \tag{44}$$

The reduction coefficient $k_{\delta T}$ is based on the 24 hour coefficient k_{24} which is entered by the user.

b. Rainfall-Runoff Models / Continuous Loss Modelling

There are two methods in the URBS model to be used for continuous rainfall runoff modelling. The first one is recovering initial loss model (RILM), and another one is third party water balance model. Details of both models are presented below:

1) URBS Recovering Initial Loss Models (RILM)

Since the continuing and proportional loss models as mentioned earlier cannot be used for recovering the initial loss. The RILM is an efficiency way developed for recovering the initial loss. There are two sub-models comprising the continuing loss and proportional loss models that can be used in this situation as presented details by the following.

- Manley-Phillips Loss Model

The initial loss is recalculated after every time step using the equation:

$$\begin{aligned} IL_{(i+1)} &= IL_i, \qquad R_i > clr_i.\delta t \\ IL_{(i+1)} &= IL_i + f.(clr_i\delta t - R_i), \qquad R_i \le clr_i.\delta t \\ IL_{(i+1)} &= IL_{\max}, \qquad IL_i > IL_{\max} \end{aligned} \tag{45}$$

where R_i is the rainfall series and clr_i is the continuing loss rate series, δt is the model time interval, and f is calibration parameter and represents the fraction of continuing loss deficit that contributes to the initial loss recovery. A value of f should be between 0.1 and 0.5 (Markar, 2001).

- Proportional Loss Model

The initial loss is recalculated after every time step using the equation:

$$\begin{aligned} IL_{(i+1)} &= IL_i, \qquad prR_i > rlr_i.\delta t \\ IL_{(i+1)} &= IL_i + rlr_i\delta t - R_i, \qquad R_i \le rlr_i.\delta t \\ IL_{(i+1)} &= IL_{\max}, \qquad IL_i > IL_{\max} \end{aligned} \tag{46}$$

where R_i is the rainfall series and pr is the proportional runoff coefficient, rlr is the recovering loss rate. When the rainfall rate is less than this rate, the initial loss can be recovered.

2) Third party water balance models.

The AWBM model is one of a water balance model, which can be used for rainfall loss estimation for a given event (Boughton, 1993). The model generally produces un-routed runoff or rainfall excess to a location of runoff station. The URBS model can access these data and disaggregate the excess for each upstream sub-catchment based on the volume of total rainfall that fell on each sub-catchment. When this loss model is used you should ensure that the parameters for the event based loss models (i.e. either uniform, proportional or Manley-Phillips) are set so that there is no generated loss.

2.4 SWAT Model

SWAT is an acronym for Soil and Water Assessment Tool. It is a public domain model developed by Dr. Jeff Arnold for the United States Department of Agriculture – Agricultural Research Service (USDA-ARS). The development of model has an objective to predict the impact of watershed management practices on water, sediment and agricultural chemical yields in large complex watersheds. The

model has been developed since 1990's, and the latest version is SWAT2000. Geographic Information System (GIS) is also applied to this latest version called AVSWAT (Arcview SWAT) to be a convenient tool for model simulation (Neitsch *et al.*, 2002).

For the model application, the catchment will be separated into a number of small sub-catchments according to their land use and soil type. There are several input data for each sub-basin such as climatological data, land covering and soil type, sub-basin and the main channel characteristic, and groundwater level.

The SWAT model simulation based on hydrologic cycle can be divided into 2 parts comprising land phase, and routing phase. For the land phase particularly consider the quantity of water, sediment, nutrient and pesticide loadings of each sub-basin before flow to the main channel, while routing phase consider the movement of water, sediment, etc. through the channel network to the outlet.

The hydrologic cycle as simulated by SWAT is based on the water balance equation as follow:

$$SW_t = SW_0 + \left(R_{day} - Q_{surf} - E_a - w_{seep} - Q_{gw}\right)_{i=1}^{t} \qquad (47)$$

where SW_t is the final soil water content (mm), SW_0 is the initial soil water content (mm), t is the time (days), R_{day} is the precipitation on day i (mm), Q_{surf} is the surface runoff on day i (mm), E_a is the evapotranspiration on day i (mm), W_{seep} is the percolation into soil on day i (mm), and Q_{gw} is the return flow on day i (mm).

SWAT model provides two methods for surface runoff estimation comprising the SCS curve number procedure (SCS, 1972) and the Green and Ampt infiltration method (1911). The theory and concept of both methods are similar to the details of sub model in HEC-HMS model as mention earlier. The estimated surface runoff will be then routed through the channel using a variable storage coefficient

method or the Muskingum routing method (Neitsch *et al*., 2002a). The model also includes controlled reservoir operation, groundwater flow model and a weather generator that generates daily values (precipitation, air temperature, solar radiation, wind speed and relative humidity) from average monthly values.

For model application, the SWAT model requires a significant amount of data and empirical parameters for model calibration and verification (Benaman *et al*., 2001). Most of the model calibration and verification were based on monthly time scale. Generally, the SWAT model predicts monthly flows well except during extreme hydrologic conditions (Shirmohammadi *et al*., 2001; Arnold *et al*., 2000; Rosenthal *et al*., 1995). Daily flow simulations were investigated in a few of the applications: Peterson and Hamlett (1998); Benaman *et al*. (2001); Varanou *et al*. (2002); Spruill *et al*. (2000); and King *et al*. (1999). In general, SWAT's daily flow predictions are not as good as monthly flow predictions.

3. Weather Radar

Rainfall is a main source of water in the hydrological processes, accurate measurement and prediction of the spatial and temporal distribution of rainfall is therefore a basic issue in hydrology (Uijlenhoet, 2001). Weather radar, which is a widely used basis for measuring rainfall at fine spatial and temporal resolutions (Collinge and Kirby, 1987; Sun *et al*., 2000; Uijlenhoet, 2001; Vieux, 2003), is an alternative measurement used for rainfall estimation. Details of weather radar in rainfall estimation are presented follow.

3.1 History of weather radar

Heinrich Hertz is the first physicist who discovered that the radio waves can be transmitted through different materials since 1887. His experiment thus becomes the fundamental of radio communication including RADAR. RADAR is an acronym for RAdio Detection And Ranging. It was developed during the Second World War since 1940s (Hitschfield, 1986; Doviak and Zrnic, 1992). In this situation,

there were many countries comprising Germany, France, Great Britain, and the United States of America used radar for many purposes such as ship navigation, airplanes guide, and enemy craft detection.

Radar system composes of two main processes which are transmitter and receiver. The transmitter emits the electromagnetic wave out toward a target through an antenna. The signal emitted from the radar is in the upper radio range of the microwave region of the electromagnetic spectrum. When the transmitted energy strikes a target, the energy is then scattered in all directions. Some portion of that scattered energy will return to the radar antenna. Once the receiver detects that backscattered radiation, the received signal will then be converted to low-frequency signal for further analysis (Collier, 1996).

Weather radar was developed for weather observation and forecasting over the last 40 years, and now it is installed in many parts of the world particularly in the developed countries (Collier, 1996). It is very useful for location detection of the precipitation and its intensity. Later, Doppler weather radar, which is another kind of radar, was developed in the early 1940s using Doppler technique (Doviak and Zrnic, 1992). This system not only detects meteorological targets with greater detail, but also measures the velocity of the detected object. For this study, the Doppler weather radar will be applied to assess areal rainfall as the input data to the selected hydrologic model for flood and runoff estimation.

3.2 Basic principles of weather radar

In the beginning stage of radar development, the electromagnetic wave which is in the form of continuous waves (CW) was transmitted into the atmosphere in radar measurement process. However, there is no distinguishing between start and stop of the echo signal using the CW, inability for estimating the target distance from radar is therefore a disadvantage of using this continuous wave in the radar process. To improve the ability on target range measurement, G. Breit and M. A. Tuve (1925) discovered a new technique by emitting the signal with pulsed radio waves instead of

continuous wave transmission. As a result, pulse radar has been used as general radar in the present including Thailand.

The radar system transmits a conical beam of energy in discrete pulses through radar antenna at approximately the speed of light (3×10^8 m/s). The volume of each pulse of energy will determine how many targets are illuminated. This directly determines how much power is returned to the radar. For the receive power from a single target is given by:

$$P_r = \frac{P_t G^2 \lambda^2 \sigma}{(4\pi)^3 r^4} \tag{48}$$

where P_t is the transmitted power, P_r is the received power, G is the gain for the radar, λ is the wavelength of radar, and *r* is the range from the radar to the target, and σ is the backscattering target cross-section. In the case of multiple targets the equation (48) will be changed as:

$$\overline{P}_r = \frac{P_t G^2 \lambda^2}{(4\pi)^3 r^4} \sum_{i=1}^{n} \sigma_i \tag{49}$$

where n is the amount of targets. Probert-Jones (1962) developed a new radar equation to describe the received power of over all targets within the pulse volumes as:

$$\overline{P}_r = \frac{P_t G^2 \lambda^2}{(4\pi)^3 r^4} V \sum_{vol} \sigma_i \tag{50}$$

where V is the effective radar pulse volume, and $\sum_{vol} \sigma_i$ is the summation of each target backscatter cross section area over a unit pulse volume. The equation for estimating V can be written as:

$$V = \frac{1}{8} \times \frac{\pi r^2 \theta \phi h}{2\ln(2)} \tag{51}$$

where θ and ϕ are the horizontal and vertical beam widths in degree unit, h is the pulse length. Substitution of equation (51) into equation (50) including the atmospheric attenuation denoted by "L" gives:

$$\overline{P_r} = \frac{P_t G^2 \lambda^2 \theta \phi h L}{512(2\ln 2)\pi^2 r^2} \sum_{vol} \sigma_i \tag{52}$$

According to scattering theory, the total energy backscattered depends upon the number of particles within the pulse volume of the radar beam. However, the particles do not scatter isotropically, thus a backscattering cross-section σ is defined as equivalent area required for an isotropic scatter to return to a receiver the power actually received. When the water drop diameter (D_i) is small compared with the wavelength$\left(\frac{Di}{\lambda} < \frac{1}{16}\right)$, the Rayleigh's law (1871) can be applied. As a result, σ can be simplified as follow:

$$\sigma_i = \frac{\lambda^2 a^6}{\pi} \left| \frac{m^2 - 1}{m^2 + 2} \right|^2 \tag{53}$$

where *m* is the complex index of refraction, and a is electrical size ($a = \pi D / \lambda$). The equation (53) can be simplified by substituting $a = \pi D / \lambda$ and $(m^2 - 1)/(m^2 + 2) = K$ into the equation (53). The equation is then changed by:

$$\sigma_i = \frac{\pi^5 |K|^2 D_i^6}{\lambda^4} \tag{54}$$

where $|K|$ is the physical properties of the target substance. For liquid water at 10^{o}C, it is equal to 0.93, and for ice particles, it is equal to 0.19 (Battan, 1973). Substitution of equation (54) into equation (52) gives:

$$\overline{P}_r = \frac{P_t G^2 \lambda^2 \theta \phi h L \pi^3}{1024 \ln 2 \pi^2 r^2} |K|^2 \sum_{vol} D_i^6 \tag{55}$$

Normally, the summation of particles diameters term ($\sum_{vol} D_i^6$) is usually refer as reflectivity factor (Z) in mm^6/m^3 unit, therefore the equation (55) can be rewritten as:

$$\overline{P}_r = \frac{P_t G^2 \lambda^2 \theta \phi h L \pi^3}{512 (2 \ln 2) \pi^2 r^2} |K|^2 Z \tag{56}$$

Equation (56) can be simplified to:

$$\overline{P}_r = \frac{C |K|^2 Z}{r^2} \tag{57}$$

where C is radar constant depending upon wavelength, transmitted power, antenna gain, beam width, pulse length, sum of all losses, and range of target. From the above equation, if we know backscattering power and the other variables, we can calculate the reflectivity factor. However, the calculated reflectivity factor (*Z*) is in mm^6/m^3 unit, which varies across many orders of magnitudes. It is therefore usually more convenient to express Z in dBZ unit using the following equation:

$$dBZ = 10 \log_{10} Z \tag{58}$$

3.3 Doppler processing

When the radar emit the frequency (f_0) strikes a moving target, the returned frequency to the radar antenna is shifted. This situation is known as the Doppler effect. The Doppler shift frequency (f_D) returned to the antenna can be written as:

$$f_D = \frac{2V}{\lambda} \tag{59}$$

where V is the velocity of the target in direction of radar transmission.

According to Doppler effect hypothesis, if the target is moving towards the radar, the received frequency can be calculate from $f_0 + f_D$. On the other hand, if the object is moving away from the radar, the received frequency can be calculate from $f_0 - f_D$. When f_D is measured, the velocity of the target can be calculated.

3.4 Range ambiguities

Radar systems radiate each pulse during transmits time. It waits for returning echoes from the previous pulse, and then radiates a next pulse, as shown in Figure 8. The number of pulses radiated in one second is called the pulse-repetition frequency (PRF), or the pulse-repetition rate (PRR). The time between the beginning of one pulse and the start of the next pulse is called pulse repetition time (PRT) and is equal to the reciprocal of PRF.

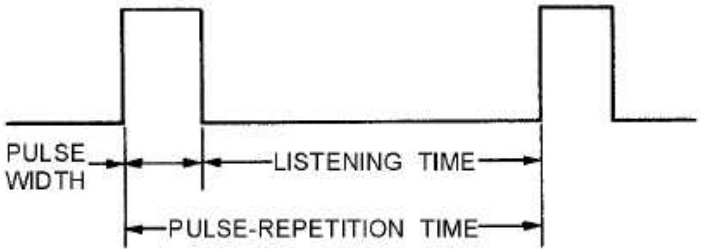

Figure 8 Radar pulse relationships.

The PRF of the radar is important for maximum range determination. Any echoes which return after the transmission of the next pulse, will give a misleading range on the radar screen. This incorrect range is called ambiguous range. The maximum unambiguous range (R_a) defined by PRF for given radar system can be determined by the following formula:

$$R_a = \frac{c}{2PRF} \tag{60}$$

where $c = 2.998 \times 10^8 m/s$ is the speed of light.

3.5 Relation between radar reflectivity, rainfall rate and raindrop size distribution

The weather radar is a widely used basis for measuring rainfall at fine spatial and temporal resolutions (Collinge and Kirby 1987; Sun et al. 2000; Uijlenhoet 2001; Vieux 2003). Nevertheless, the weather radar does not measure rainfall directly, inferring the rainfall based on the power of electromagnetic waves backscattered by raindrops in the atmosphere and intercepted by the radar. This backscattered power is represented as the radar reflectivity (Z), and related to a rainfall rate (R) through a power law relationship $Z = AR^b$, referred to as the Z-R relationship. This section aims to explain the fundamental reason of this empirical power law relationship.

The reflectivity in mm^6/m^3 unit is related to the raindrop size distribution in the radar sample volume as: (Atlas, 1964; Battan, 1973)

$$Z = \int_0^\infty D^6 N_V(D) dD \tag{61}$$

where $N_V(D)dD$ (the subscript V standing for volume) represents the mean number of raindrops with equivalent spherical diameters between D and $D + dD$ (mm) present per unit volume of air in unit of $1/m^3$. $N_V(D)$ represents raindrop size distribution in 1/mm m^3 unit. From the equation (61), it demonstrates that the Z is a purely meteorological quantity that is independent of any radar property (Uijlenhoet, 2001). While the rainfall rate (mm/h) is also computed by using the raindrop size distribution relationship according to.

$$R = \frac{6\pi}{10^4} \int_0^\infty D^3 v(D) N_V(D) dD \tag{62}$$

where $v(D)$ is the relationship between the raindrop fall speed in still air v (m/s) and its diameter D (mm). It can be approximated using a power law as presented below:

$$v(D) = cD^\gamma \tag{63}$$

Atlas and Ulbrich (1977) suggested that the coefficient c and γ are 3.778 (ms^{-1}) and 0.67, respectively.

Marshall and Palmer (1948) proposed a simple negative exponential raindrop size distribution $N_V(D)$ as shown in equation (64). This equation is widely used to compute rainfall rates from reflectivity measurements (Doviak and Zrnic, 1992).

$$N_V(D) = N_0 e^{-\Lambda D} \tag{64}$$

where N_0 is a shorthand notation for $N_V(0)$, and Λ is the slope of the $N_V(D)$ curve on a semilogarithmic plot. Both parameters are constant for any rainfall rate. N_0 = 8,000 1/mm m^3, and $\Lambda = 4.1R^{-0.21}$ (Marshall and Palmer, 1948).

Besides, raindrop size distribution can be written in the form of $N_V(D)$, it can be written in the form of $N_A(D)$ (mm^{-1} m^{-2} s^{-1}) as well. $N_A(D)d(D)$ (m^{-2} s^{-1}) is defined as the mean number of raindrops in a particular diameter interval arriving at a surface per unit area and per unit time (Uijlenhoet and Stricker, 1999). If the effects of wind, turbulence and raindrop interaction are neglected, the relationship between $N_A(D)$ and $N_V(D)$ in stationary rainfall becomes:

$$N_A(D) = \nu(D) N_V(D) \tag{65}$$

and

$$N_V(D) = \nu(D)^{-1} N_A(D) \tag{66}$$

By substituting the Equation (63) and (64) into the Equation (65) into, we obtained

$$N_A(D) = cN_0 D^{\gamma} e^{-\Lambda D} \tag{67}$$

From consideration of the Equations (61), (62), (65), and (66), the definitions of the radar reflectivity factor Z and the rainfall rate R can be rewritten as:

$$Z = \int_0^{\infty} D^6 N_V(D) dD \tag{68}$$

and

$$R = \frac{6\pi}{10^4} \int_0^{\infty} D^3 N_A(D) dD \tag{69}$$

Hence, Z is most naturally defined in terms of $N_V(D)$ and R is in terms of $N_A(D)$. This is because Z is a state variable an R is a flux variable (Uijlenhoet and Stricker, 1999).

Because reflectivity factor (Z) and rainfall rate (R) are related to the raindrop size distribution, it is possible to derive a power law relationship between Z and R (Marshall, 1969; Battan, 1973; Wilson and Brandes, 1979; Austin, 1987; Rinehart, 1991; Uijlenhoet, 2001) as presented below.

$$Z = AR^b \tag{70}$$

where A and b are model parameters which vary from one location to the next and form one season to the next. This power law equation has been common practice to convert measured radar reflectivity into rainfall rate (Chumchean, 2004)

MATERIALS AND METHODS

Materials

1. A laptop computer
2. Topographic map (scale 1:250,000 and 1:50,000) of the upper Ping river basin and the surrounding areas
3. Rain gauge rainfall data, runoff data, and radar reflectivity data in the upper Ping river basin
4. Rain gauge rainfall data, and radar reflectivity data in Bangkok
5. Rain gauge rainfall data, and radar reflectivity data in Sydney and Brisbane, Australia
6. Microsoft office, version 2003
7. URBS model
8. NAM model
9. Microsoft visual basic, version 6.0
10. ArcView GIS software, version 3.3

Methods

Based on the objectives of this thesis, methodologies were separated into 6 sections. Data collection used in this study is presented in section 1. The next section presents the methodology for selecting a suitable hydrologic model for flood and runoff estimation in the upper Ping river basin. The method for testing the selected model performance for flood estimation in gauged catchment in the study area, and the technique for the selected model application on the ungauged catchment were presented in section 3. Section 4 presents the calibration of a climatological Z-R relationship for the upper Ping river basin. Section 5 describes the method for studying an effect of rain-gauge temporal resolution on the specification of a Z-R relationship. Application of a simple scaling hypothesis for constructing a scaling transformation equation to ascertain the A parameters at finer temporal resolution was also described in this section. The last section presents the methodologies for

estimating different types of rainfall (daily rain gauge, daily radar, and hourly radar rainfall) to be used as input data to the selected hydrologic model for different runoff stations in the upper Ping river basin. Details of each section are described as in the followings.

1. Data collection

1.1 Rain gauge rainfall data

Rain gauge rainfall data from the networks located in the upper Ping river basin and Bangkok, as well as in Sydney and Brisbane, Australia were collected for this study. Details of data collection for each location are explained below.

1) The upper Ping river basin

In this study, rain gauge rainfall from 80 rainfall stations located in the upper Ping river basin and the surroundings (see Figure 9) during 1952 until 2005 were collected. Five automatic rain gauges providing continuous rainfall data are owned and operated by the Thailand Meteorological Department (TMD), whereas the remaining 46 and 29 stations owned and operated by the TMD and the Royal Irrigation Department (RID), respectively, are non-automatic stations providing daily rainfall.

The collected rain gauge rainfall data will be used for two applications: 1) used as the input data to the selected hydrological model for flood estimation at runoff stations located in the upper Ping river basin, 2) used in climatological Z-R calibration process for the upper Ping river basin.

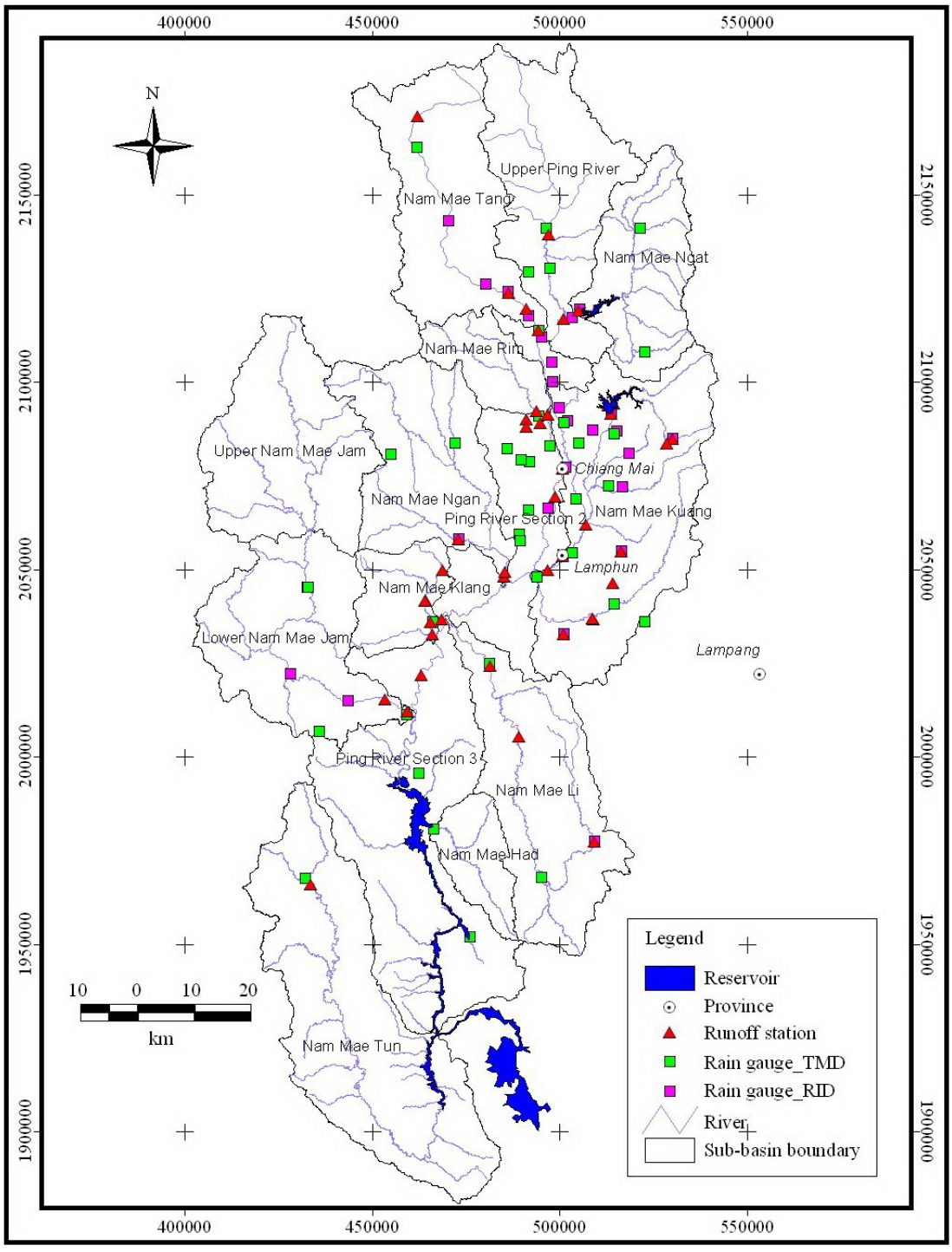

Figure 9 Locations of rain gauges and runoff stations in the upper Ping river basin and surroundings.

2) Bangkok

Rain gauge rainfall data used in this study were obtained from the network of 61 continuous tipping-bucket gauge stations located within 100 km from the Pasicharoen radar as illustrated in Figure 10. The rain gauges are owned and operated by the Bangkok Metropolitan Administration (BMA).

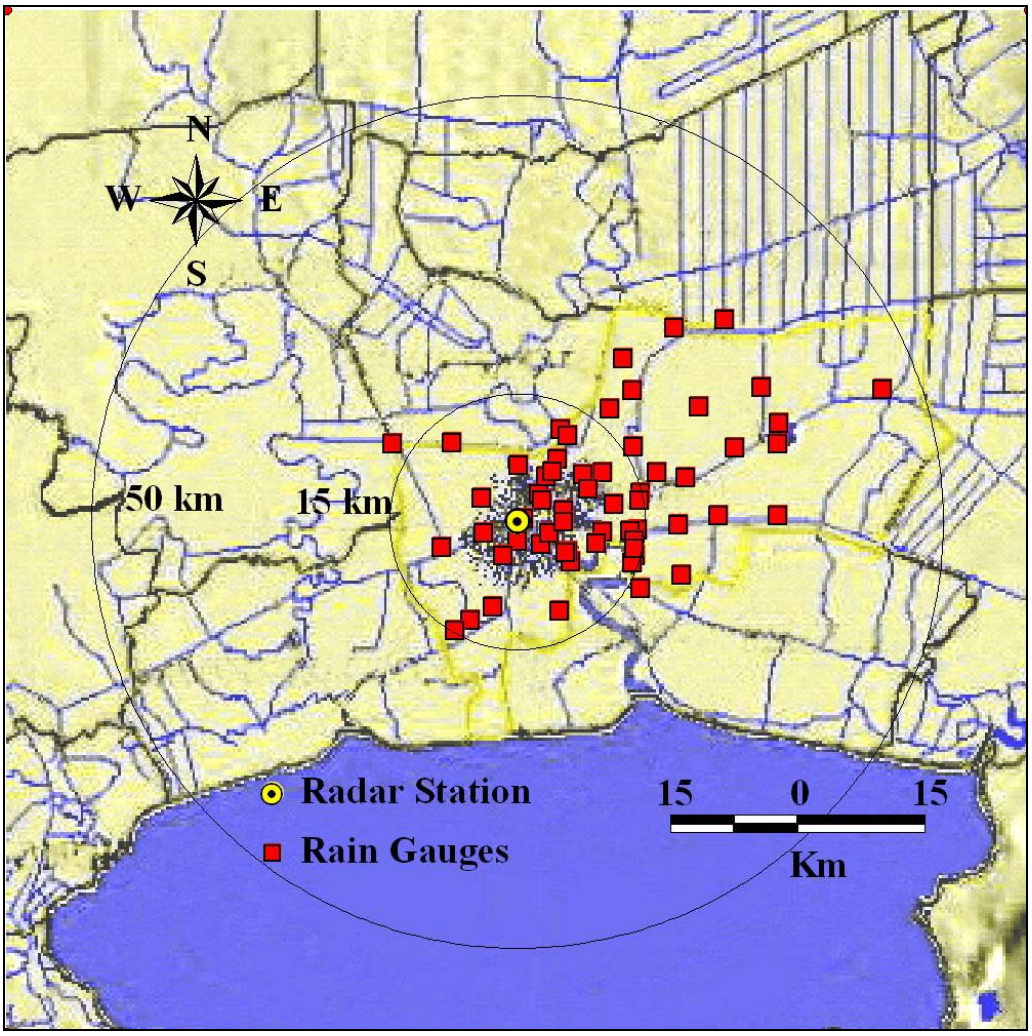

Figure 10 Locations of tipping-bucket rain gauges within the Pasicharoen radar radius.

3) Sydney

Rain gauge rainfall data used in this study were obtained from the network of 227 continuous tipping-bucket gauge stations located within 100 km from the Kurnell radar as illustrated in Figure 11. The rain gauges are owned and operated the Australian Bureau of Meteorology and the Sydney Water Corporation.

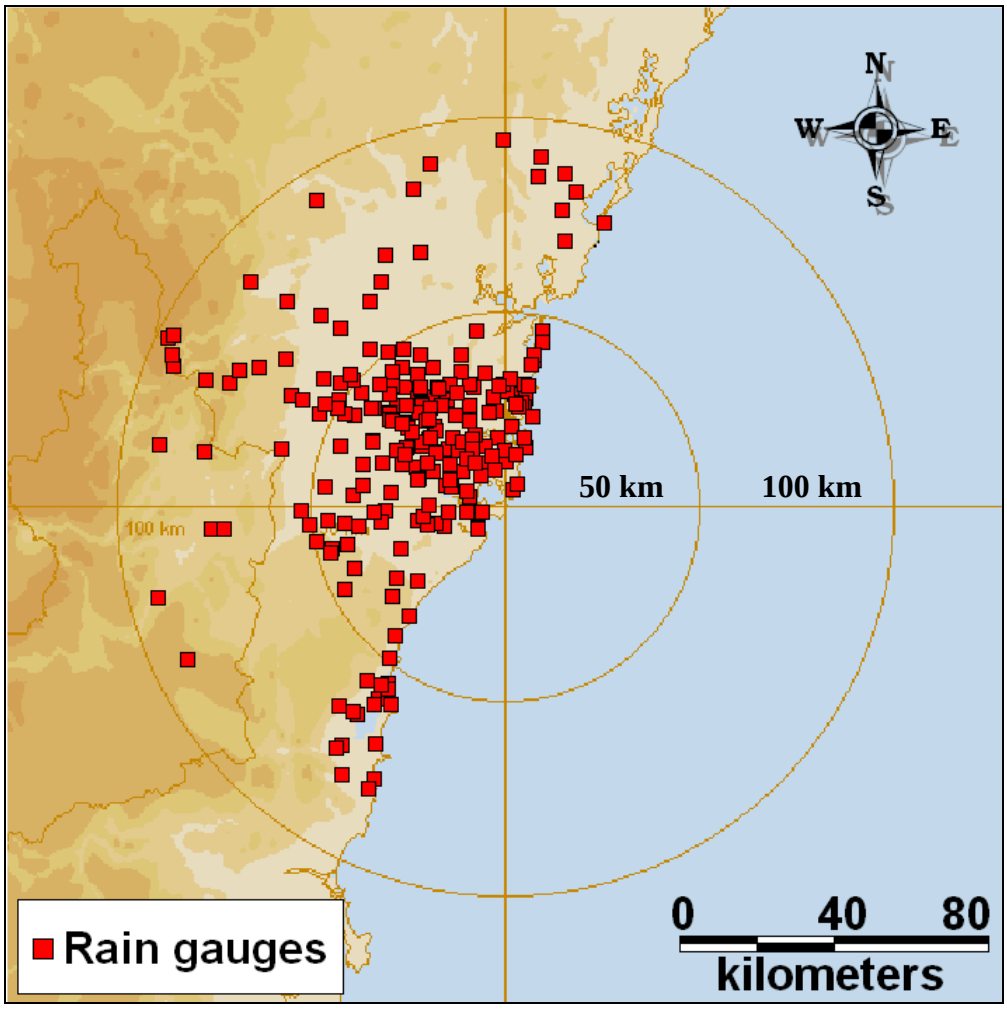

Figure 11 Locations of tipping-bucket rain gauges within the Kurnell radar radius.

4) Brisbane

Rain gauge rainfall data used in this study were obtained from the network of 202 continuous tipping-bucket gauge stations located within 100 km from the Mt Stapylton radar as illustrated in Figure 12. The rain gauges are owned and operated the Australian Bureau of Meteorology and the Sydney Water Corporation.

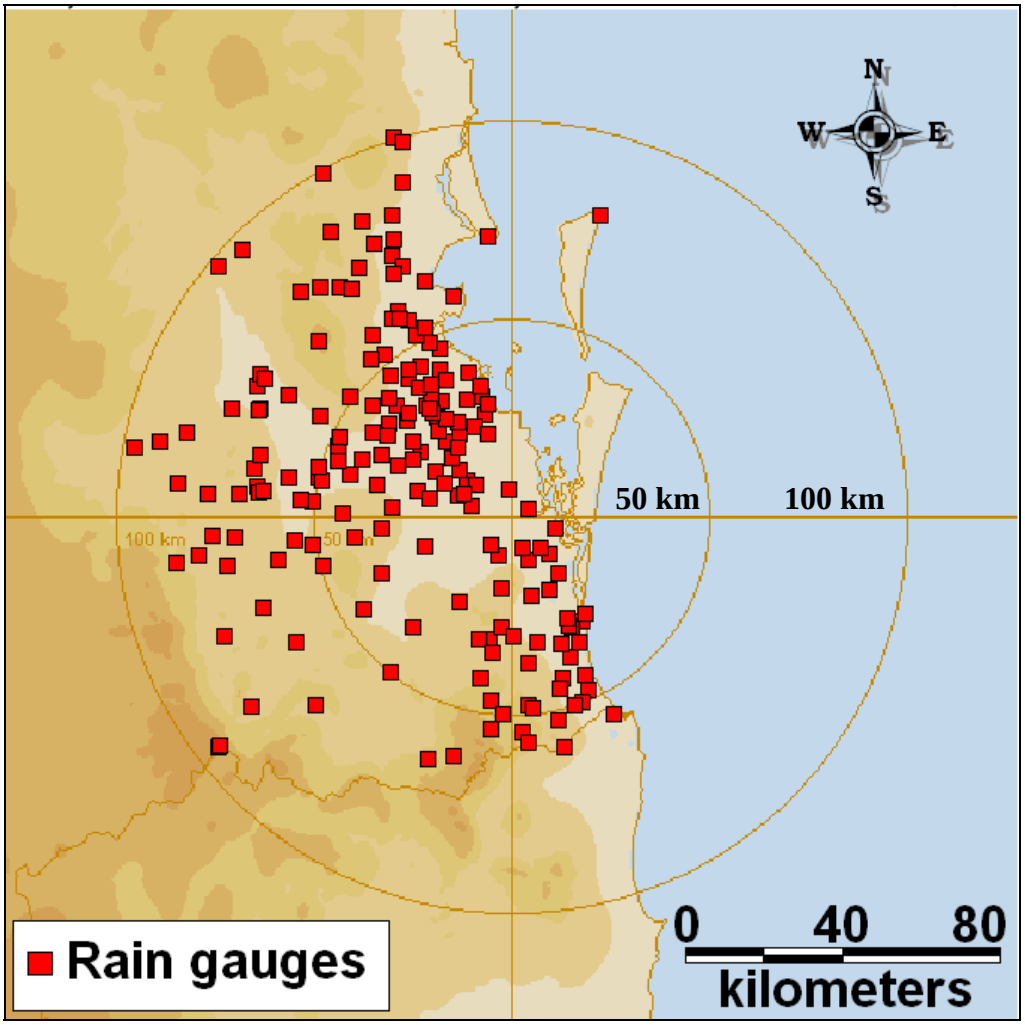

Figure 12 Locations of tipping-bucket rain gauges within the Mt Stapylton radar radius.

1.2 Runoff data

Thirty six runoff stations situated in the upper Ping river basin as illustrated in the Figure 9 were collected in this study. Two stations are floating gauges, while the rest 34 stations are vertical staff gauges. All runoff stations are owned and operated by the RID. The runoff data during 1952 until 2005 were collected for model calibration and verification purpose.

1.3 Radar reflectivity data

Radar reflectivity data from the Omkoi, the Pasicharoen, the Kurnell, and the Mt Stapylton radars located in Chiang Mai (represent the upper Ping river basin), Bangkok, Sydney, and Brisbane, respectively were collected for this study. Details of data collection for each location are explained below.

1) The upper Ping river basin

In the upper Ping river basin, two departments – the Thai Meteorological Department (TMD) and the Bureau of Royal Rainmaking and Agricultural Aviation (BRRAA) - collect reflectivity data at Amphor Muang Chiang Mai and Amphor Omkoi, respectively as illustrated in Figure 13. The reflectivity data from the Omkoi radar collected by the BRRAA is chosen for an investigation of the Z-R relationship for the following reasons.

Firstly, the BRRAA uses the S-band Doppler radar, whereas the C-band radar is used by the TMD. These different kinds of radar transmit radiation at different wavelengths, which is highly related to beam attenuation error. The shorter wavelengths are more attenuated in power by the vibration of particles in the atmosphere and absorbed by water than the longer wavelength (Hildebrand, 1978). Attenuation is therefore a severe problem for the X-band radar, which has quite short wave length of radiation of 2.8 cm. It can also be a problem for the C-band radar with the wave length of 5.5 cm. However it is not a problem for the S-band radar, which

has the longer wave length of 10.7 cm (Hitschfeld and Bordan, 1954; Delrieu *et al*., 2000).

Secondly, the BRRAA has collected the reflectivity data as volume scans, which are derived at 6-min interval using radar beam with different elevation angles (0.6, 1.4, and 2.2). The reflectivity products with a maximum range of 240 km provided by the BRRAA are in the form of PseudoCAPPI. This PseudoCAPPI reflectivity is the data obtained from the 2.5-km CAPPI (Constant Altitude Plan Position Indicator) and PPI (Plan Position Indicator) products. At a constant altitude of 2.5 km, the data collected within the radar range of approximately 135 km is considered as the CAPPI data, and the data beyond the range of 135 km is produced from the lowest PPI (0.6 degree). On the other hand, the TMD has collected hourly PPI which is extracted from the raw reflectivity data from the beam at the elevation angle of 0.75 degree.

Lastly, the data collected by the BRRAA are within smaller temporal resolutions of around 5 to 6 minutes compared to the TMD's data that are within one hour resolution. The data collected by the BRRAA has higher temporal resolution than the data collected by the TMD.

The S-band Doppler radar at Omkoi station transmits the radiation with the wave length of 10.7 cm, and produces a beam width of 1.2 degrees and a 240 km maximum range. The PseudoCAPPI reflectivity products with the spatial resolution of 1 km^2 for wet season (May - September) in 2003 to 2005 were collected for radar rainfall estimation in the upper Ping river basin because of its accuracy and the suitability of the rainfall data within the same periods as the reflectivity data.

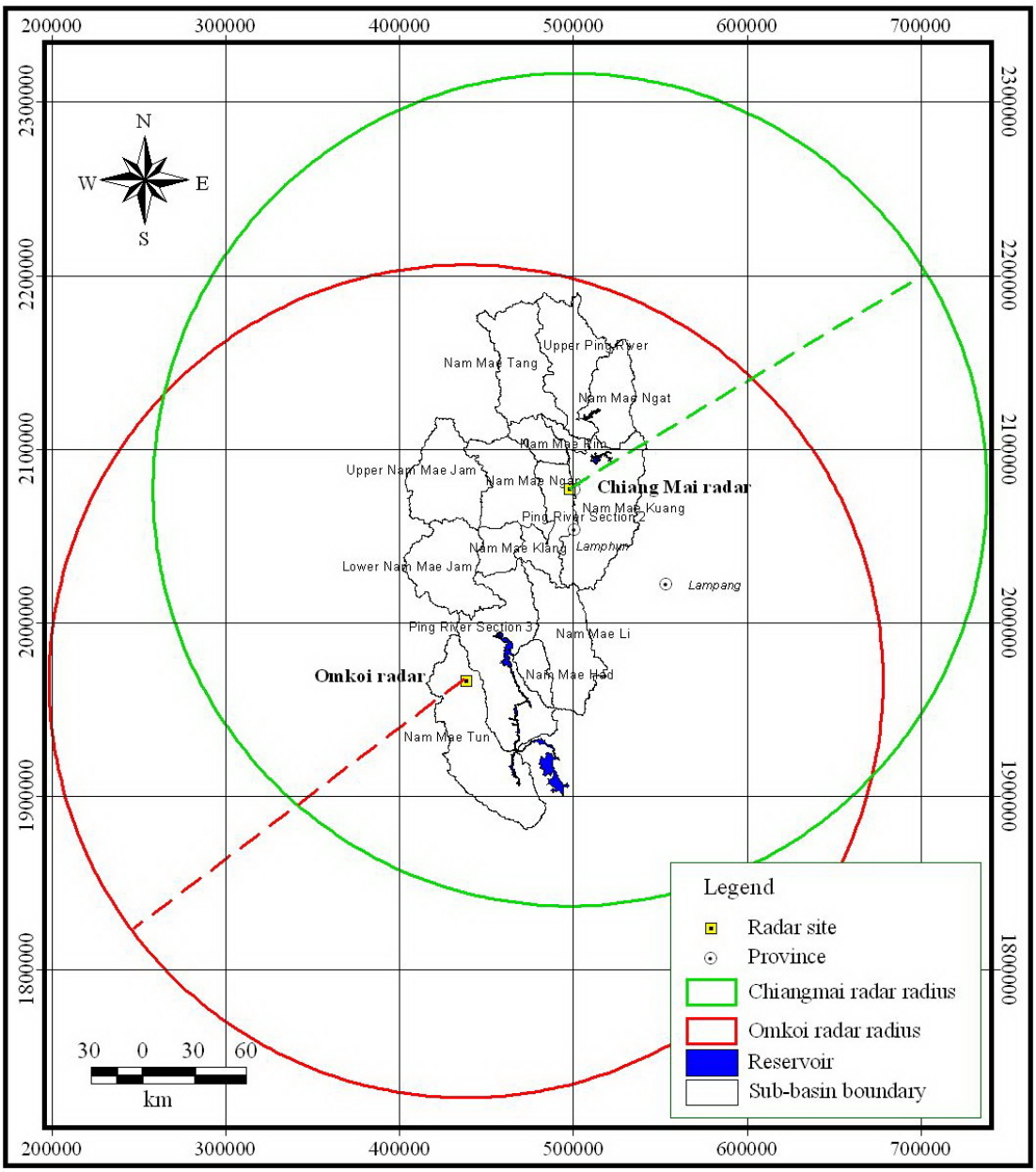

Figure 13 Location of weather radar belonged to the BRRAA and the TMD coving the upper Ping river basin.

2) Bangkok

For the *Z-R* calibration in Bangkok area, one dataset of the 0.5^{o} PPI (Plan Position Indicator) reflectivity data at Pasicharoen radar and 15-minute rain gauge data obtained from a 61 rain gauge network (see Figure 10) during June 2005–October 2006 were used. The Pasicharoen radar is a C-band Minimax Doppler radar which transmits the radiation with the wave length of 5.4 cm and produces a beam width of 0.90^{o}. The radar reflectivity data achieved from Bangkok station are in Cartesian grid with 240 km × 240 km extent with 1 km^2 spatial resolution and 10 minute temporal resolution.

3) Sydney

Three datasets of the 1.5-km CAPPI (Constant Altitude Plan Position Indicator) reflectivity data at the Kurnell radar and hourly rain gauge data obtained from a 227 rain gauge network (see Figure 11) during November 2000 – April 2001, August – December 2006, and January – May 2007 were used for the *Z-R* development for the Sydney area. The Kurnell radar is a C-band Doppler radar which transmits the radiation with the wave length of 5.3 cm and produces a beam width of 0.94^{o}. The radar reflectivity data achieved from Sydney station are in Cartesian grid with 256 km × 256 km extent with 1 km^2 spatial resolution and 10 minutes temporal resolution.

4) Brisbane

One dataset of the 1.5-km CAPPI (Constant Altitude Plan Position Indicator) reflectivity data at the Mt Stapylton radar and hourly rain gauge data obtained from a 202 rain gauge network (see Figure 12) during November 2006–March 2007 were used for the *Z-R* development for the Brisbane area. The Mt Stapylton is a S-band Doppler radar which transmits the radiation with the wave

length of 10.7 cm and produces a beam width of 1^{o}. The radar reflectivity data achieved from Brisbane station are in Cartesian grid with 256 km × 256 km extent with 1 km^2 spatial resolution and 10 minutes temporal resolution.

2. Hydrologic model selection

In this section, the most suitable hydrologic model for flood estimation in the upper Ping river basin will be chosen by considering the theory and the concepts of the four hydrologic models (NAM, HEC-HMS, URBS, and SWAT models) as presented in section 2 of the literature review. Methodology for hydrologic model selection is shown in the following.

2.1 Model selection criteria

To select a suitable hydrologic model for flood estimation in this study, the selection criteria is necessary to be established. The order of the selection criteria which are ranked according to its importance are presented below.

1) The model should be a public domain model or low cost model.

2) Model input and output facilities should be easily to carry out.

3) The model can be applied not only to a specific river basin but also to other river basins. Model users can change model parameters to be suited with their study areas. The recommendation for the suitable parameters to be applied for different basin characteristics would be benefit for model usages.

4) The model has an ability to simulate both single and continuous flood events.

5) Concept, theory, user manual and source code of the models can be obtained.

6) Input data needed for model applications are available for Thailand river basins.

2.2 Models comparison

Four hydrological models namely NAM, HEC-HMS, URBS, and SWAT models (see the details of their theory and concept in the section of "Hydrological models" in the literature review) were compared by considering the selection criteria as presented in Table 1. The most suitable hydrologic model will be chosen for flood estimation in this study.

2.3 Model selection

From Table 1, it can be seen that these four models have their own advantages and disadvantages on each selection criteria. To be able to choose the most appropriate model for this study, scores need to be given for a particular criterion of each model. The model which obtains the maximum score will be chosen for further investigation. Score evaluation is given as in the followings.

1) Since there are six selection criteria ranking according to its importance, weighing factors 6 to 1 are given to the selection orders 1 to 6, respectively.

2) For each selection criterion, the scores 0, 1, and 2 are given according to its low, medium, and high performance, respectively. Results of the rated score are presented in Table 2.

Table 1 Model ability according to the selection criteria.

Selection criterion	NAM model	HEC-HMS model	URBS model	SWAT model
1. The model should be a public domain model or low cost model	A high cost model (approximately 200,000 baht)	A public domain model	A low cost model (approximately 30,000 baht)	A public domain model
2. Model input and output facilities should be easily to carry out.	The NAM model provides a friendly graphic user interface for ease of use. User has alternatives to complete all input data via the graphic user or to prepare the data in the form of text file, which is very easily to be handle and it can be later imported to the model. For the output display, flood estimation result will be presented as a time series plot via graphic interface. The user can also export the output as text file for further analysis.	The HEC-HMS model comprise a graphical user interface, integrated hydrologic analysis components, data storage system (DSS) and management capabilities, and graphics and reporting facilities (US-ACE, 2001). DSS can be used to prepare time series data, but it is more complicated than using the text file. Thorough investigation of using the HEC-DSS model is therefore necessary. For the output display, the result of flood hydrograph is presented as a time series plot or table via graphic interface.	There is no user interface available for preparing the input data for the usage of the URBS model. All input data, which mostly are the time series data, need to be prepared in the form of text file. Locations of input data are specified via user interface or batch file, which is ready to be executed. The output data are displayed as time series plot and table via user interface. Text file of the output data are also available, and can easily be exported to be used as the input data for some hydrodynamic models such as the MIKE 11 and HEC-RAS models.	Since the SWAT model was developed using the Fortran code, the input and output data are necessary to be prepared in the form of text files. Presently, the model has an ability to link to the ArcView GIS software using the extension AVSWAT-2000 for arranging the input and output data.

Table 1 (Continued)

Selection criterion	NAM model	HEC-HMS model	URBS model	SWAT model
3. The model can be applied not only to a specific river basin but also to other river basins. Model users can change model parameters to be suited with their study areas. The recommendation for the suitable parameters to be applied for different basin characteristics would be benefit for model usages.	The model can be applied for general river basin using model calibration and verification techniques to ascertain the most suitable set of model parameters for a particular basin. Ranges of the suitable parameters are also provided in the user manual. However, the model parameters can be out of the recommended ranges.	There are several sub-models for flood estimation available in the HEC-HMS model. Some sub-models cannot be applied for general river basin using model calibration and verification techniques. This is because these sub-models include empirical parameters, which cannot be changed by user. Examples of these sub-models are as follows. In the SCS unit hydrograph (UH) model, the dimensionless unit hydrograph - which was synthesized using the data in USA – cannot be changed to suit the study area. In the SCS hypothetical storm model, there are four -	The model can be applied for general river basin by model calibration and verification processes to ascertain the most suitable set of model parameters for a particular basin. Ranges of the suitable parameters are also provided in the user manual but can be out of the recommended ranges. However, the URBS model can be simplified and the number of model parameters will be reduced to ease the model application.	Surface runoff volume in the SWAT model is computed using a modification of the SCS curve number method (USDA Soil Conservation Service, 1972) or the Green & Ampt infiltration method (Green and Ampt, 1911). For the curve number method, CN value is the main parameter which can be estimated as a function of land use, soil type, and antecedent watershed moisture, using tables published by the SCS. For the Green & Ampt method, loss rate can be calculated as a function of the wetting front matric potential and effective hydraulic conductivity. Both parameters can be estimated as a function of -

Table 1 (Continued)

Selection criterion	NAM model	HEC-HMS model	URBS model	SWAT model
3. (Continued)		- types of storm distribution that can be chosen by the user. However, they are not covered all storm types occurring around the world. The application of these sub-models would cause significant errors in flood estimation.		- soil type using a table proposed by Rawls, *et al*. (1982). The SWAT model allow user to change those parameters to be suited to the study area. Since land use and soil type are important information for model application, unfortunately these data are not easily measured from a general topography map.
4. The model has an ability to simulate both single and continuous flood events.	The NAM model was designed to simulate the components of surface runoff comprising the overland flow, interflow and baseflow. All flow components based on physical structures and semi-empirical equations can continuously be connected and transported to each others. As a result, the -	The HEC-HMS model was designed to simulate both single and continuous flood events over a long period of time. The model consists of 4 model groups (24 sub-models), which are runoff-volume models, direct-runoff models, baseflow models, and routing models, to be used for -	The URBS model has an ability to simulate both single and continuous flood events depending upon the loss model. For the single loss model, an initial loss will first be specified, and a continuing loss rate (cl) or a proportional amount of runoff (pr) will thereafter be applied to the -	The SWAT model provides two methods for calculating the rainfall loss rate comprising the SCS curve number procedure (SCS, 1972) and the Green and Ampt infiltration method (1911). These two techniques are however appropriate for single flood event (HEC-HMS). An application of -

Table 1 (Continued)

Selection criterion	NAM model	HEC-HMS model	URBS model	SWAT model
4. (Continued)	- NAM model can reasonably be used to simulate both single and continuous flood events.	- the calculation of rainfall loss rate, rainfall-runoff transformation, baseflow estimation, and flow routing, respectively. Single and continuous flood events can be distinguished using 7 sub-models of the rainfall loss rate which are available in the runoff-volume models. Within these sub-models, there are 3 sub-models (deficit and constant rate, Soil Moisture Accounting (SMA), Gridded SMA models) can be used for calculating the continuous flood events. Users can choose the appropriate method to calculate flood events according to their needs.	- rainfall. For the continuous simulation, the initial loss can be recovered if there is no rainfall for a long period.	- the model for continuous flood events would possibly contains significant errors.

Table 1 (Continued)

Selection criterion	NAM model	HEC-HMS model	URBS model	SWAT model
5. Concept, theory, user manual and source code of the models can be obtained.	Theory and concept of the model are presented in the user manual, but the source code of the model is not available.	Theory, concept, user manual, and source code for most of sub-models of the HEC-HMS model are available via internet. Further details can be obtained by direct contact to their website.	Theory and concept of the model are presented in the user manual, but the source code of the model is not available. The problems occur while using the model can be directly consulted to the developer.	Theory, concept, user manual, and source code of the model are available via internet. Further details can be obtained by direct contact to their website.
6. Input data needed for model applications are available for Thailand river basins.	Data needed for model applications comprise rainfall, runoff, and evaporation data which are available in Thailand river basins.	Data needed for model applications comprise rainfall, runoff, and evaporation data which are available in Thailand river basins.	Data needed for model applications comprise rainfall, runoff, rating curve, and evaporation data which are available in Thailand river basins.	Data needed for model applications comprise rainfall, runoff, evaporation, climate, land used, and soil type data which are available in Thailand river basins.

Table 2 Rated score for each model and selection criterion.

Selection Criterion Number	Weighing factor	Score				Score × weighing factor			
		NAM model	HEC-HMS model	URBS model	SWAT model	NAM model	HEC-HMS model	URBS model	SWAT model
1	6	0	2	1	2	0	12	6	12
2	5	2	1	2	1	10	5	10	5
3	4	2	1	2	2	8	4	8	8
4	3	2	2	2	1	6	6	6	3
5	2	1	2	2	2	2	4	4	4
6	1	2	2	2	2	2	2	2	2

The URBS model has shown the full score for five out of six criteria, while other three models receive the full score for four out of six criteria. With a

consideration of weighting factors, the URBS model has shown slightly advantage over other three models. Additionally, two experts on the URBS model application had visited the Water Resources Department for two weeks during the early stage of this research, therefore the URBS was finally chosen for further application in this study.

3. Testing the URBS model performance and extending its application to the ungauged catchments

An effectiveness of the URBS model performance can be evaluated by calibrating the model on runoff stations in the upper Ping river basin. To be more confident on applying the URBS model to the study area, the URBS model performance will also be compared to the NAM model performance. This is because the NAM model, a sub-module of the MIKE 11 model package, is one of the commercial hydrologic models that has been accepted worldwide (Knudsen *et al*., 1986; Refsgaard and Knudsen, 1996; Madsen 2000) and also generally applied for many river basins in Thailand for runoff and flood assessment (Poomthaisong, 1997; Tingsanchali and Gautam, 2000; Pawattana *et al*., 2007). The URBS and NAM models were setup for different runoff stations in the upper Ping river basin using gauge rainfall as the input data. The performance comparison between the URBS and the NAM model were thereafter verified at some gauging stations in the upper Ping river basin.

Since the URBS model can only be applied on the gauged catchment - which model parameters can be specified by the calibration and verification processes - the potential of the URBS model application on the ungauged catchment for the upper Ping river basin was extended in this study. After the URBS model was applied for different runoff stations in the upper Ping river basin, the ungauged relationship between model parameters and catchment characteristics will be constructed to be used for ungauged catchment in the basin.

3.1 Hydrological model description

3.1.1 URBS model

In this study, catchment and channel storage as shown in the Eqs. (39) and (40), respectively, were simplified by setting the afforestation factor, *F*, and urbanization factor, *U*, to be zero for the catchment routing component. The channel routing component, Muskingum non-linearity parameters (n_1) and the reach length factor (*f*) are set to be 1, while Manning's n and channel slope S_c were neglected. The simplified equations are then:

$$S_{catch} = \beta\sqrt{A}Q^m \tag{71}$$

and

$$S_{chnl} = \alpha L\left(xQ_u + (1-x)Q_d\right) \tag{72}$$

Excess rainfall estimation is crucial for the rainfall - runoff modeling (Malone and Cordery, 1989). For the URBS model, excess rainfall can be assessed using different rainfall loss models (see more details in the section "Hydrologic model" in the literature review). In this study, the initial loss - proportional runoff model (IL-PR) coupled with the spatial variability parameters loss model were chosen. The assumption of IL-PR model is that an initial loss (il, mm) will be deducted from rainfall following by the proportional loss (pr, mm) and then excess rainfall will occur. Spatial variability of infiltration was also accounted using the Eqs. (42) and (43).

As the URBS model equations have been simplified, there are only 7 model parameters necessary for the model application. These parameters are: 1) the channel lag parameter (α), 2) the catchment non-linearity parameter (m), 3) the Muskingum translation parameter (x), 4) the catchment lag parameter (β), 5) the initial loss (IL), 6) the proportional amount of runoff (PR), and 7) the maximum

infiltration rate (IF). The first four parameters are related to runoff routing behavior and the last three parameters are related to rainfall loss estimation. However, m and x parameters do normally not vary significantly from 0.8 and 0.3, respectively (Malone, 2000; Jordan *et al*., 2004). In this study, the values of the x and m parameters were therefore fixed at 0.8 and 0.3, respectively, for flood investigation. The remaining five model parameters are determined during the calibration process. For model application, each particular gauged basin needs to be divided into sub-catchments of at least 5 sub-catchments (Carroll, 2004). Each sub-catchment should have a similar size and also similar catchment characteristics.

3.1.2 NAM model

According to model description as presented in the section "Hydrologic models" in the literature review, there are 8 parameters needed for the NAM model application comprising: 1) the maximum water content in surface storage (U_{max}), 2) the maximum water content in root zone storage (L_{max}), 3) the overland flow runoff coefficient (*CQOF*), 4) the root zone threshold value for overland flow (*TOF*), 5) the time constant for routing overland flow (CK_1), 6) the time constant for routing interflow (CK_2), 7) the root zone threshold value for groundwater recharge (*TG*), and 8) the time constant for routing baseflow (*CKBF*). For model calibration, the U_{max} value is suggested to be ten percent of the L_{max} value, and the values of CK_1 and CK_2 are the same. Therefore six parameters have to be identified during the calibration process.

3.2 Method for comparing the URBS and NAM models for flood estimation

In the upper Ping river basin, there are 80 rainfall stations and 44 runoff stations located in the upper Ping river basin and its surroundings, but only 19 rainfall stations and 15 runoff stations have sufficient data available for this study. These stations are non-automatic stations with only daily data available for model application. Locations of the rainfall and runoff stations used in this study are shown in Figure 14.

Table 3 presents the number of rainfall stations and flood events used in hydrograph simulation for each of the 15 runoff stations in the upper Ping river basin. Note that, the flood events used in the analysis were selected to cover medium to severe levels of flooding with the respective annual probabilities of flood exceedence being 40 and 10% suggested by Paiva (1993). For the URBS model application, each runoff station needs to be separated into smaller sub-catchment as described earlier. Numbers of sub-catchment for each runoff station are also shown in Table 3.

Only the first 5 runoff stations namely P.20, P.4A, P.28, P.21, and P.71 presented in Table 3 were used in model comparison purpose. Model calibration and verification processes were carried out to define the most suitable set of control parameters of each model and each station. In these processes, goodness of fit between the observed and calculated discharges was evaluated using three statistical measures: the correlation coefficient (Chapra and Canale, 2002), root mean square error (Madsen, 2000), and the efficiency index or Nash-Sutcliffe criterion (Nash and Sutcliffe, 1970; Krause *et al*., 2005). Equations used to calculate these statistical measures are expressed in Table 4.

Table 3 Data used for the URBS and the NAM model application.

Runoff station code	Catchment Name	Catchment Area (km^2)	Amount of Sub-catchment	Number of rainfall station	Number of flood event	Range of probability of exceedance (%)
P.20	Upper Ping River	1,339	25	2	5	8 – 38
P.4A	Nam Mae Tang	1,939	30	3	5	14 – 40
P.28	Nam Mae Ngat	1,267	27	3	5	6 – 40
P.21	Nam Mae Rim	510	5	3	4	10 – 39
P.71	Nam Mae Ngan	1,727	15	2	5	11 – 40
P.1	Ping River section 2	1,112	15	4	6	15 – 40
P.77	Nam Mae Kuang	544	5	1	2	30 – 40
P.24A	Nam Mae Klang	454	5	2	4	28 – 39
P.29	Nam Mae Li	1,966	14	2	2	15 – 26
P.76	Nam Mae Li	1,543	11	2	2	20 – 40
P.73	Ping River section 3	2,242	14	8	3	14 – 40
P.5	Nam Mae Kuang	1,777	15	5	3	21 – 40
P.14	Nam Mae Jam	3,853	25	4	3	8 – 39
P.75	Ping River section 3	771	6	3	3	15 – 40
P.67	Ping River section 3	498	13	4	3	20 – 40

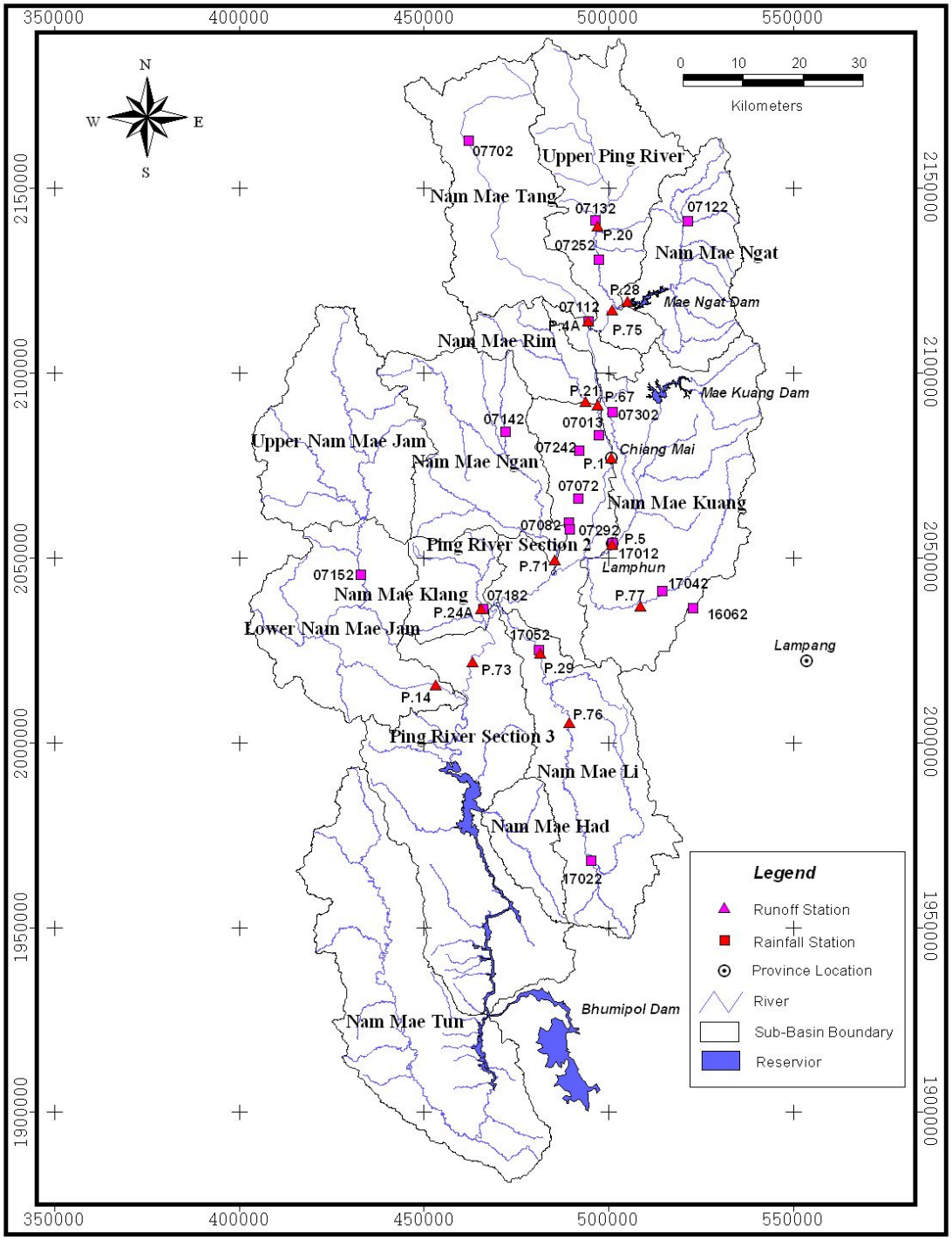

Figure 14 Locations of rainfall and runoff stations used for the analysis of testing the URBS model performance and extending its application to the ungauged catchments.

Table 4 Statistical measures used to identify the goodness of fit of flood discharges.

Statistical Measures	Equations
Correlation Coefficient (r)	$r = \frac{\sum_{i=1}^{N}(Q_{mi} - \overline{Q}_m) \times (Q_{ci} - \overline{Q}_c)}{\sqrt{\left[\sum_{i=1}^{N}(Q_{mi} - \overline{Q}_m)^2 \times \sum_{i=1}^{N}(Q_{ci} - \overline{Q}_c)^2\right]}}$
Root Mean Square Error (RMSE)	$RMSE = \left(\frac{\sum_{i=1}^{N}(Q_{mi} - Q_{ci})^2}{N}\right)^{0.5}$
Efficiency Index (EI)	$EI = 1 - \frac{\sum_{i=1}^{N}(Q_{mi} - Q_{ci})^2}{\sum_{i=1}^{N}(Q_{mi} - \overline{Q}_m)^2} \times 100\%$

where, Q_{mi} is daily the observed discharge at time i, $\overline{Q}_m$ is an average value of observed discharge, Q_{ci} is the calculated discharge at time i, $\overline{Q}_c$ is the average value of the calculated discharge, N is the number of data points. The best fit between the calculated and observed discharges using these parameters occurs when the correlation coefficient (r) approaches 1, the root mean square error ($RMSE$) approaches zero, and the efficiency index (EI) approaches 100 percent.

3.3 Method for model application for the ungauged catchments in the upper Ping river basin

Model parameters for gauged catchment can be achieved by the best fit between the observed and calculated discharges at a particular runoff station. Unfortunately most of the catchments are ungauged including the upper Ping river basin. To be able to apply the URBS model to the ungauged catchments in the upper Ping river basin, the ungauged relationships between model parameters and catchment characteristics, which can be measured from topographical maps, were formulated in this study. In this analysis, the URBS model will be further used to find model

parameters suitable for other 6 runoff stations namely P.1, P.77, P.24A, P.29, P.76, and P.73 presented in Table 3. Model parameters of the first 11 runoff stations shown in Table 3 and their catchment characteristics will be used to formulate the best ungauged relationships for the upper Ping river basin.

To test an effectiveness of the proposed ungauged relationships, these equations will be then used to calculate the model parameters of the last 4 runoff stations namely P.5, P.14, P.75, and P.67, which has not been applied in formulating the ungauged relationships process and also presented in the Table 3. The model parameters estimated using the gauged catchment approach (obtained by the best fit between the observed and calculated hydrograph) at the 4 runoff stations were also carried out to compare with the parameters obtained from the ungauged relationships. The results of flood estimation at the last 4 runoff stations calculated using the ungauged and gauged catchment approaches were later compared to the observed flood hydrograph to show the performance of ungauged catchment approach. If the estimated flood hydrographs attained from the ungauged and gauged catchment approaches are not significantly different with acceptable statistical measure values, it could be concluded that the proposed relationships between model parameters and catchment characteristics can also be applied to estimate the model parameters for other ungauged catchments in the upper Ping river basin.

4. Climatological Z-R relationship for radar rainfall estimation in the upper Ping river basin

Weather radar can potentially provide the spatial and temporal rainfall data as input to hydrologic models with the aim of increasing the accuracy of flood estimations. The basic principle of radar meteorology for rainfall estimation is discussed by many researchers Battan (1973); Rinehart (1991); Doviak and Zrinc (1992); Collier (1996). Nevertheless, the weather radar does not measure rainfall directly, it measures the power of electromagnetic waves backscattered by raindrops in the atmosphere (P_r) that can be performed as shown in the following equation (Battan, 1973; Rinehart, 1991; Doviak and Zrinc, 1992; Collier, 1996).

$$P_r = \frac{C|K|^2 Z}{r^2} \tag{73}$$

where C is a radar constant depending upon wavelength, transmitted power, antenna gain, beam width, pulse length, and sum of all losses; r is radar range; $|K|^2$ is the dielectric factor depending on the physical properties of the target; and Z is radar reflectivity factor. The radar reflectivity factor can be calculated using the above equation from the known backscattering power and the other variables. For radar rainfall estimation, an empirical power relationship between the reflectivity and rainfall rate ($Z=AR^b$) called the Z-R relationship is generally used to assess the radar rainfall rate.

Various forms of *Z-R* relations have been suggested in the literature (Marshall and Palmer, 1948; Joss and Waldvogel, 1970; Battan, 1973). However these relationships cannot be directly used in any region. This is because the *A* and *b* parameters of the *Z-R* relationship vary depending on many factors which include their dependence on the rainfall drop size distribution which varies in both space and time. Reflectivity (*Z*) and rainfall rate (*R*) can be estimated directly from the raindrop size distribution (DSD) measured using a disdrometer. These *Z* and *R* values can then be used to construct a *Z-R* relationship (Atlas, 1964; Battan, 1973; Krajewski and Smith, 2002; Russo *et al*., 2005). However, disdrometers are relatively expensive and complicated equipments to operate, and hence it is uncommon for more than one (or even any) of them to be operated in conjunction with a weather radar. The use of DSD to ascertain a Z-R relationship is not possible at all locations. In places where accurate measurements of the DSD are not possible, the option of using reflectivity data measured by the radar and the rainfall recorded in rain gauges within the radar coverage is generally used.

The methodology for developing an appropriate climatological Z-R relationship to be used for rainfall estimation in the upper Ping river basin is presented

in this section. However, the DSD data has not been measured in Thailand, calibration of the Z-R relationship will therefore be carried out using the radar reflectivity and rain gauge rainfall data located within the radar coverage.

4.1 Radar reflectivity and rain gauge rainfall data

4.1.1 Radar reflectivity data

Radar reflectivity data from the Omkoi radar located in Chiang Mai, Thailand were used for the analyses presented in this paper. The instantaneous 2.5-km PseudoCAPPI reflectivity data during June and October in 2003 and 2004 were used for an investigation of the Z-R relationship in the upper Ping river basin because of its accuracy and the suitability of the rainfall data within the same periods as the reflectivity data.

To avoid the bright band effect, the PseudoCAPPI reflectivity data lying within the radar range that causes the height of the upper beam below the freezing level was chosen for the analysis. Silverman and Sukarnjanaset (2000) recommended that the freezing levels in Chiangmai, Thailand are between approximately 4.9 and 5.5 km. The maximum radar range (calculated using the equation proposed by Doviak and Zrnic (1992) that gives the height of the upper beam below the freezing level of 4.9 km is about 160 km. The reflectivity and rain gauge data that lie within the range of 160 km from the radar were therefore used for the analysis. It was concluded that this 2.5-km PseudoCAPPI reflectivity data is free from the bright band effect.

4.1.2 Rain gauge rainfall data

Most of rainfall stations in and around the upper Ping river basin are daily read (non-automated) stations providing daily rainfall data. Consequently, the climatological Z-R relationship was determined based on a daily data basis. There are 50 rain gauges located in the basin and nearby area; but only 42 stations are

situated in the range of 160 km from the radar. The available data within the period between June and October in 2003 and 2004 collected at these 42 stations were therefore used for the calibration of the Z-R relationship. Locations of daily rainfall stations operated by the Royal Irrigation Department (RID) and the Thai Meteorological Department (TMD) within the Omkoi radar radius are shown in Figure 15.

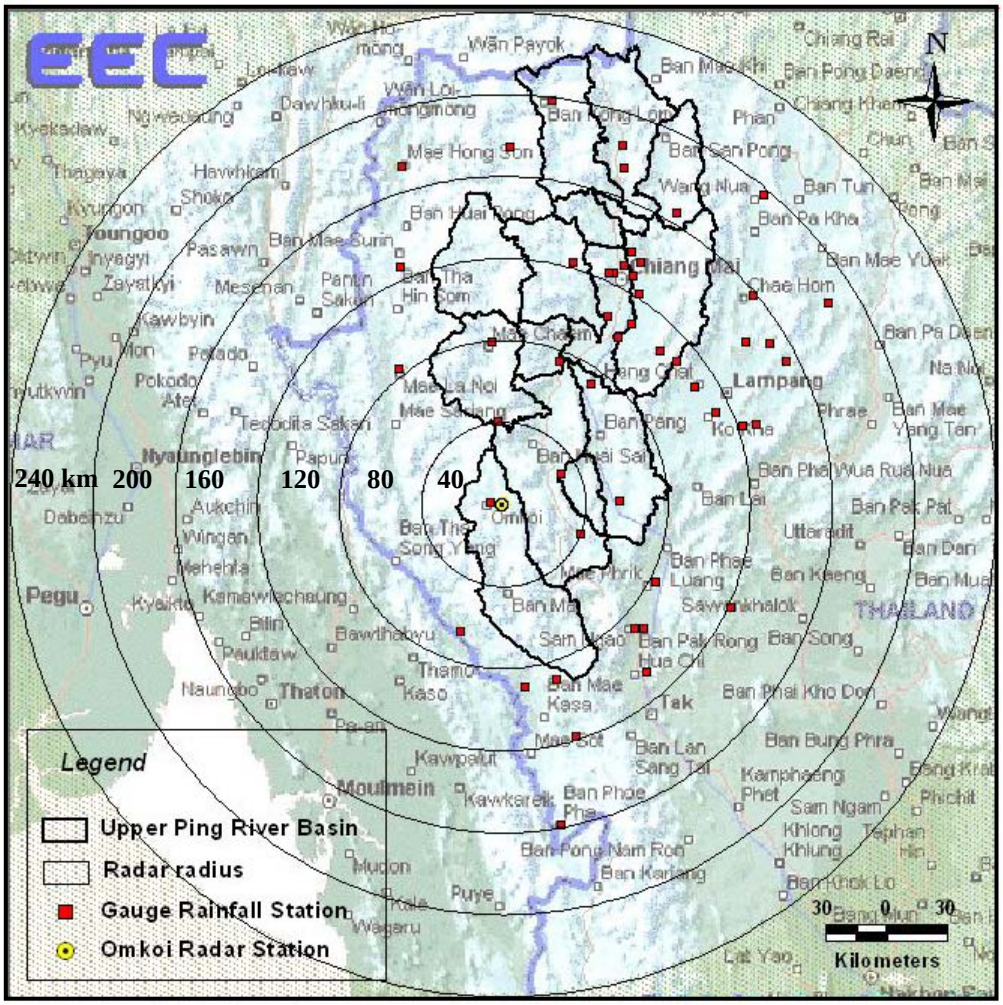

Figure 15 Locations of daily rainfall stations within the Omkoi radar radius.

4.2 Radar reflectivity measurement errors

Weather radar can commonly measure the signal that is backscattered by targets that include not only the raindrops, but also any objects in the atmosphere leading to some errors in reflectivity measurement. During the Z-R relationship calibration process, the following errors have to be removed to improve the accuracy of the reflectivity values.

1) Height sampling errors caused by the bright band that result in a range dependent bias (Fabry *et al*., 1994; Kitchen *et al*., 1994; Andrieu and Creutin, 1995; Fabry and Zawadzki, 1995; Vignal and Andrieu, 1999; Vignal and Krajewski, 2001).

The radar antennas transmit the signals at several elevation angles. The Earth's curvature and the refraction of the radar beam through the atmosphere cause the height of the beam to increase in a non-linear fashion with range (Doviak and Zrnic, 1992). Bright band contamination occurs where the radar beam intersects the melting layer. During the melting process in this layer, snowflakes and hail become coated with a film of water leading to the appearance of giant raindrops. The reflectivity in the bright band is generally 5-10 dB stronger than in the rain below or the snow directly above (Stewart *et al*., 1984; Klaassen, 1988; Fabry *et al*., 1992; Andrieu and Creutin, 1995; Williams and Ecklund, 1995). The PseudoCAPPI reflectivity data at the altitudes below the freezing levels is therefore selected for further analysis to avoid the bright band effect that could cause radar rainfall overestimation.

2) Ground clutter (Collier, 1996)

Ground clutter is non-precipitation radar echo occurring where the main or side lobes of radar beam encounter other targets such as mountains, ground, buildings, and trees. The backscattered radar signals from those objects result in strong persistent radar reflectivity leading to an overestimation of the radar rainfall.

Gabella and Perona (1998) have suggested that the ground clutter effect can be significantly reduced by increasing the elevation angle of the radar beam. However, ground clutter correction using this strategy may cause increases in height sampling error (Chumchean, 2004). Another strategy involves using a topography map of known ground clutter locations and discarding radar measurement in these areas (Gabella and Perona, 1998; Chumchean, 2004) is an easier alternative and was therefore applied in this study.

3) Radar beam attenuation (Hildebrand, 1978)

Attenuation of radar power (electromagnetic wave) transmitted into the atmosphere can be caused by atmospheric gases in the clear atmosphere and by precipitation. Water vapor and oxygen are the major atmospheric gases that need to be considered as absorbers (Battan, 1973). The basic principle of the attenuation by these gases was explained by Vleck (1974a, 1974b).

Attenuation caused by rain may vary strongly according to rainfall rate (Chumchean, 2004). As mentioned in the sub-section “Radar reflectivity data”, the sensitivity of the radar beam attenuation due to atmospheric gases and precipitation is higher at shorter wavelength. Since the reflectivity data used in this study is categorized as the S-band radar - with the longer wavelength compared to the X-band and C-band radars - the beam attenuation effect is not significant for this kind of radar and it was therefore not considered in this study.

As mentioned earlier regarding the properties of reflectivity values collected by the Omkoi radar, some of the errors comprising beam attenuation and bright band are not included. Moreover, the errors by ground clutter and beam blocking were already removed by using the correction strategy recommended by Gabella and Perona (1998) and Chumchean (2004) as mentioned above in the sub section on “Ground Clutter”.

To avoid the effect of noise and hail in the measured radar reflectivity, the reflectivity values that are less than 15 dBZ were assumed to represent a reflectivity of 0 mm^6/m^3, and the reflectivity values that are greater than 53 dBZ were assumed to be 53 dBZ.

To avoid the effect of noise and hail, the reflectivity values that that are less than 15 dBZ were assumed to represent a reflectivity of 0 mm^6/m^3, and the reflectivity values that are greater than 53 dBZ were assumed to be 53 dBZ (Chumchean *et al*., 2004, 2005, 2006a, 2006b). Once these errors are removed, the reflectivity values can be used for further analysis.

4.3 Radar rainfall accumulation

For a conventional practice in radar rainfall estimation, a Z-R relationship is used to convert the reflectivity into the rainfall intensity. Since most of rainfall stations in the upper Ping river basin are non-automatic, the daily rainfall data were used to calibrate the climatological Z-R relationship in this study. As the gauge rainfall data are in mm per day and the reflectivity data are in mm^6/m^3 per 6 minute interval, the measured instantaneous reflectivity needs to be converted as the radar rainfall rate in mm/hr using an original Z-R relationship (see details in the next item). However, the units of the radar rainfall rate and gauge rainfall need to be expressed as mm per day for calibrating the Z-R relationship. Radar rainfall rates are therefore converted into daily radar rainfall in mm unit using a radar rainfall accumulation algorithm, which is developed in this study and based on the method proposed by Fabry *et al*. (1994). In this method, the rainfall field is assumed to remain stationary in space and intensity during the sampling interval. The radar rainfall accumulation is therefore computed by multiplying the radar rainfall rates (mm/hr) by the reflectivity data interval and thereafter adding radar rainfall data for each interval to become the daily radar rainfall in mm.

4.4 Calibration of climatological Z-R relationship for the upper Ping river basin

As there was no calibrated Z-R relationship available for the Omkoi radar, the BRRAA has been using the relationship of $Z=200R^{1.6}$ proposed by Marshall and Palmer (1948) to convert the reflectivity data recorded from the Omkoi radar into radar rainfall. In this study, the most suitable climatological Z-R relationship of Omkoi radar for daily radar rainfall estimation in the upper Ping river basin was therefore calibrated using several events of the measured instantaneous reflectivity and daily rain gauge rainfall data during June and October in 2003 and 2004. Since rain gauge rainfall data in the upper Ping river basin are in the daily basis, the calibration techniques based on daily basis proposed by Seed *et al*. (2002) and Fields *et al*. (2004) were applied to attain the suitable Z-R relationship. Using this technique, the instantaneous reflectivity values are initially converted into radar rain rates using the standard Z-R relationship ($Z=200R^{1.6}$) and then accumulated into daily radar rainfall. The most suitable relationship will be calibrated by minimising the errors between the accumulated daily radar and rain gauge rainfall. The calibrated results carried out by Seed *et al*. (2002) and Fields *et al*. (2004) showed that the multiplicative term A based on daily basis by using the data from Sydney, Melbourne, Darwin, and Brisbane, Australia are within the ranges of 50 to 280. Details of the methodology in Z-R calibration used in this study can be summarized as follows.

1) Parameters A and b in the Z-R relationship were initially specified as 200 and 1.6, respectively, which are suitable for the stratiform rainfall (Marshall and Palmer, 1948), to be used to convert instantaneous reflectivity data into initial radar rain rates.

2) The instantaneous radar reflectivity data during 2003 and 2004 of all radar pixels that contain the rainfall stations were converted into rain rates using the initial Z-R relationship ($Z=200R^{1.6}$). The estimated radar rain rate for each time interval at a particular rainfall station was then accumulated into daily radar rainfall in mm using the radar rainfall accumulation algorithm as mentioned earlier.

3) Mean gauge rainfall and mean radar rainfall of each day were estimated using the equations (3) and (4), respectively.

$$\overline{G}_j = \frac{1}{N}\sum_{i=1}^{N} g_{ij} \tag{74}$$

where $\overline{G}_j$ is the mean gauge rainfall on day j; g_{ij} is gauge rainfall at station i and on day j; and N is the total rain gauge numbers.

$$\overline{R}_j = \frac{1}{N}\sum_{i=1}^{N} r_{ij} \tag{75}$$

where $\overline{R}_j$ is the mean radar rainfall on day j; and r_{ij} is radar rainfall accumulation computed using the relationship; $Z=200R^{1.6}$, for day j at the radar pixels that contain the N rainfall gauges.

4) Estimated mean radar rainfall and mean gauge rainfall were compared using four statistical measures recommended by Seed *et al*. (2002) as explained below.

Mean Error,

$$ME = \frac{1}{n}\sum_{i=1}^{N} (\overline{R}_i - \overline{G}_i) \tag{76}$$

Mean Absolute Error,

$$MAE = \frac{1}{n}\sum_{i=1}^{N} \left|\overline{R}_i - \overline{G}_i\right| \tag{77}$$

Root Mean Square Error,

$$RMSE = \sqrt{\frac{1}{n}\sum_{i=1}^{N}(\overline{R_i} - \overline{G_i})^2} \quad (78)$$

Bias,

$$B = \frac{\sum_{i=1}^{n}\overline{G_i}}{\sum_{i=1}^{n}\overline{R_i}} \quad (79)$$

where n is the number of mean daily rainfall records.

Several Z-R relationships would be specified by repeating the calculation of steps 1 to 4. Whichever relationship gives the minimum of the four statistical measures will be chosen as the most suitable relationship for the study.

Many researchers suggested that parameter b does not need to be varied as much as the parameter A (Seed *et al*., 1996; Steiner *et al*., 1999; Seed *et al*., 1002). Chumchean (2004) summarized the suitable values of A and b that are within the ranges of 31 to 500 and 1.1 to 1.9, respectively. To reduce the complicating in minimization process, the algorithm proposed by Fields *et al*. (2004) was applied to estimate the appropriate parameter that would give the minimum errors. The exponent b was fixed as 1.6 and only the multiplicative term A was adjusted to minimize the errors. The new parameter A can be determined from the following equation.

$$A_1 = \frac{A_0}{m^b} \quad (80)$$

where A_1 is the new multiplicative term A in Z-R relationship; A_0 is the initial parameter A; m is the gradient of the regression line between the predicted radar rainfall and the observed gauge rainfall obtained from an original Z-R relationship; and b is the exponent (1.6) in the Z-R relationship.

5. Effect of rain-gauge temporal resolution on the specification of a Z-R relationship

The approach followed to specify the *Z-R* relationship at a location involves collating ground rainfall data at the finest temporal resolution possible, accumulating the reflectivity to the same resolution, and ascertaining the parameters using a suitable optimization rationale. This relationship is generally used at a resolution finer than the ground measured rainfall, under the assumption that the relationship is independent of the temporal resolution it is developed at.

While past studies have calibrated the *Z-R* relationship at a range of temporal rainfall resolutions such as hourly, daily, weekly, monthly, seasonal, or even longer (Hitchfeld and Bordan, 1954; Smith *et al*., 1975; Wilson and Brandes, 1979; Klazura, 1981; Steiner *et al*., 1995), little has been done to investigate the sensitivity of the relationship to the temporal resolution that is used. While the assumption that a *Z-R* relationship developed using hourly rainfall data is not different to application at finer resolutions (such as 6 minute) may be appropriate, can the same assumption be made if the relationship is developed using only coarse daily observations instead? This is the main question we investigate in this analysis, proposing a rationale for scaling the *Z-R* relationship developed at one temporal resolution to another, thereby providing an option for specifying the *Z-R* relationship in locations where sub-daily rainfall measurements on a dense rainfall network are not available.

There are two objectives in this analysis. The first objective is to study the effect of using rain gauge data of different temporal resolutions for calibrating climatological Z-R relationships. Different climatological Z-R relationships were estimated using rainfall aggregated over 1 to 24 hours. Radar reflectivity data from the Kurnell, the Mt Stapylton, and the Pasicharoen radars located in Sydney, Brisbane, and Bangkok, respectively, and corresponding rain gauges data in the three cities, were used in the analysis. The second objective is to propose a generic scaling rule that can be used to estimate radar rainfall at fine temporal resolution for the cases

where only daily rain gauge rainfall data are available for use in the Z-R calibration. A simple scaling hypothesis was applied to construct a scaling transformation equation to ascertain the A parameters at finer temporal resolution.

The method for calibrating different climatological Z-R relationships using rainfall aggregated over 1 to 24 hours and the simple scaling hypothesis for the multiplicative term A are presented in this section.

5.1 Radar and rain gauge data

Radar reflectivity data from the Kurnell, the Mt Stapylton, and the Pasicharoen radars located in Sydney, Brisbane, and Bangkok, respectively, and corresponding rain gauges data representing large networks in the three cities, were used for the analyses. Locations of tipping-bucket rain gauges within the Kurnell, the Mt Stapylton, and the Pasicharoen radars radius are presented in Figure 11, 12, and 10, respectively. Three datasets of the 1.5-km CAPPI (Constant Altitude Plan Position Indicator) reflectivity data at the Kurnell radar and hourly rain gauge data obtained from a 227 rain gauge network during November 2000 – April 2001, August – December 2006, and January – May 2007 were used for the Z-R development for the Sydney area. The Mt Stapylton radar data used represented the November 2006– March 2007 period, with corresponding rain gauge data obtained from a 202 rain gauge network. For the Z-R calibration in Bangkok area, one dataset of the 0.5o PPI (Plan Position Indicator) reflectivity data at Pasicharoen radar and 15-minute rain gauge data obtained from a 61 rain gauge network during June 2005–October 2006 were used.

Rain gauge rainfall data used in this study were obtained from the networks of 227, 202, and 61 continuous tipping-bucket gauge stations located within 100 km from the Kurnell, the Mt Stapylton, and the Pasicharoen radars as illustrated in Figure 11, 12, and 10, respectively. The tipping bucket gauge can systematically under-record the true rainfall accumulation during the hour by the volume of water

required to initially wet the funnel plus the volume of water stored in the tipping bucket at the end of hour. However, the amount of rainfall required to wet the funnel of the gauge before it starts to drain into the tipping bucket is very small, and considered to be insignificant in this study. The rain gauges used in this study have a tipping bucket size of 1.0 mm and 0.5 mm. Because tipping bucket rain gauges record the time of the tips, they are subject to significant high quantization error at low rainfall intensity (Chumchean *et al*., 2003, 2004, 2006a, 2006b). Therefore, only the rainfall amounts that are greater than the volume of that gauge's tipping bucket were used in this analysis. It should be noted that quality control of these data has been performed by considering rainfall data from adjacent gauges and the plots of time series. If unusual rainfall data were found, these data were excluded from the analysis.

To avoid the effects of bright band and different observation altitude in radar reflectivity, the CAPPI reflectivity data at the altitude below the climatological freezing levels of the Sydney and Brisbane, and the PPI reflectivity data of the Pasicharoen radar at the lowest elevation angle within the radar range that give the height of radar beam below the freezing level were used in the analyses.

The climatological freezing levels for Sydney, Brisbane, and Bangkok is about 2.5 km, 3.0 km, and 4.7 km, respectively (Chumchean *et al*., 2003, 2004). In this study, the 1.5-km CAPPI reflectivity data of both radars in Australia and 0.5^{o} PPI reflectivity data of Bangkok and only the reflectivity and rain gauge data that lie within 100 km from the radars were used. It is to be noted that the height of the base scan beam center at this range is about 1.8 km above the ground which is also below the freezing levels for the three cities and it can be considered to be not overly different from the 1.5 km CAPPI height. Therefore, we consider that the reflectivity data used in this study are free from the effects of bright band and different observation altitude.

To avoid the effect of noise and hail in the measured radar reflectivity, the reflectivity values that are less than 15 dBZ were assumed to represent a reflectivity

of 0 mm^6/m^3, and the reflectivity values that are greater than 53 dBZ were assumed to be 53 dBZ. . Additionally, the errors due to effect of ground clutter were also removed from the reflectivity data by finding the clutter locations from the map and discarding the radar measurements in these areas.

5.2 Calibration of the Climatological Z-R relationship

The *Z-R* conversion error is an important source of error in radar rainfall estimates. The following empirical power law relationship is used to estimate radar rainfall using measured reflectivity (Battan, 1973; Rinehart, 1991; Doviak and Zrinc, 1992; Collier, 1996):

$$Z = AR^b \tag{81}$$

Here, *A* and *b* are the radar parameters to be estimated which depend on the DSDs that have been sampled, assuming that the terminal velocity of the raindrops is a function of their diameter, and that they are falling at terminal velocity through still air (Chumchean *et al*., 2008), *Z* is radar reflectivity expressed in $mm^6\ m^{-3}$, and R is the rainfall rate in mm hr^{-1}. While the parameter *A* is observed to change significantly from one region to another depending on the nature of the rainfall events that occur, many researchers have suggested that the exponent b does not change as much (Seed *et al*., 1996; Steiner *et al*., 1999; Seed *et al*., 2002; Chumchean *et al*., 2003). Typical values of the multiplicative term A may range from 100 to 500 (Battan, 1973), whereas the exponent b varies from 1 to 3 (Smith and Krajewski, 1993), with typical values between 1.2 and 1.8 (Battan, 1973; Ulbrich, 1983). Doelling *et al*. (1998); Steiner and Smith (2000); and Hagen and Yuter (2003) investigated an appropriate value of the *b* parameter using several years of reflectivity data measured by a disdrometer. They found that a value of 1.5 was suitable to represent the *b* parameter in the *Z-R* relation. Seed *et al*. (2002) illustrate that the root-mean-square error (RMSE) of radar-rainfall estimates are quite insensitive to the value of b over the range (b = 1.6, 1.5, and 1.4). Based on the above arguments and

the result of a climatological calibration using the datasets analysed in this study, the *b* parameter of the *Z*-*R* relation was fixed at 1.6 while the *A* parameter was ascertained using the procedure described next.

To study the effect of using rain gauge data of different temporal resolutions on *Z*-*R* relationships, different *Z*-*R* relationships were estimated using rainfall aggregated over 1 to 24 hours. The logic used was as follows:

1) Convert instantaneous radar reflectivity into an initial radar rainfall intensity using the relationship $Z=200R^{1.6}$ (Marshall and Palmer, 1948). Note our earlier comment on the relative insensitivity of results to changes in the *b* exponent as our rationale for keeping it fixed equal to 1.6 in our study.

2) Accumulate the initial instantaneous radar rainfall into 1-hour to 24-hour rainfall resolutions using the accumulation algorithm proposed by Fabry *et al*. (1994). In this method, the rainfall field is assumed to move at constant velocity and to vary linearly in intensity during the sampling interval. The storm velocity was first computed for each time interval and then used to simulate a 1 min sampling rate by advecting the field observed at the start of the interval toward the field observed at the end of the interval. Represent the accumulated rainfall now via a variable *A* parameter, denoted A_a, where the subscript denoted the time resolution the rainfall is aggregated over. The resulting radar rainfall (which is a function of A_a) is denoted as $R_{i,t,a}$ where the subscripts denote the gauge, time-step and temporal resolution respectively.

3) Ascertain the rain gauge rainfall at station i for time-step t for temporal resolution a (denoted $G_{i,t,a}$) by accumulating it from a 1-hour to the other durations (1 to 24-hours) considered.

4) Estimate the optimal value of A_a for each time resolution a considered by minimizing the Mean Absolute Error (MAE) between the gauge and radar rainfall estimates. The Mean Absolute Error is expressed as:

$$MAE_a = \frac{1}{N_{t,a} N_G} \sum_{t=1}^{N_{t,a}} \sum_{i=1}^{N_G} \left| R_{i,t,a} - G_{i,t,a} \right| \tag{82}$$

where $R_{i,t,a}$ is the radar rainfall accumulation at the pixel corresponding to the i^{th} rain gauge for hour t for a temporal resolution a, $G_{i,t,a}$ is the corresponding gauge rainfall for hour t, N_G is the number of rain gauges, and $N_{t,a}$ is the number of time periods for each time resolution a.

It should be pointed out that this study used the Mean Square Error (MSE) and the Mean Absolute Error as two separate error criteria. While the results from both criteria were similar, the MSE exhibited greater instability for results for larger time resolutions than the MAE, possibly because of fewer gauge-radar pairs being available, and the tendency of the measure to magnify the larger differences. As a result, the results presented in the next main section "Results and Discussion" are based on the MAE error criterion alone.

5.3 Climatological Z-R relations for variable temporal resolutions

The five datasets considered in this study were used to develop Z-R relationships by following the calibration procedure outlined in the sub-section 5.2. Numbers of radar-gauge pairs used for Z-R calibration for each temporal resolution in each dataset are also presented in the Table 5. As mentioned before, the results presented here correspond to the use of the Mean Absolute Error as the objective function to be minimized. The A parameters of Z-R relationships derived by using different temporal rainfall resolutions for the five datasets are illustrated in the Figure 16. Note that, datasets Sydney (1), Sydney (2) and Sydney (3) represent data for

periods November 2000 – April 2001, August – December 2006, and January – May 2007, respectively. The results in Figure 16 illustrate clearly that the highest value of parameter A is obtained when the temporal resolution is one hour, with the parameter value decreases as the aggregation period increases. The difference between the calibrated A parameters for Sydney, Brisbane, and Bangkok are large, while there are only small differences between Sydney (1) to Sydney (3). This is to be expected given the differences in the dominant storm types that could be expected between the three cities.

From the above results, it can be seen that the multiplicative term A of the Z-R relationship varies as a function of the temporal resolution of the rainfall used in the calibration. Derivation of the A parameter using coarse (say daily) rainfall and subsequently applying it to estimate fine resolution (say hourly or sub-hourly) rainfall can lead to significant biases in the resulting estimates. For situations where only daily rain gauge rainfall data is available for use in the Z-R calibration, a transformation function for converting the A parameters to other resolutions is needed.

Table 5 Number of radar-gauge pairs used for Z-R calibration at each temporal resolution.

a) Sydney datasets

Temporal resolution (hour)	Sydney (1)			Sydney (2)			Sydney (3)		
	0-100 km	0-50 km	50-100 km	0-100 km	0-50 km	50-100 km	0-100 km	0-50 km	50-100 km
1	31,405	22,527	8,878	9,664	7,857	1,807	17,294	13,299	3,995
2	20,298	14,676	5,622	6,514	5,281	1,233	11,891	9,151	2,740
3	15,649	11,384	4,265	5,195	4,175	1,020	9,319	7,134	2,185
4	13,143	9,567	3,576	4,385	3,565	820	7,815	6,003	1,812
5	11,165	8,119	3,046	3,862	3,119	743	7,057	5,423	1,634
6	9,871	7,200	2,671	3,582	2,885	697	6,290	4,806	1,484
7	8,959	6,576	2,383	3,136	2,522	614	5,773	4,427	1,346
8	8,622	6,305	2,317	2,930	2,310	620	5,253	4,033	1,220
9	7,454	5,428	2,026	2,878	2,284	594	4,903	3,752	1,151
10	6,890	4,965	1,925	2,544	2,001	543	4,771	3,628	1,143
11	6,414	4,612	1,802	2,300	1,811	489	4,490	3,408	1,082
12	6,009	4,401	1,608	2,357	1,884	473	4,061	3,072	989
13	5,760	4,184	1,576	2,146	1,724	422	4,116	3,119	997
14	5,550	4,087	1,463	2,130	1,683	447	3,825	2,881	944
15	5,145	3,746	1,399	1,872	1,468	404	3,701	2,757	944
16	5,135	3,759	1,376	1,806	1,422	384	3,476	2,634	842
17	4,741	3,474	1,267	1,793	1,403	390	3,516	2,644	872
18	4,563	3,351	1,212	1,892	1,497	395	3,189	2,388	801
19	3,987	2,901	1,086	1,802	1,404	398	3,289	2,486	803
20	3,883	2,792	1,091	1,676	1,311	365	3,007	2,238	769
21	3,749	2,722	1,027	1,579	1,227	352	3,196	2,402	794
22	3,879	2,827	1,052	1,519	1,158	361	2,952	2,181	771
23	3,639	2,655	984	1,548	1,197	351	2,695	1,989	706
24	3,424	2,479	945	1,438	1,112	326	2,653	1,983	670

b) Brisbane and Bangkok datasets

Temporal resolution (hour)	Brisbane			Bangkok		
	0-100 km	0-50 km	50-100 km	0-50 km	0-15 km	15-50 km
1	14,949	8,696	6,253	868	563	305
2	9,849	5,747	4,102	703	467	236
3	7,652	4,485	3,167	645	418	227
4	6,628	3,880	2,748	567	371	196
5	5,908	3,489	2,419	536	345	191
6	5,222	3,033	2,189	548	354	194
7	4,902	2,878	2,024	503	325	178
8	4,514	2,636	1,878	473	298	175
9	3,914	2,265	1,649	506	336	170
10	3,680	2,142	1,538	471	301	170
11	3,864	2,259	1,605	493	323	170
12	3,875	2,239	1,636	471	306	165
13	3,229	1,880	1,349	458	293	165
14	3,308	1,926	1,382	465	306	159
15	3,122	1,805	1,317	422	278	144
16	3,067	1,765	1,302	414	272	142
17	2,892	1,718	1,174	493	312	181
18	2,758	1,616	1,142	490	315	175
19	2,712	1,570	1,142	554	344	210
20	2,477	1,420	1,057	450	288	162
21	2,566	1,479	1,087	526	326	200
22	2,730	1,558	1,172	510	325	185
23	2,555	1,477	1,078	476	323	153
24	2,378	1,376	1,002	465	316	149

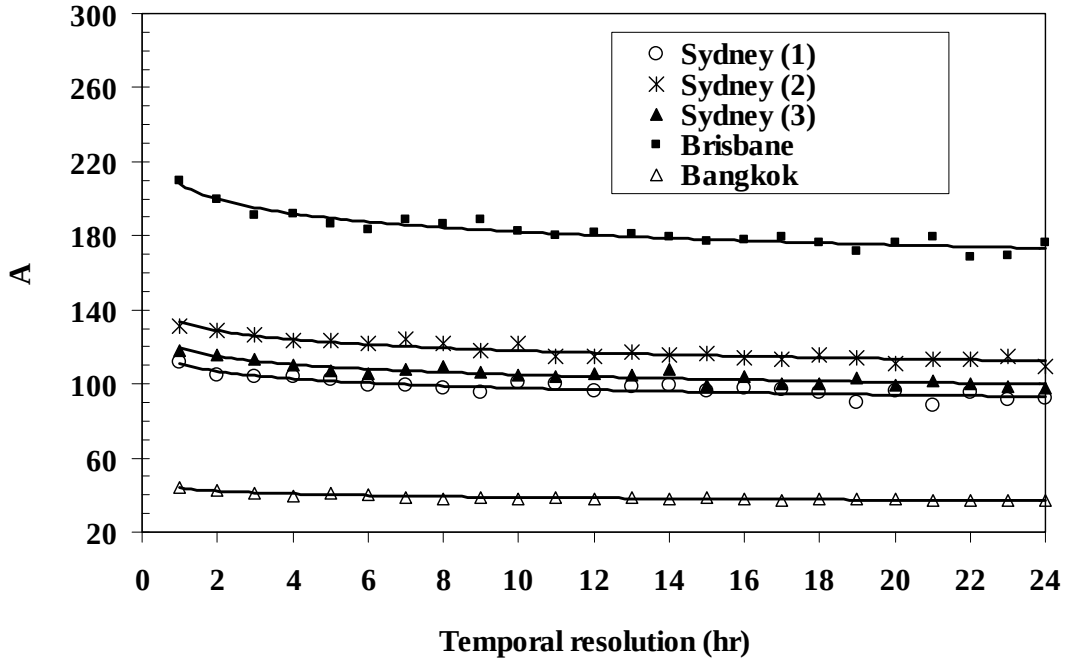

Figure 16 Coefficient A of the *Z-R* relationship, derived using a fixed exponent b equal to 1.6, for the Kurnell, the Mt Stapylton, and the Pasicharoen radars, as a function of varying temporal rainfall resolutions.

5.3 Simple Scaling Hypothesis for the multiplicative term A

As a means of explaining the variation of A with temporal resolution in Figure 16, we hypothesis here that A exhibits simple scaling behaviour in time (Mandelbrot, 1982; Chumchean *et al*., 2004). Such a hypothesis has been used by others to describe rainfall extremes at fine temporal resolutions (Menabde *et al*., 1999), to develop cascade models of rainfall disaggregation in time (Sivakumar and Sharma, 2007) and to explain bias in radar rainfall estimates in space (as a function of distance from the radar) (Chumchean *et al*., 2004). The simple scaling hypothesis (as defined by Gupta and Waymire (1990) and used by Chumchean *et al*. (2004) in a spatial scaling context) can be expressed as:

$$A_t \overset{dist}{=} (t/T)^{-\eta} A_T \tag{83}$$

where $\overset{dist}{=}$ represents the equality of the probability distribution for the multiplicative factor *A*, *t/T* is a scale factor, *t* (hr) is the temporal resolution at which the rainfall needs to be estimated, *T* (hr) is the reference temporal resolution of the radar rainfall, η is a scaling exponent that needs to be ascertained, and A_T and A_t represent the parameter *A* at temporal resolutions *T* and *t* respectively. The distributional equality represented in (3) implies that the quantiles and the moments of any order of the calibrated multiplicative term *A* are scale-invariant. Raising both sides of Eq. (3) with different power q, the relationship between the q^{th} moment can be written as:

$$\left\langle A_t^q \right\rangle = (t/T)^{-\eta q} \left\langle A_T^q \right\rangle \tag{84}$$

The brackets denote the expected value of the q'th order moment for the multiplicative term A. Estimation of the scaling exponent η that best describes the distributional equality expressed in equations (83) and (84) now proceeds by fitting the relationship in (4) across a range of moment orders q.

Moment orders q equal to 0.5, 1.0, 1.5, 2.0, 2.5, 3.0, 3.5, 4.0, 4.5, 5.0, 5.5, and 6.0, were used to ascertain the optimal value of η for the five rainfall datasets used. A scaling transformation equation for calculating A parameters at finer temporal resolution in a situation where only daily rain gauge rainfall data is available can therefore be written as:

$$A_t = (t/24)^{-\eta} A_{24} \tag{85}$$

The result of an optimal value of η was presented in the next main section "Results and Discussion".

6. Improvement in runoff estimation accuracy using radar

Measured rainfall is one of the most significant input data in applying the hydrological models for runoff and flood estimations. Unfortunately, the distribution of rainfall usually varies significantly in both space and time (Seed and Austin, 1990); therefore, the limited number of rainfall stations in the catchment can have a major impact on the accuracy of runoff and flood estimations (Wilson *et al*., 1979; Bevan and Hornberger, 1982; Hamlin, 1983). The accurate estimation of the spatial distribution of rainfall therefore requires a very dense rainfall network, which involves high installation and operational costs (Goovaerts, 2000). Radar rainfalls estimated from the weather radar are the alternative rainfall products which are spatially distributed over the catchment using the available rainfall network. The weather radar, which is a widely used basis for rainfall estimation at fine spatial and temporal resolutions (Collinge and Kirby, 1987; Sun *et al*., 2000; Uijlenhoet, 2001; Vieux, 2003), can better capture the spatial variation of rainfall fields than rain gauge rainfall data in areas where rain gauges are distributed sparsely (Yang *et al*., 2004; Segond *et al*., 2007). There are number of papers shown the improvements in flood estimation and flood forecasting using radar rainfall as the input data to hydrological models (Wyss *et al*., 1990; Pessoa *et al*., 1993; Borga *et al*., 2000; Sun *et al*., 2000). Spatial rainfall estimation over the upper Ping river basin using the weather radar was therefore investigated in this study and then was used as the input data for the selected hydrologic model to see whether there is any improvement to the accuracy in runoff estimations.

Use of a Z-R relationship ($Z=AR^b$) - calibrated using radar reflectivity data (Z) and corresponding rain gauge rainfall data (R) located within the radar coverage - is a traditionally technique for radar rainfall estimation. The gauge rainfall data at the finest temporal resolution possible is collected, and the reflectivity data is then accumulated to the same resolution of rain gauge to ascertain the Z-R parameters using a suitable optimization rationale. This calibrated relationship is generally used

at a resolution finer than the ground measured rainfall, under the assumption that the relationship is independent of the temporal resolution it is developed at. However, there might be a significant error on radar rainfall estimates caused by applying the Z-R relationship developed using rain gauge data at coarse temporal resolutions (say daily) to estimate radar rainfall at finer temporal resolution. To reduce this error, the transformation equation proposed in this thesis as presented the methodology in earlier section was used in this analysis.

In this study, radar rainfalls at hourly and daily temporal resolution were estimated to be used as different input data to the selected hydrological model (URBS model). Since only daily gauge rainfall data is sufficiently available in the upper Ping river basin, a calibration process of the Z-R relationship as presented the methodology in section 4 was therefore undertaken based on the daily basis. This calibrated daily Z-R relationship and mean field bias technique were applied here to estimate the daily radar rainfall over the study area. For hourly radar rainfall estimation, there are two estimation approaches proposed in this study. Firstly, the daily Z-R relationship was directly used to estimate radar rainfall at hourly time scale. Secondly, the scaling equation was applied to the daily Z-R relationship for hourly rainfall estimation. The daily gauge rainfall, daily radar rainfall, and two types of hourly radar rainfall were later used as different input data to the hydrological model at particular runoff stations in the study area. Results of flow hydrograph estimated by these four types of rainfall data were compared for their accuracy and effectiveness. Capabilities and advantages of using rain gauge rainfall and radar rainfall as the input data to the hydrological model for runoff estimation were finally defined. The data collection and methodology for estimating the four types of rainfall data are described as follows.

6.1 Data collection

6.1.1 Radar reflectivity data

Radar reflectivity data recorded from the Omkoi radar, which is own and operated by the Bureau of Royal Rainmaking and Agricultural Aviation (BRRAA), was used for daily and hourly radar rainfall estimation in some sub-catchments of the upper Ping river basin.

Because of the accuracy of the recorded reflectivity data and their suitability to the gauge rainfall and runoff data within the same periods, three datasets in rainy season (May – October) of the 2.5-km pseudoCAPPI reflectivity data at the Omkoi radar during June – October 2003, May – September 2004, and May – July 2005 were therefore used for the analysis.

Since the reflectivity data used in this study was ascertained from the S-band radar, beam attenuation effect was therefore considered to be insignificant (Hitschfeld and Bordan, 1954; Delrieu *et al*., 2000).

To avoid the effects of bright band and different observation altitude in radar reflectivity, the pseudoCAPPI reflectivity data lying within the radar range that causes the height of the upper beam to be below the climatological freezing level of Chaing Mai was therefore used in the analysis. The climatological freezing level for Chiang Mai is about 4.9 km (Silverman and Sukarnjanaset, 2000). The maximum radar range (calculated using the equation proposed by Doviak and Zrnic (1992)) that gives the height of the upper beam below the freezing level of 4.9 km is about 160 km. The reflectivity that lies within a range of 160 km from the radar was therefore used for the analysis. Consequently, we consider that the reflectivity data used in this study are free from the effects of bright band and different observation altitude.

To avoid the effect of noise and hail in the measured radar reflectivity, the reflectivity values that are less than 15 dBZ were assumed to represent a reflectivity of 0 mm^6/m^3, and the reflectivity values that are greater than 53 dBZ were assumed to be 53 dBZ. Additionally, the errors due to effect of ground clutter were also removed from the reflectivity data by finding the clutter locations from the map and discarding the radar measurements in these areas.

6.1.2 Rain gauge rainfall data

There are 35 rain gauge rainfall stations located within 160 km range from the Omkoi radar. Thirty two stations are non-automatic stations providing daily rainfall data, while only 3 rain gauges are automatic station. Since most of gauges in and around the project are daily rain gauges, three datasets of rain gauge rainfall data obtained from the networks of 35 gauge stations at the same period of the reflectivity data were therefore used in this study. These rain gauges are owned and operated by the Royal Irrigation Department (RID) and the Thai Meteorological Department (TMD). The quality control of these rain gauge rainfall data has also been performed by considering rainfall data from adjacent gauges and the plots of time series. If unusual rainfall data were found, these data were excluded from the analysis. Locations of rain gauge rainfall used in this analysis are presented in Figure 17.

6.1.3 Runoff data

As the reflectivity data lying within a range of 160 km from the Omkoi radar were used in this study, runoff data obtained from the 6 stations namely P.21, P.71, P.14, P.24A, P.77, and P.73, which have sufficient data available and located in the upper Ping river basin within that range, were therefore used for the analysis. These runoff stations, which have the catchment areas of 510, 1,727, 3,853, 454, 544, and 2,242 km^2, respectively, are owned and operated by the RID.

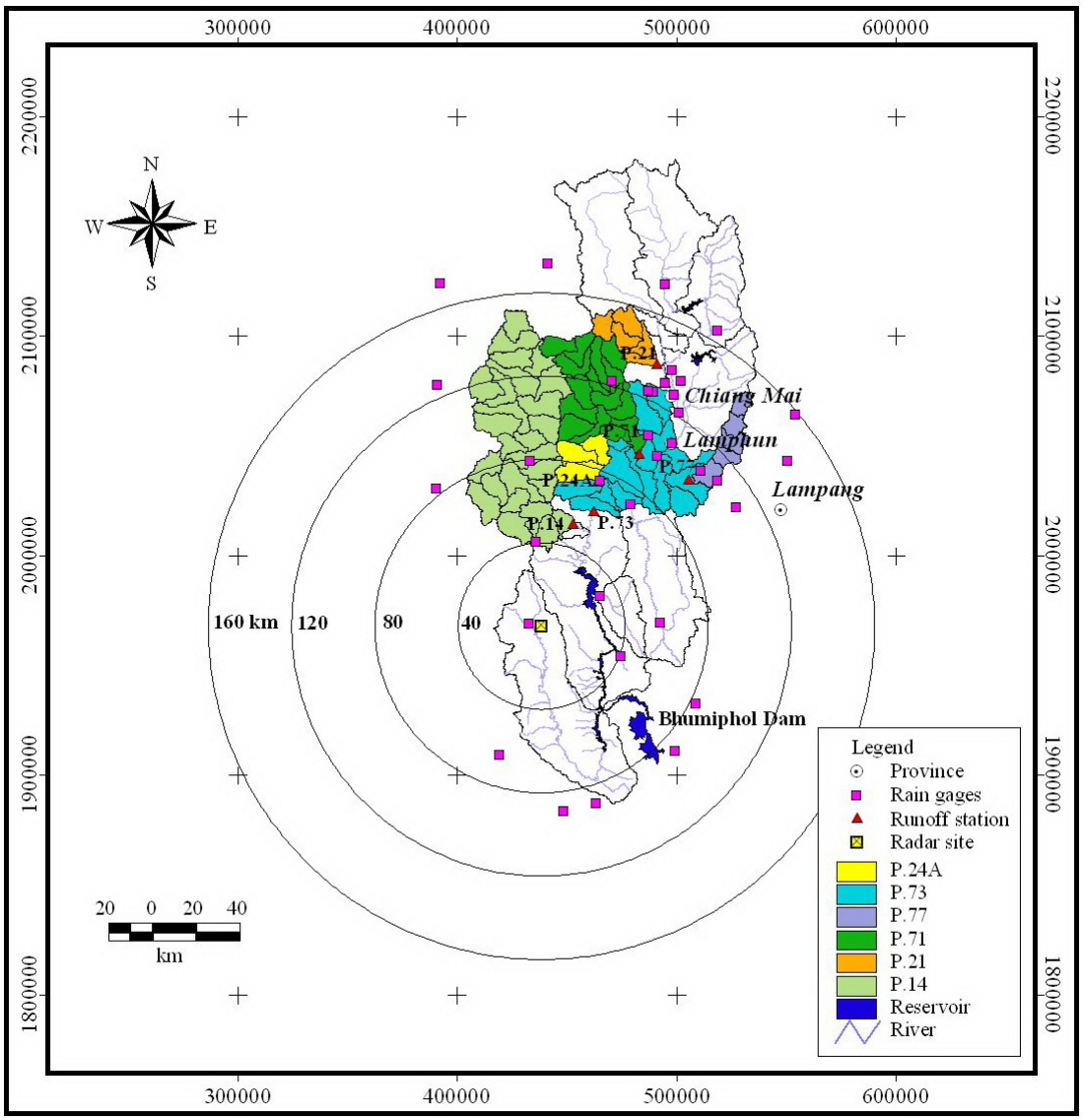

Figure 17 Locations of rainfall and runoff stations in the upper Ping river basin.

Three datasets of hourly flow hydrograph data for these 6 runoff stations at the same period of reflectivity and rain gauge rainfall data were used in this study. Note that, the P.73 actually is the most downstream runoff station of the upper Ping river basin with the catchment area of approximately 12,910 km^2. However, the catchment area of the P.73 used in this study is the area (2,242 km^2) which is excluded sub-catchment area of main tributaries of the Ping river (see Figure 17). For model calibration and verification at this station, only rainfall on this incremental catchment was transformed to be runoff using the URBS model, while the runoff data

from the main tributaries was obtained from the runoff stations located at their downstream.

6.2 Catchment rainfall estimation

There are four types of catchment rainfall that have been calculated to be used as the input data for the URBS model for runoff estimation at the six runoff stations in the upper Ping river basin during three period of the datasets. These comprise the daily gauge rainfall, the daily radar rainfall, and the hourly radar rainfall with and without scaling logic. Catchment rainfall estimation methods for different rainfall types are explained as follows.

6.2.1 Daily rain gauge rainfall estimation

Rainfall data measured from rain gauges installed on the ground has generally been used as the input data to a hydrological model for runoff and flood estimation. In this study, the catchment rainfalls for the sub-catchments of each runoff station were calculated using the Thiessen polygon technique - which is a spatial interpolation technique and usually applied in the area with non-uniform distribution of the rain gauges (Chow *et al*., 1988). Thirty five daily rain gauges located in and around the upper Ping river basin were used to construct the Thiessen polygons. Daily catchment rainfalls for each sub-catchment were calculated by the multiplication between the daily gauge rainfalls and its corresponding weighting factor estimated from the generated polygons.

6.2.2 Daily radar rainfall estimation

Typically, a Z-R relationship is used to estimate radar rainfall using measured reflectivity data (Battan, 1973; Rinehart, 1991; Doviak and Zrinc, 1992; Collier, 1996). Various forms of *Z-R* relations have been suggested in the literatures (Marshall and Palmer, 1948; Joss and Waldvogel, 1970; Battan, 1973).

However, these relationships cannot be directly applied in all regions, a climatological Z-R relationship for daily radar rainfall estimation in the upper Ping river basin was therefore developed in this thesis as presented the methodology in section 4. This proposed equation was used to convert three data sets of instantaneous radar reflectivity data recorded at the Omkoi radar at the pixel located in the target area into the instantaneous radar rainfall intensity. The instantaneous radar rainfalls were thereafter accumulated into 24-hour rainfall resolution using the accumulation algorithm proposed by Fabry *et al*. (1994).

Although the errors caused by reflectivity measurement process were corrected and the Z-R relationship suitable for the study area was used in radar rainfall estimation, there remain errors in the radar rainfall estimates (Chumchean *et al*., 2006). These residual errors are due to the *A* and *b* parameters of the *Z-R* relationship vary depending on many factors which include the rainfall drop size distribution which varies in both space and time. Additionally, there are some differences between the two different types of rainfall measuring sensors. That is a rain gauge records rainfall at a point on the ground while radar measures instantaneous rainfall at some height (1-3 km) above the ground. To improve the accuracy on radar rainfall estimation, these residual errors needs to be eliminated. A mean field bias correction technique (Wilson, 1970; Battan, 1973; Brandes, 1975; Collinge, 1991; Seo and Breidenbach, 2002; Chumchean *et al*., 2006) was used to eliminate these errors in this study. An adjustment factor -computed as the ratio of the mean-areal gauge rainfall to the corresponding radar rainfall (Anagnostou *et al*., 1998; Borga *et al*., 2000) - was first assessed, and the radar rainfall estimated by the proposed daily Z-R relationship for the upper Ping river basin was thereafter adjusted by multiplying the adjustment factor to the initial radar rainfall

There are many mean field bias techniques, and each technique can be used to correct the errors caused by temporal and/or spatial variability. However, rain gauge networks located in the target basin are too sparse (1 gauges/600 km^2) to represent spatial rainfall distribution, estimation of mean field bias adjustment factor were therefore consider to be uniform in space but vary in time. In this study, the

mean field bias was computed at the daily time scale using the recorded daily gauge rainfall data and initial daily radar rainfall (estimated using the proposed Z-R relationship for the study area) during the three dataset of 2003, 2004, and 2005. An adjustment factor for day t (B_t) was calculated as:

$$B_t = \frac{\text{Mean areal gauge rainfall}}{\text{Mean areal radar rainfall}} \tag{86}$$

Mean areal gauge rainfall was calculated using the Thiessen polygon technique. All 35 rain gauges in the upper Ping river basin located within the range of 160 km from the Omkoi radar were used in the analysis. Mean areal radar rainfall was computed by averaging the initial daily radar rainfall at all radar pixels located within the 160 km range. Mean areal gauge and radar rainfall can be written as:

$$\text{Mean areal gage rainfall} = \frac{1}{A}\sum_{i=1}^{N_{G,t}} A_{i,t} G_{i,t} \tag{87}$$

where A is the catchment area of the upper Ping river basin located within 160 km range from the Omkoi radar, $A_{i,t}$ is the sub-area of Thiessen polygon corresponding to the i^{th} rain gauge for day t, $G_{i,t}$ is the corresponding daily gauge rainfall (mm) for day t, and $N_{G,t}$ is the number of sub-area of the polygon over the basin for day t.

$$\text{Mean areal radar rainfall} = \frac{1}{N_P}\sum_{i=1}^{N_P} R_{i,t} \tag{88}$$

where, R_i is the initial daily radar rainfall (mm) estimated using the proposed Z-R relationship for Omkoi radar at the i^{th} pixel for day t, N_P is the number of radar pixels in the upper Ping river basin situated within the 160 km range.

It should be noted that the daily rainfall at the current day is available at the end of the day, the mean field bias for day *t* will therefore be computed at the end of the day *t*. However, radar can estimate rainfall since the commencement of the day *t*. The mean filed bias for the previous day (*t-1*) was therefore used for radar rainfall correction at day *t*, under the assumption that the mean field bias will be the same between yesterday and today.

The initial daily radar rainfall for day *t* at all pixels located in the 6 gauged catchments was multiplied by B_{t-1} to obtain adjusted daily radar rainfall. For sub-catchment rainfall estimation in each gauged catchment, the corrected daily radar rainfall at all pixels located in the sub-catchment was averaged using the simple arithmetic averaging method to ascertain the total daily rainfall input for the URBS model.

6.2.3 Hourly radar rainfall estimation

Because of the limitation in obtaining continuous rain gauge rainfall data for the upper Ping river basin, the mean filed bias correction was undertaken based on daily basis. The daily radar rainfall adjusted by the mean field bias values was also applied for hourly radar rainfall estimation in this study. When the daily radar rainfall were adjusted by the mean field bias, as a result, the original 24-hour *A* parameter (obtained using the reflectivity data from the Omkoi radar and corresponding rain gauge rainfall data) was changed with day depending upon the mean field bias used for correcting daily radar rainfall. The update 24-hour *A* parameter for day *t* $(A_{24new})_t$ was therefore computed using the following equation.

$$(A_{24new})_t = \frac{A_{old}}{B_{t-1}^b} \tag{89}$$

where A_{old} is the 24-hour A parameter used in daily rainfall estimation before applying mean field bias correction (see results of climatological Z-R

relationship for the upper Ping river basin), B_{t-1} is the adjustment factor for day *t-1*, and *b* is the radar parameter which was fixed as 1.6.

For hourly radar rainfall estimation at day *t* covering the project area, three datasets of the recorded instantaneous radar reflectivity at the pixel located in the target area were converted into radar rainfall using the updated 24-hour Z-R relationship that A parameter was calculated using Equation (89), and b parameter was fixed at 1.6. The calculated instantaneous radar rainfall was thereafter accumulated into 1-hour rainfall resolution using the accumulation algorithm proposed by Fabry *et al*. (1994). For sub-catchment rainfall estimation in each gauged catchment, the estimated hourly radar rainfall at all pixels located in the sub-catchment was averaged using the simple arithmetic averaging method to ascertain the hourly rainfall input for the URBS model.

6.2.4 Hourly radar rainfall estimation using the scaling transformation equation

Since the A parameter of the Z-R relationship tends to decrease with a decrease in the rainfall temporal resolution used to develop the relationship, application of the 24-hour Z-R relationship to estimate radar rainfall at finer temporal resolution may give significant error on rainfall estimates. For situations where only daily rain gauge rainfall data is available for Z-R calibration, a climatological scaling transformation equation for converting the A parameter to finer resolutions was proposed as presented Equation (85). Note that, the results of scaling exponent (η) was later presented in the "results and discussion" at the sub-section "Effect of rain-gauge temporal resolution on the specification of a Z-R relationship". Consequently, that scaling transformation equation was also used for hourly rainfall estimation in this study.

From the Equation (85), there are two parameters (*t* and A_{24}) needed for A_t estimation. The *t* was substituted as 1 hour. Since the mean field bias correction based on daily time scale was applied in this study, the original A_{24} was

therefore changed with day depending upon the mean field bias used for correcting daily radar rainfall as presented in Equation (89). The 1-hour A parameter for day *t* $(A_1)_t$ was therefore derived using the following equation.

$$(A_1)_t = (\frac{1}{24})^{-\eta}(A_{24new})_t \quad (90)$$

For hourly radar rainfall estimation at day *t* covering the project area, the calculated $(A_1)_t$ parameter and the b parameter fixed at 1.6 will be applied to the three datasets of the recorded instantaneous radar reflectivity for the pixel located in the target area.

6.3 Model calibration and verification

Model calibration and verification processes were carried out to define the most suitable set of control parameters of the URBS model for each rainfall dataset and each runoff station. For each runoff station, the 4 estimated catchment rainfall fields for the first dataset (June – October 2003) and the last 2 datasets (May – September 2004, and May – July 2005) were separately used as the input data to the URBS model for model calibration and verification, respectively. The individual set of model parameters for each rainfall input type that produced the goodness of fit between the hourly observed and the simulated flow hydrographs for both in calibration and verification processes were identified as the most suitable set.

Four statistical measures: the correlation coefficient (r), the efficiency index (EI) or Nash-Sutcliffe criterion (Nash and Sutcliffe, 1970; Krause *et al*., 2005), overall root mean square error (RMSE), and average RMSE of peak flow events ($RMSE_{peak}$) (Madsen, 2000) were considered to provide a general guide in the assessment of the overall performance of the observed and calculated hydrographs. Equations used to calculate these statistical measures are expressed in Table 6.

Table 6 Statistical measures used to identify the goodness of fit of flood hydrographs.

Statistical Measures	Equations
Correlation Coefficient (r)	$r = \frac{\sum_{i=1}^{N}\left(Q_{m,i} - \overline{Q}_m\right)\times\left(Q_{c,i} - \overline{Q}_c\right)}{\sqrt{\left[\sum_{i=1}^{N}\left(Q_{m,i} - \overline{Q}_m\right)^2 \times \sum_{i=1}^{N}\left(Q_{c,i} - \overline{Q}_c\right)^2\right]}}$
Efficiency Index (EI)	$EI = 1 - \frac{\sum_{i=1}^{N}\left(Q_{m,i} - Q_{c,i}\right)^2}{\sum_{i=1}^{N}\left(Q_{m,i} - \overline{Q}_m\right)^2} \times 100\%$
Overall root mean square error (RMSE)	$RMSE = \left(\frac{\sum_{i=1}^{N}(Q_{m,i} - Q_{c,i})^2}{N}\right)^{0.5}$
Average root mean square error of peak flow event ($RMSE_{peak}$)	$RMSE_{peak} = \frac{1}{P}\sum_{j=1}^{P}\left[\frac{1}{M_j}\sum_{i=1}^{M_j}\left(Q_{m,i} - Q_{c,i}\right)^2\right]_j^{1/2}$

where, $Q_{m,i}$ is the observed discharge at time i, $\overline{Q}_m$ is the average value of observed discharge, $Q_{c,i}$ is the calculated discharge at time i, $\overline{Q}_c$ is the average value of the calculated discharge, N is the number of data points, P is the number of peak flow events, M_j is the number of data points at peak flow event j. Note that, peak flow events are defined as periods where the observed discharge is above a 10 % probability of exceedance (Paiva, 1993). The best fit between the calculated and observed discharges using these parameters occurs when the correlation coefficient (r) approaches 1, the efficiency index (EI) approaches 100 percent, the overall root mean square error (RMSE) and average root mean square error of peak flow event ($RMSE_{peak}$) approach zero.

RESULTS AND DISCUSSION

According to the objectives of this thesis, results and discussion of this study corresponding to the topic of methodologies described above can be summarized below.

1. Hydrologic model selection

According to the results of hydrologic model selection as presented in the section of methodology for model selection, the URBS model is the most appropriate hydrologic model for flood and runoff estimation in this thesis.

2. Testing the URBS model performance and extending its application to the ungauged catchments

2.1 Results of the URBS and the NAM model calibrations and verifications for flood estimation in the upper Ping river basin

Applications of the URBS and the NAM models on particular runoff stations and flood events were undertaken by adjusting model parameters to achieve the best fit between the observed and the simulated flood hydrographs for both in calibration and verification processes. The simulation results showed that both models can simulate flood hydrographs close to the observed hydrographs for most flood events as shown by acceptable average statistical values for model parameters in Figure 18. Examples of model application results for the three calibrated runoff stations are shown in Figures 19 to 23. It should be noted that both models cannot simulate flood hydrographs accurately for a few flood events, this most likely is attributable to inaccuracy of daily rainfall data, which is the most significant input data for model estimation, and only few rainfall stations are located within the catchment areas of some of the runoff stations.

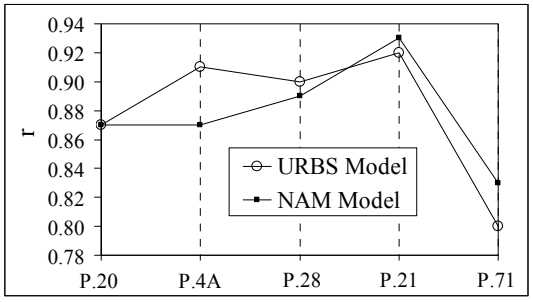

a) Correlation Coefficient (r)

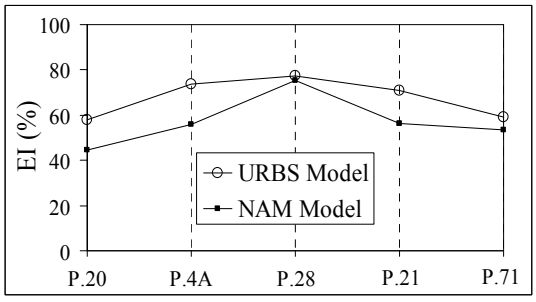

b) Efficiency Index (EI)

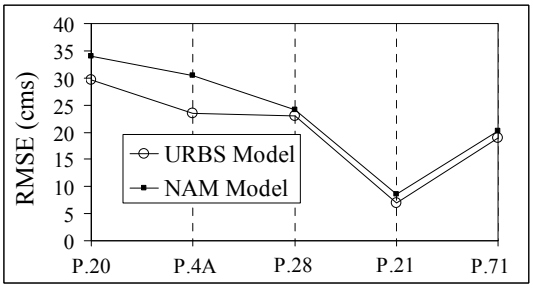

c) Root Mean Square Error (RMSE)

Figure 18 Average statistical measures of the URBS and the NAM models.

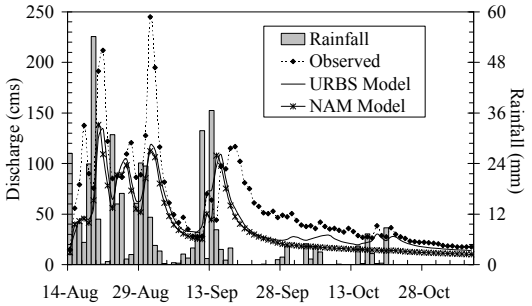

a) Flood hydrograph in 1994

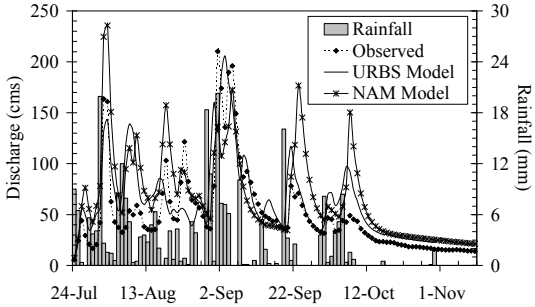

b) Flood hydrograph in 1995

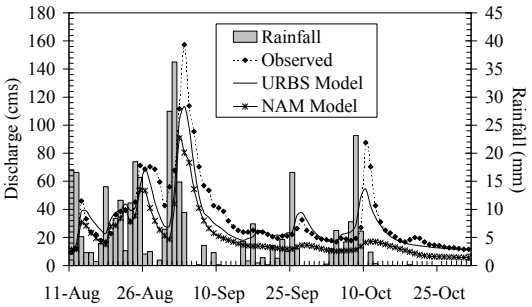

c) Flood hydrograph in 1996

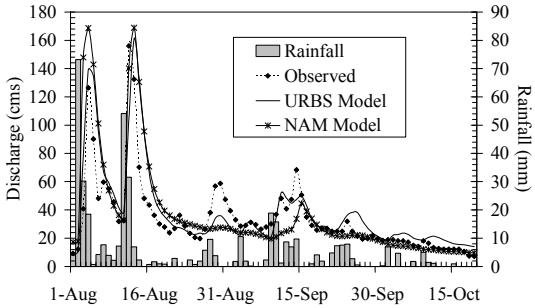

d) Flood hydrograph in 2001

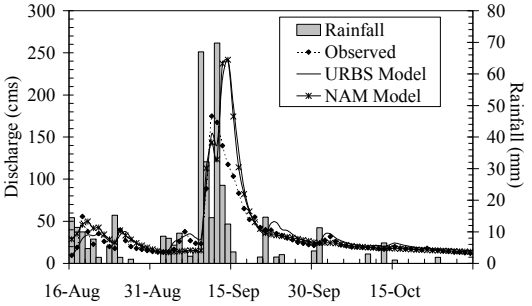

e) Flood hydrograph in 2003

Figure 19 Observed and calculated flood hydrographs at the runoff station P.20.

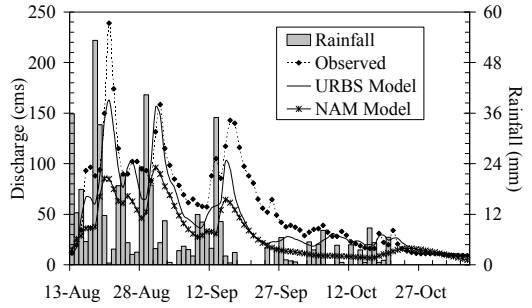

a) Flood hydrograph in 1994

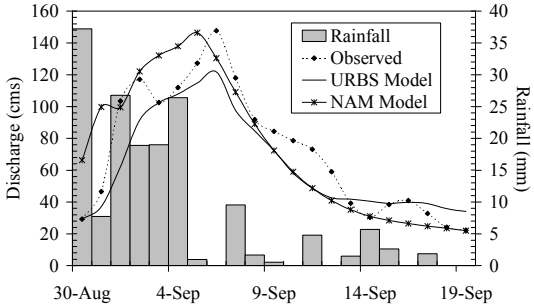

b) Flood hydrograph in 1995

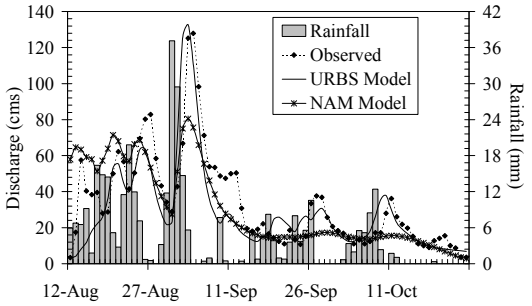

c) Flood hydrograph in 1996

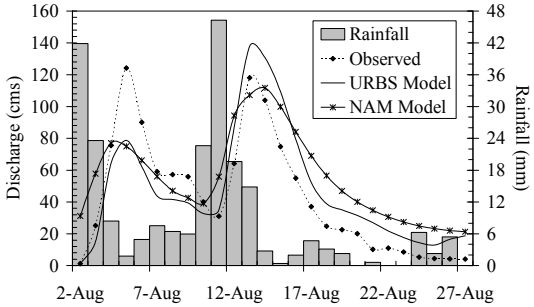

d) Flood hydrograph in 2001

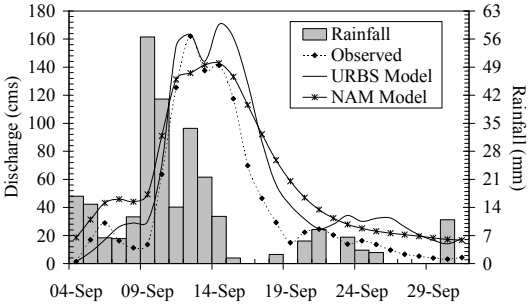

e) Flood hydrograph in 2003

Figure 20 Observed and calculated flood hydrographs at the runoff station P.4A.

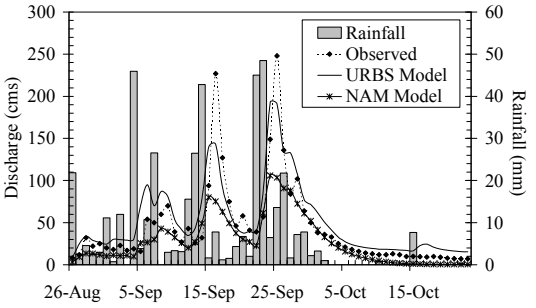

a) Flood hydrograph in 1967

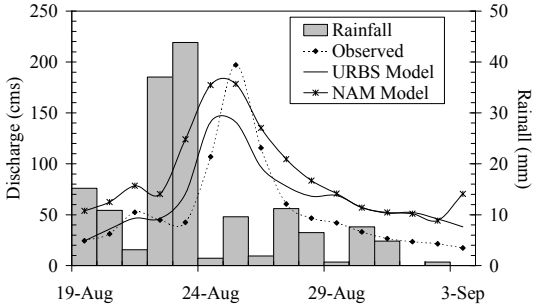

b) Flood hydrograph in 1970

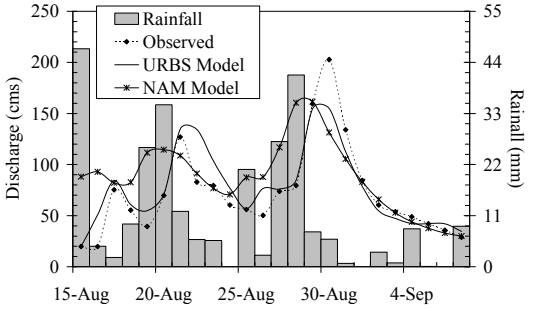

c) Flood hydrograph in 1971

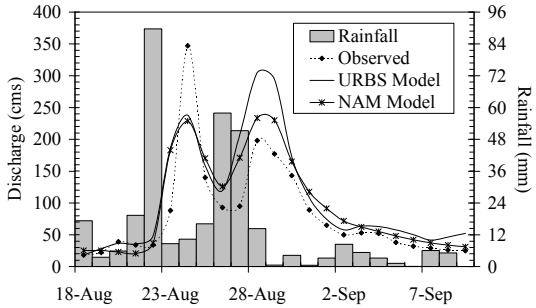

d) Flood hydrograph in 1973

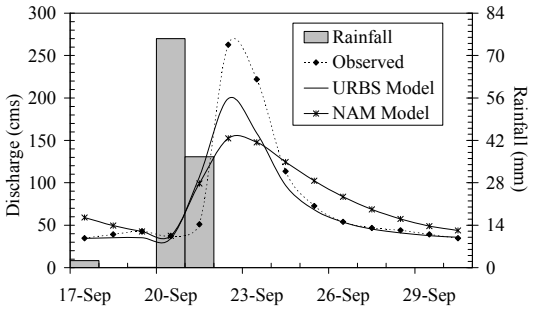

e) Flood hydrograph in 1975

Figure 21 Observed and calculated flood hydrographs at the runoff station P.28.

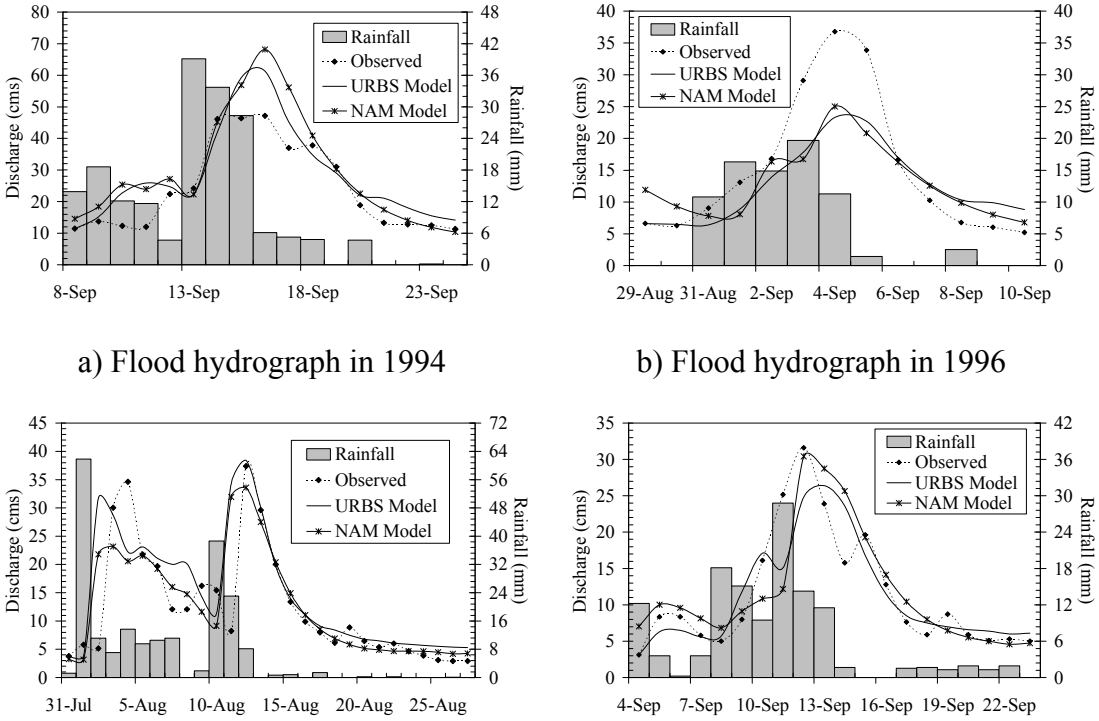

a) Flood hydrograph in 1994

b) Flood hydrograph in 1996

c) Flood hydrograph in 2001

d) Flood hydrograph in 2003

Figure 22 Observed and calculated flood hydrographs at the runoff station P.21.

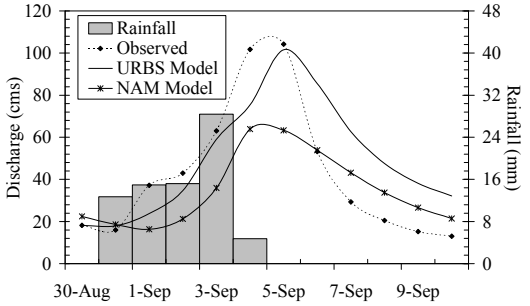

a) Flood hydrograph in 1996

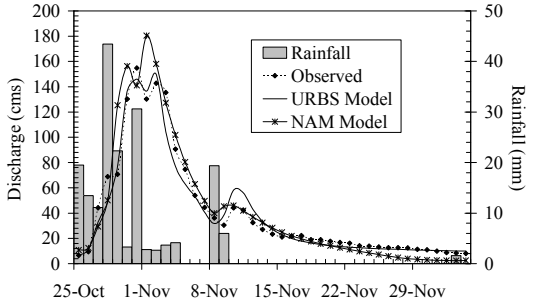

b) Flood hydrograph in 1999

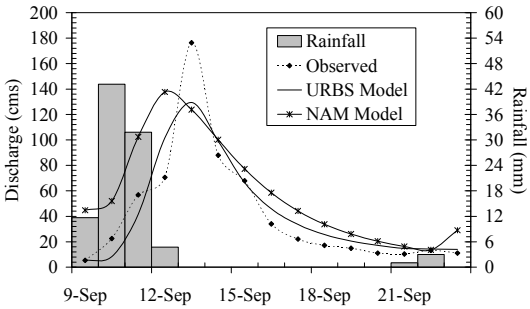

c) Flood hydrograph in 2000

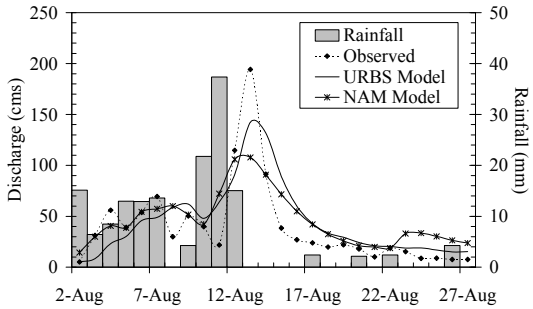

d) Flood hydrograph in 2001

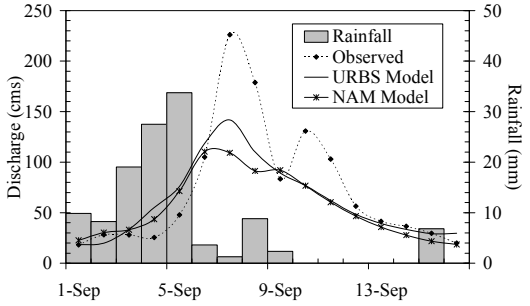

e) Flood hydrograph in 2002

Figure 23 Observed and calculated flood hydrographs at the runoff station P.71.

Table 7 Results of the URBS and the NAM model applications.

Runoff station	Control parameters gained from model calibration and verification processes										
	URBS model					NAM model					
	α	β	IL	PR	IF	L_{max}	CQOF	TOF	CK1	TG	CKBF
P.20	0.30	9	0	0.21	550	350	0.5	0.4	26	0.4	1,500
P.4A	0.35	9	0	0.15	700	520	0.5	0.3	48	0.1	1,000
P.28	0.35	8	0	0.22	400	330	0.5	0.1	42	0.9	2,000
P.21	0.20	6	0	0.15	600	450	0.6	0.6	30	0.7	5,000
P.71	0.40	8	0	0.22	350	480	0.5	0.1	40	0.9	3,000

Table 7 shows that there are 5 parameters necessary to be calibrated for the URBS applications. However, the parameter IL (the initial loss) was set to be zero to give the best fit between the observed and calculated flood hydrographs. This is because the model was used to simulate large flood events that occur in the wet season after some previous flood events, whereby soil moisture is expected to be saturated. This brings the number of parameters to four compared with six parameters that need to be calibrated for the NAM model. As less model parameters are needed for model application and slightly better flood hydrograph results were obtained using the URBS model, this model was chosen for further investigation to formulate the ungauged relationships that could be applied on the ungauged catchments of the upper Ping river basin.

2.2 Generalised URBS model parameters and catchment characteristics for the upper Ping river basin

As mentioned in section 5.1, the URBS model has proved to be simpler than the NAM model with slightly better calibration results. As such the URBS model was calibrated to other 6 runoff stations: P.1, P.77, P.24A, P.29, P.76, and P.73 as previously stated. Model parameters gained from model application of all 11 runoff stations are summarized in Table 8. The catchment characteristics of each runoff station comprising the catchment area (A), main channel length (L), main channel

length from the centroid (L_c), channel slope (S), and the percentage of land use consisting of agricultural (Ag) and forest areas (F), are presented in Table 9.

Table 8 Model parameters of the 11 runoff stations used in ungauged relationship formulation.

Runoff Station	Control parameters of the URBS model				
	α	β	IL	PR	IF
P.20	0.30	9	0	0.21	550
P.4A	0.35	9	0	0.15	700
P.28	0.35	8	0	0.22	400
P.21	0.20	6	0	0.15	600
P.71	0.40	8	0	0.22	350
P.1	0.30	7	0	0.17	500
P.77	0.20	5	0	0.20	350
P.24A	0.20	5	0	0.25	280
P.29	0.40	8	0	0.26	200
P.76	0.40	8	0	0.26	200
P.73	0.45	9	0	0.25	250

Table 9 Catchment characteristics of the 11 runoff stations used in ungauged relationship formulation.

Runoff Station	Catchment characteristic parameters					
	A (km^2)	L (km)	L_c (km)	S	Agricultural Area(%)	Forest Area(%)
P.20	1,355	85.0	44.0	0.00942	17.3	81.9
P.4A	1,902	148.1	69.0	0.00411	13.9	85.5
P.28	1,261	81.4	37.1	0.00699	19.6	78.1
P.21	515	47.3	26.6	0.01213	35.3	63.1
P.71	1,771	112.4	53.4	0.00666	18.9	78.8
P.1	1,322	97.9	45.0	0.00058	31.2	61.5
P.77	547	72.1	26.3	0.00625	12.3	86.0
P.24A	460	41.9	24.7	0.03510	23.0	75.9
P.29	1,970	179.0	60.0	0.00271	12.7	84.8
P.76	1,541	144.4	47.8	0.00277	14.9	82.2
P.73	2,284	96.1	44.2	0.00038	34.4	55.5

To apply the URBS model on ungauged catchments, four model parameters α, β, PR, and IF need to be correlated with the proposed catchment characteristics comprising A, L, L_c, and S using the multiple linear regression analysis. Multiple linear regression relationships between each model parameter and catchment characteristics are shown in Equations. (91) to (94). These relationships have very high correlation coefficients (r) with the values of 0.97, 0.91, 0.95, and 0.94, respectively, as shown in Table 10.

$$\alpha = 0.163 + 0.0002A + 0.001L - 0.003L_c + 0.456S \quad (91)$$

$$\beta = 4.499 + 0.002A - 0.018L + 0.057L_c - 18.574S \quad (92)$$

$$PR = 0.176 + 0.0001A + 0.002L - 0.006L_c + 3.498S \quad (93)$$

$$IF = 386.94 - 0.329A - 7.037L + 28.624L_c - 10{,}024S \quad (94)$$

Table 10 Correlation coefficients (r) for the relationships between the model parameters and catchment characteristics.

Model Parameter	Four catchment characteristics (A, L, L_c and S)		Six catchment characteristics (A, L, L_c, S, A_g, and F)	
	Multiple linear regression analysis	Multiple power regression analysis	Multiple linear regression analysis	Multiple power regression analysis
α	0.97	0.98	0.97	0.99
β	0.91	0.95	0.95	0.96
IL	0.95	0.79	0.97	0.80
PR	0.94	0.75	0.96	0.82

Multiple power regression analysis was then used to create the relationships between model parameters and catchment characteristics. The results show that the correlation coefficients for the relationships between catchment characteristics and model parameters α and β slightly increase to 0.98 and 0.95, respectively, as shown in Table 10. However, the correlation coefficients between catchment characteristics and model parameters PR, and IF reduce to 0.79 and 0.75, respectively, as shown in Table 10. Therefore, only the power relationships between catchment characteristics and model parameters α and β are shown in the Equations. (95) and (96), respectively.

$$\alpha = 0.006(A^{0.784} L^{0.179} L_c^{-0.608} S^{0.041}) \tag{95}$$

$$\beta = 0.484(A^{0.484} L^{-0.199} L_c^{0.102} S^{0.035}) \tag{96}$$

Finally these four model parameters were correlated with the extra catchment characteristics, the percentage of agricultural and forest areas, along with the four primary catchment characteristics. The results show that the correlation coefficients for the relationships between all six catchment characteristics and the model parameters α and β, using multiple power regression analysis (as shown in

Equations. (97) and (98)), slightly increase to 0.99 and 0.96, respectively, as shown in Table 10. Similarly, the correlation coefficients of the relationships between the six catchment characteristics and model parameters PR, and IF, calculated using linear multiple regression analysis (as shown in Equations. (99) and (100)), also slightly increase to 0.97 and 0.96, respectively, as shown in Table 10.

$$\alpha = 0.0002(A^{0.758}L^{0.599}L_c^{-0.893}S^{0.083}Ag^{0.385}F^{0.389}) \quad (97)$$

$$\beta = 0.006(A^{0.485}L^{-0.137}L_c^{0.012}S^{0.01}Ag^{0.289}F^{0.792}) \quad (98)$$

$$PR = 0.346 + 0.0001A + 0.001L - 0.006L_c + 3.273S - 0.003Ag - 0.001F \quad (99)$$

$$IF = -1{,}742 - 0.265A - 5.962L + 24.72L_c - 10{,}774S + 26.74Ag + 20.37F \quad (100)$$

The relationships of the four parameters that use the percentage of agricultural and forest areas were not adopted for use because these two catchment characteristics are more difficult to measure than the four catchment characteristics A, L, L_c, and S. Moreover the correlation coefficients between the URBS model parameters and catchment characteristics using the percentage of agricultural and forest areas are not improved much compared with not using them. The proposed ungauged relationships presented in Equations. (93) to (96) are therefore recommended to be used for estimating the model parameters PR, IF, α, and β, respectively, for the ungauged catchments in the upper Ping river basin.

2.3 Verification of the proposed relationships for flood estimation in ungauged catchment

Once the relationships between the URBS model parameters and catchment characteristics have been created, flood hydrographs at the 4 runoff stations (P.5, P.14, P.75, and P.67) gained from the ungauged and gauged catchment approaches were compared to the observed data. The three statistical measures (r, EI, and RMSE) were then calculated to identify the effectiveness of the ungauged catchment approach. The URBS model parameters PR and IF were evaluated using the linear relationships between these parameters and the catchment characteristics A,

L, L_c, and S, as shown in Equations. (93) and (94). The model parameters α and β were evaluated using the multiple power relationships between these parameters and the catchment characteristics A, L, L_c, and S, as shown in Eqs. (95) and (96).

Catchment characteristics of the 4 runoff stations used to test the proposed relationships are presented in Table 11, and the URBS model parameters assessed using the gauged and ungauged catchment approaches for the 4 runoff stations are presented in Table 12. The simulation results attained from these two approaches are presented by the average statistical measure values shown in Table 13 as well as the time series plots in Figures 24 to 27. Percentage differences of the average statistical values between the gauged and ungauged approaches were also calculated as shown in Table 13.

Table 11 Catchment characteristics for the 4 runoff stations.

Runoff Station	Catchment characteristic parameters			
	A (km^2)	L (km)	L_c (km)	S
P.5	1,777	97. 9	49.1	0.00392
P.14	3,853	194.2	99.6	0.00437
P.75	771	64.1	29.4	0.00088
P.67	498	35.4	16.3	0.00148

Table 12 Estimated URBS model parameters obtained from gauged and ungauged catchment approaches.

Runoff Station	Gauged catchment approach				Ungauged catchment approach			
	α	β	PR	IF	α	β	PR	IF
P.5	0.80	9	0.25	250	0.38	9	0.20	481
P.14	0.20	5	0.11	500	0.52	12	0.23	560
P.75	0.30	7	0.17	500	0.22	5	0.18	430
P.67	0.30	7	0.17	500	0.24	6	0.16	520

Table 13 Average statistical measures corresponding to flood events used in verification process.

Runoff Station ID	Gauged approach			Ungauged catchment approach (percentage difference from gauged approach)		
	r	EI (%)	RMSE (m^3/s)	r	EI (%)	RMSE (m^3/s)
P.5	0.85	64.98	26.76	0.75 (-11.56)	47.98 (-26.15)	31.74 (18.63)
P.14	0.86	67.33	36.13	0.70 (-18.51)	36.98 (-45.08)	54.24 (50.13)
P.75	0.98	93.16	12.39	0.96 (-2.49)	89.35 (-4.09)	14.66 (18.40)
P.67	0.96	91.68	26.96	0.96 (0)	90.33 (-1.47)	29.73 (10.27)

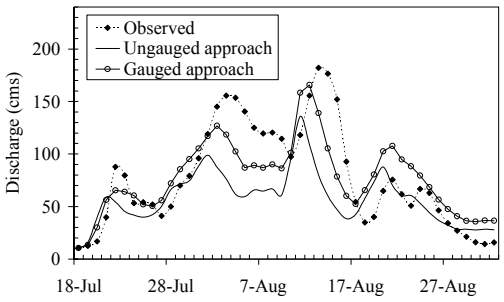

a) Flood hydrograph in 1981

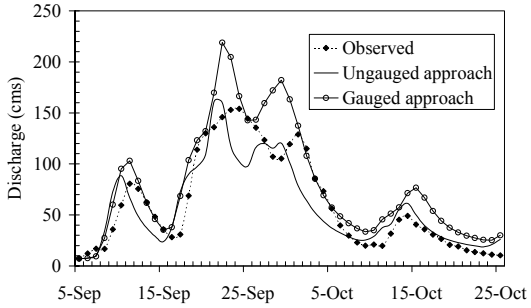

b) Flood hydrograph in 1982

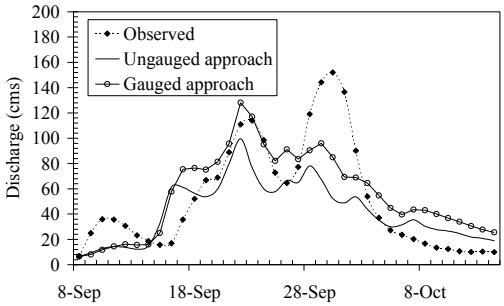

c) Flood hydrograph in 1992

Figure 24 Observed and calculated flood hydrographs at the runoff station P.5.

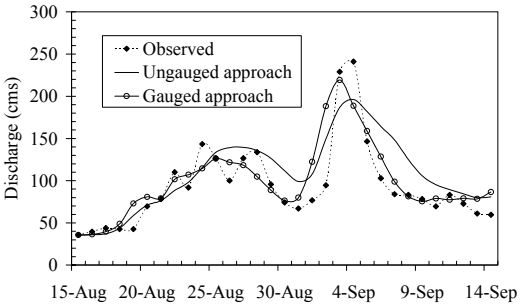

a) Flood hydrograph in 1996

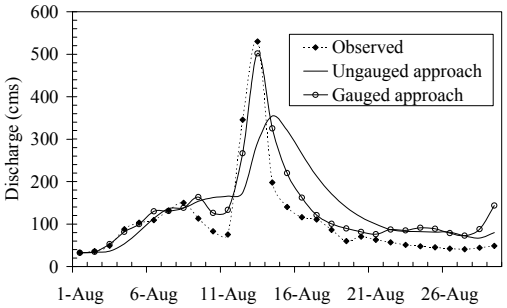

b) Flood hydrograph in 2001

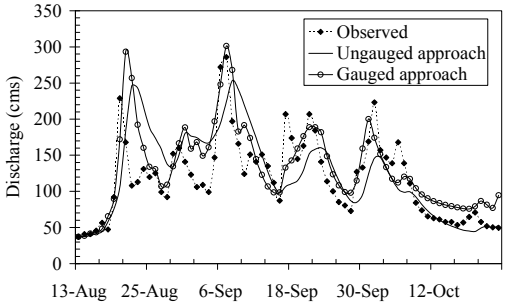

c) Flood hydrograph in 2002

Figure 25 Observed and calculated flood hydrographs at the runoff station P.14.

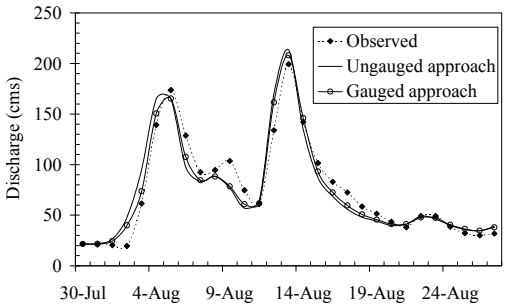

a) Flood hydrograph in 2001

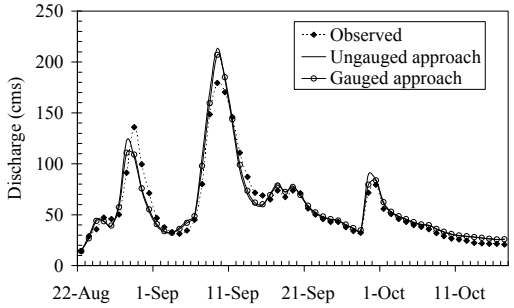

b) Flood hydrograph in 2002

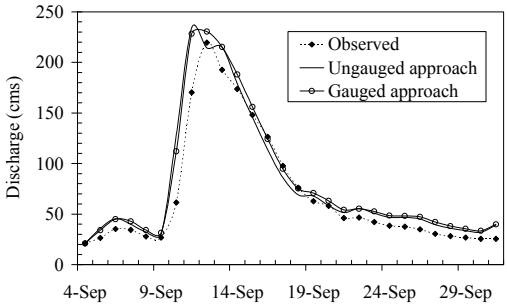

c) Flood hydrograph in 2003

Figure 26 Observed and calculated flood hydrographs at the runoff station P.75.

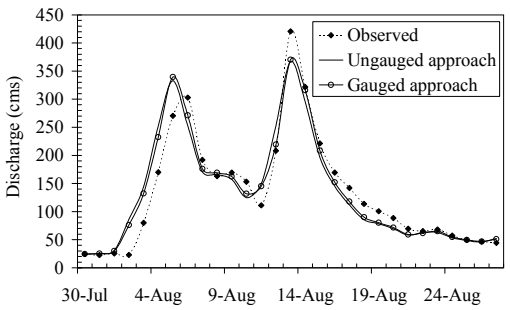

a) Flood hydrograph in 2001

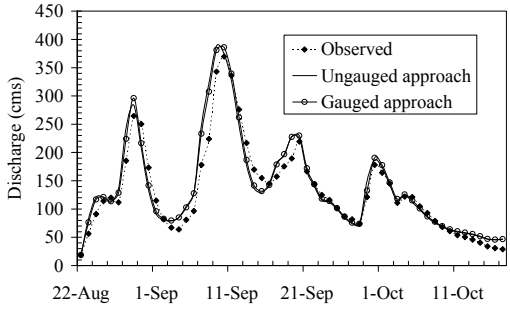

b) Flood hydrograph in 2002

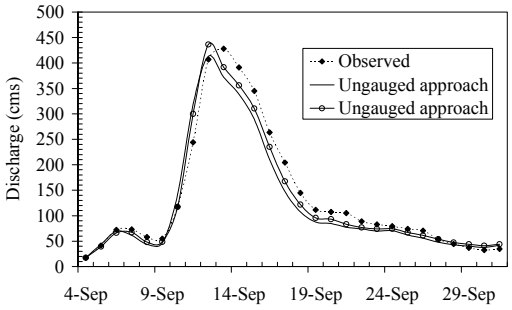

c) Flood hydrograph in 2003

Figure 27 Observed and calculated flood hydrographs at the runoff station P.67.

Table 13 shows that the average statistical values at the stations P.75 and P.67 attained from both approaches are very high with r and EI close to 1 and 100%, respectively. It also shows that the estimated flood hydrographs attained from both approaches at these two stations are very close with the only small percentage difference of the averaged statistical values. These evidences have confirmed an ability of the ungauged relationships to be confidently applied for flood estimation for the ungauged catchments at these two locations. However, the ungauged approach cannot simulate flood hydrographs at the stations P.5 and P.14 as good as the gauged approach can. As we can see the averaged statistical values of r and EI attained from the ungauged approach are lesser than that of the gauged approach while the RMSE of the ungauged approach are higher than that of the gauged approach.

It should be noted that the catchment area of the stations P.75 and P.67 are the sub-catchments of the station P.1, which is one of the 11 stations used to formulate the ungauged relationships. On the other hand, the stations P.5 and P.14 are the independent catchments which have not been used in the formulation process of the ungauged relationships. From the results, it could be concluded that the ungauged relationships can be confidently applied for flood estimation purpose only for the ungauged catchments that lay within the catchment area of the stations which are involved in formulating the ungauged relationships. More cautious is needed when these relationships are applied for general ungauged catchments located outside the basins of the 11 stations used in the formulation process of the ungauged relationships.

3. Climatological Z-R Relationship for Radar Rainfall Estimation in the upper Ping river basin

The reflectivity and gauge rainfall data between June and October in 2003 and 2004 were analysed by the steps as explained in the previous section. The results of the mean radar rainfall and mean gauge rainfall using the standard relationship of $Z=200R^{1.6}$ are compared as shown in Figure 28. The statistical measures comparing these two sets of data are also calculated as summarized in Table 14. It can be noted that the estimated radar rainfall is generally lower than the gauge rainfall. Parameter A in the Z-R relationship needs to be adjusted using the Equation (9) with the m value equal to 1.868, which is the slope gained from the relationship in Figure 28. The adjusted A value is 74, and then the new Z-R relationship; $Z = 74R^{1.6}$, was used to recalculate each step (1 to 4) as explained in the topic "Climatological Z-R relationship calibration". The results showed that the modified Z-R relationship can improve the accuracy of the mean daily radar rainfall compared to the application of $Z=200R^{1.6}$. Significant reductions of the statistical measures resulting from the calibrated relationship are shown in Table 14. Figure 29 shows that the scatter plot of the mean radar rainfall attained from the adjusted relationship ($Z = 74R^{1.6}$) and mean gauge rainfall (see Figure 29) are closer compared to the scatter plot produced using the previous relationship ($Z = 200R^{1.6}$). Radar rainfall estimated using the adjusted

relationship ($Z = 74R^{1.6}$) and gauge rainfall for the daily basis in 2003 and 2004 were plotted as shown in Figures 30 and 31, respectively. The figures show that estimated radar rainfall is not significantly lower than the gauge rainfall. An agreement between estimated radar and gauge rainfall was presented using correlation coefficient (r). The results show that the overall correlation coefficients between the estimated radar and calculated rain gauge rainfall for the data sets in 2003 and 2004 are 0.857 and 0.912, respectively (see Figure 30 and 31), which are acceptable. The calibrated Z-R relationship ($Z = 74R^{1.6}$) is therefore appropriate to be used for an estimation of daily radar rainfall in the upper Ping river basin.

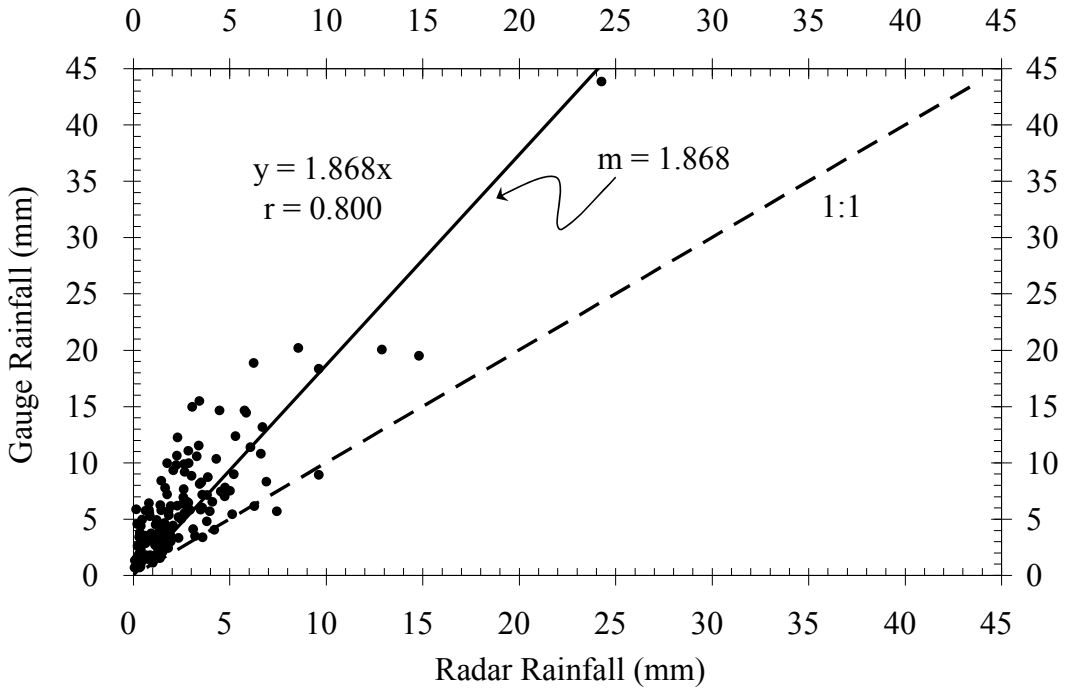

Figure 28 Scatter plot of mean radar rainfall and mean gauge rainfall based on the relationship $Z = 200R^{1.6}$.

Table 14 Comparisons of the statistical measures gained from the different Z-R relationships.

Statistical Measures	$Z = 200R^{1.6}$	$Z = 74R^{1.6}$
Mean Error (mm)	-3.47	-1.23
Mean Absolute Error (mm)	3.51	2.30
Root Mean Square Error (mm)	4.65	3.14
Bias (mm)	2.33	1.25

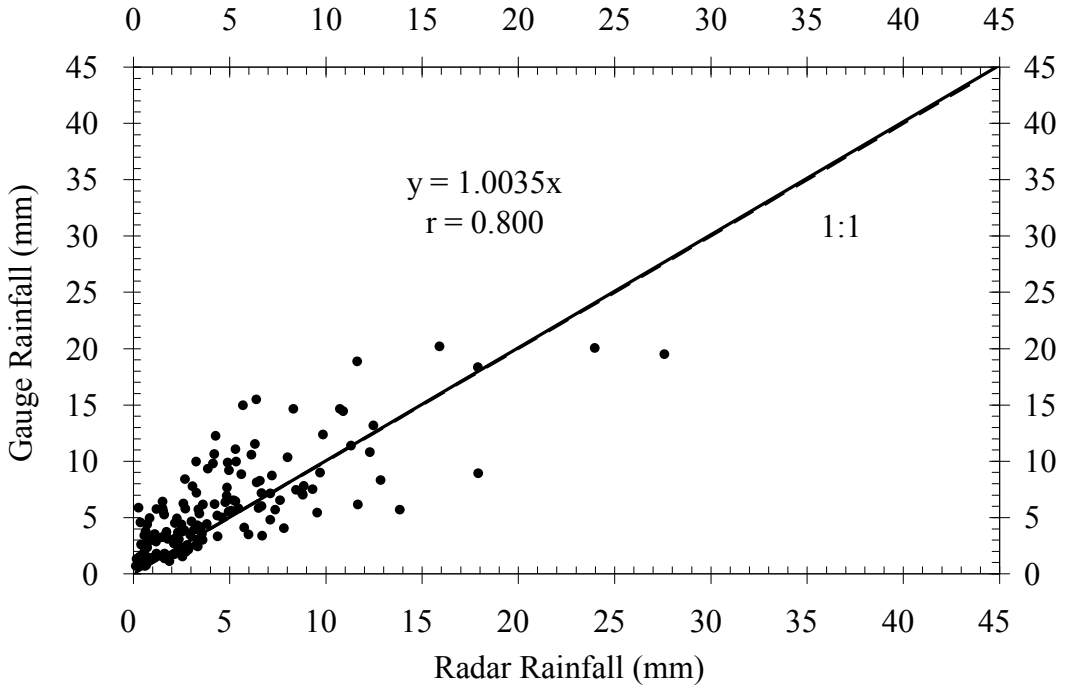

Figure 29 Scatter plot of mean radar rainfall and mean gauge rainfall based on the relationship $Z = 74R^{1.6}$.

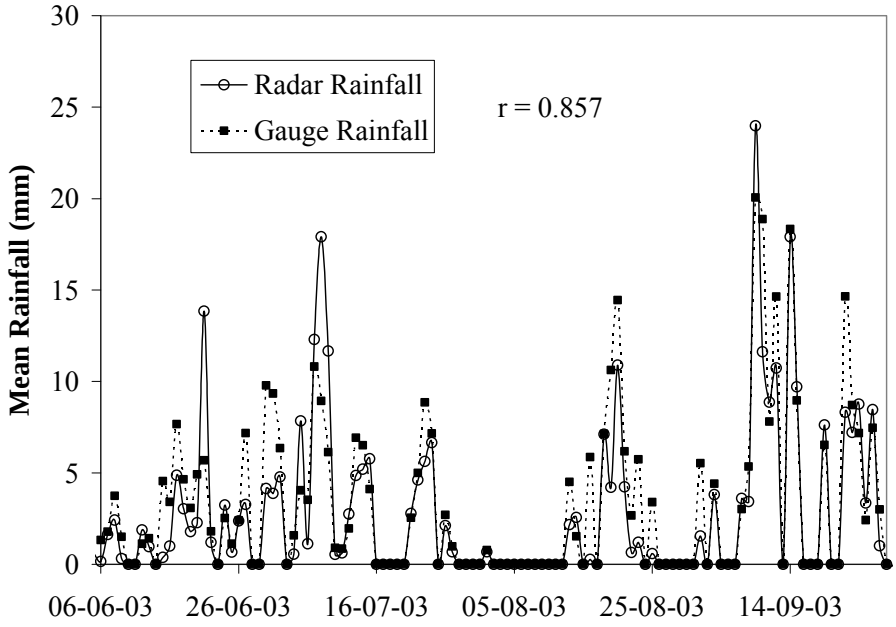

Figure 30 Time series plot of mean gauge rainfall and radar rainfall in 2003 using the relationship $Z = 74R^{1.6}$.

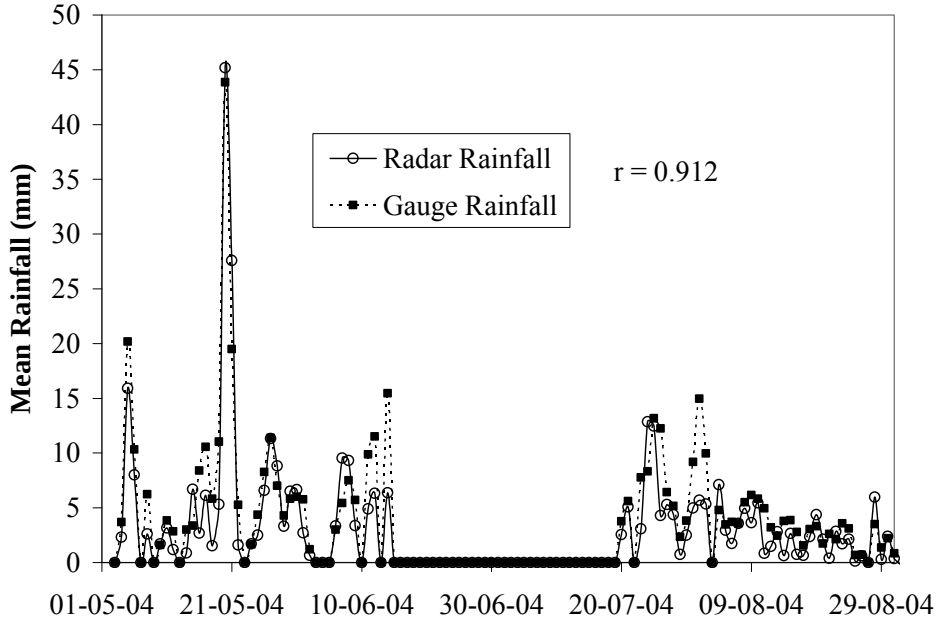

Figure 31 Time series plot of mean gauge rainfall and radar rainfall in 2004 using the relationship $Z = 74R^{1.6}$.

4. Effect of rain-gauge temporal resolution on the specification of a Z-R relationship

4.1 Result of climatological scaling transformation function

Moment orders q equal to 0.5, 1.0, 1.5, 2.0, 2.5, 3.0, 3.5, 4.0, 4.5, 5.0, 5.5, and 6.0, were used to ascertain the optimal value of η for the five rainfall datasets used. Results from this analysis are illustrated in Figure 32(a). An optimal value of η was ascertained as the slope of $\partial \log(A_t^q) / \partial \log(t)$ plotted as a function of moment order q in Figure 32(b). Note that Figure 32 represents results for the Sydney (1) data alone. Similar results were obtained for the remaining four datasets used.

The values of the scaling exponent for the other four datasets were equal to 0.0548, 0.0566, 0.0574, and 0.0528 for Sydney (2), Sydney (3), Brisbane, and Bangkok, respectively. Consequently, a uniform scaling exponent equal to 0.055 was proposed in this study. The proposed climatological scaling equation then becomes:

$$A_t = (t/24)^{-0.055} A_{24} \tag{101}$$

It should be noted that the data used in the study comprises of a range of storms that include short-lived convective events to more sustained stratiform ones. While the argument can be made that the mix of these types of events could be responsible for the scaling behavior that is observed, the fact that similar scaling relations are derived in the three climatologically different locations the study focused on, suggests the scaling may be due to other factors. However, future work in this research will investigate the effect of storm types on the temporal scaling behavior of the Z-R relationship for these two rainfall types using an operational storm classification approach of the type outlined in Chumchean *et al*. (2008).

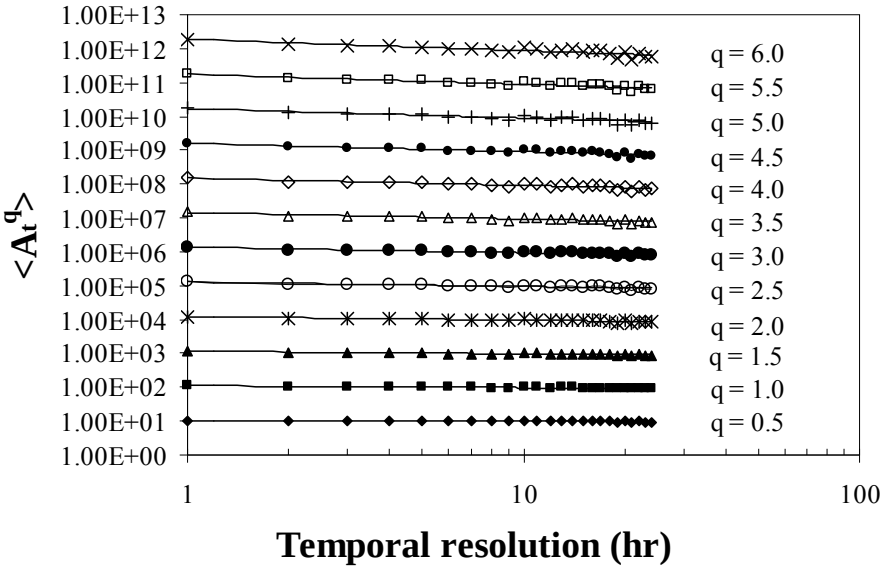

(a) Scaling of the moments for *A* parameters

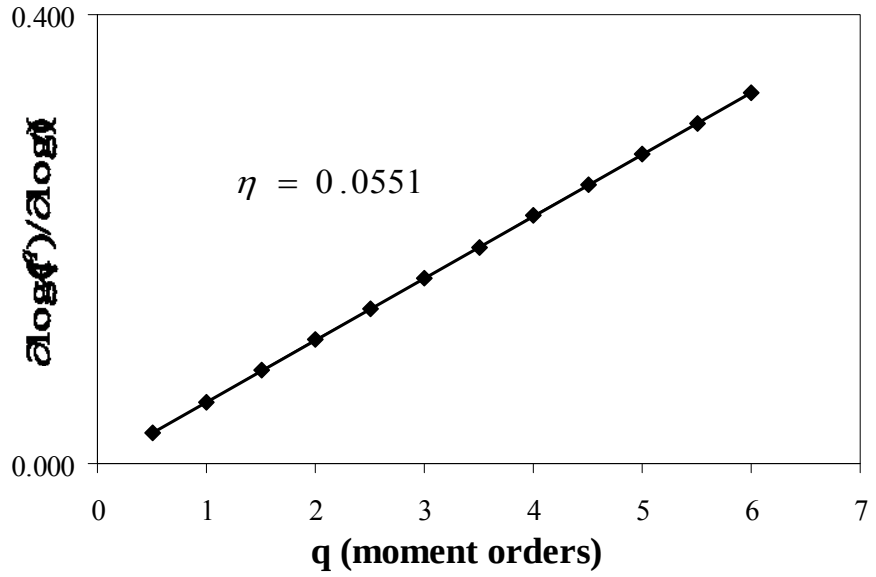

(b) Scaling exponent for *A* parameters at different moment orders (q)

Figure 32 Verification of scaling hypothesis for Sydney rainfall data (1) representing the period November 2000 – April 2001.

4.2 Investigation of impact of attenuation on the temporal scaling relationship

Attenuation for C-band radar is considered to be a severe problem for measurement of high-intensity rainfall (reflectivity > 50 dBZ) (Hildebrand, 1978; Austin, 1987). However, the impact of attenuation can be ascertained by studying the relationship between gauge and radar rainfall as a function of distance from the radar (Burrows and Attwood, 1949). In the results reported below, we investigate the effect of attenuation on the temporal scaling behavior of the Z-R relationship by considering that attenuation by rain is depending on distance from the radar site. We assume that radar data within a given range interval has common attenuation effects. According to the spatial distribution of three rain gauge networks of the three cities, three datasets for Sydney and one dataset for Brisbane were separated into 0 – 50 km and 50 – 100 km range intervals, and the dataset for Bangkok was separated into 0 – 15 km and 15 – 50 km range intervals because the farthermost gauge of the Bangkok network is located at around 46 km from the radar. To investigate the effect of attenuation on the temporal scaling of the Z-R relationship, the A parameter of each range interval of each radar was calculated and the results are presented in Figure 33.

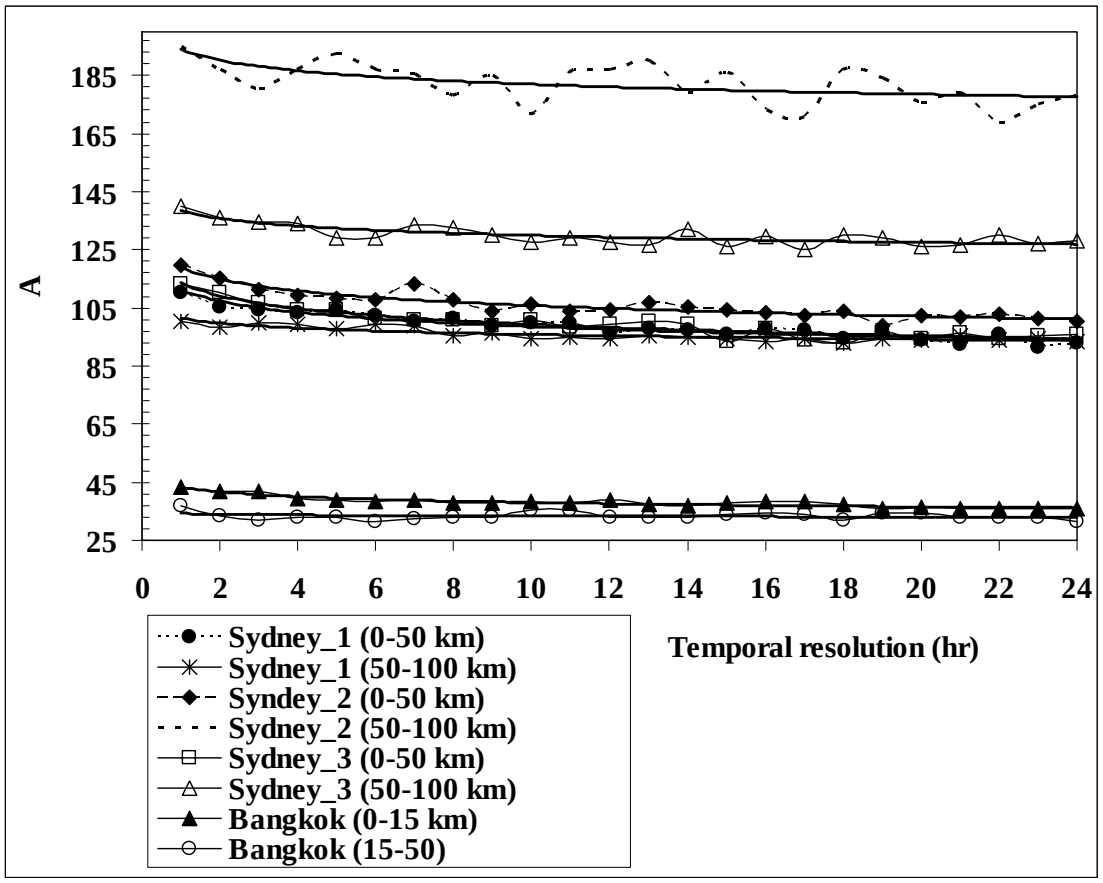

Figure 33 Coefficient A of the *Z-R* relationship at different range intervals, derived using a fixed exponent b equal to 1.6, for the Kurnell, the Mt Stapylton, and the Pasicharoen radars, as a function of varying temporal rainfall resolutions.

Difference in the A parameters of each range intervals for the same radar might be due to the differences in rainfall characteristic of each range, the differences being partly due to attenuation. Once, the A parameters of each range intervals were derived, the scaling transformation equations for each dataset were also estimated and the results are presented in Table 15. Note that, datasets Sydney (1), Sydney (2) and Sydney (3) represent data for periods November 2000 – April 2001, August – December 2006, and January – May 2007, respectively.

Table 15 Scaling exponents at different range intervals for five datasets.

City	0 - 50 km	50 - 100 km	0 - 15 km	15 - 50 km
Sydney (1)	0.0529	0.0250	-	-
Sydney (2)	0.0513	0.0276	-	-
Sydney (3)	0.0578	0.0273	-	-
Brisbane	0.0577	0.0557	-	-
Bangkok	-	-	0.0572	0.0114

From the results presented in Table 15, it can be seen that the scaling exponents (η) of the scaling transformation Z-R equations obtained from the data lying within far range intervals of the C – band radar (50-100 km for Kurnell radar and 15 – 50 for Pasicharoen radar) are lower than using the data lying in the inner range intervals. The lower scaling exponent indicates an overestimated scaling exponent since attenuation has not been corrected for the data at far ranges. From this result it is evident that attenuation has affected the temporal scaling behavior of the Z-R relations of the C-band radars. However, for the S-band radar, the scaling exponents of the two range intervals are not significant different. This confirms the temporal scaling hypothesis of the Z-R relationship since attenuation problem can be neglected for the S-band radar.

4.3 Verification of proposed scaling transformation function

As the proposed scaling transformation is based on the assumption of distributional equality, it can be expected that the function leads to reasonable results when applied to ascertain specified quantiles of the data. Consequently, the scaling function was verified by using it to ascertain the probability distribution of the maximum intensity of rainfall burst as a function of rainfall duration, and compared to the distribution of similar maximum intensity of rainfall burst observed in each rain

gauge location. It is to be noted that the term “rainfall burst” has been used to represent rainfall bursts of fixed durations. The 24-hour A parameter value was used as a reference, based on which parameters for other temporal aggregation periods were estimated. Additionally, to show an effectiveness of the proposed scaled Z-R transformation equation, the frequency distributions of the maximum radar rainfall obtained from the scaling and 24-hour Z-R relationships were also compared with rain gauge data as presented in Figures 34 to 36. It can be noted that the distributional attributes of the estimated maximum radar rainfall are more similar to those of the rain gauge rainfall than the maximum radar rainfall obtained from the 24-hour Z-R relationship. This lends further credibility to the assumptions that were used to formulate the proposed scaling transformation function.

The mean square errors for the maximum intensity of rainfall bursts for six time resolutions (1-, 2-, 4-, 6-, 12-, and 24-hour) for the combined Sydney data, the Brisbane data, and the Bangkok data are presented in Table 16. In addition to this, the mean square error for the full rainfall data excluding zero radar rainfall was also calculated. The “optimal” case in the table refers to the estimation of the optimal A coefficient based on mean absolute error as described in section 2. For contrast, values of the error that would be expected were the 24 hour A parameter be used, are also given. Percentages of error in radar rainfall estimates based on two different A parameters that were derived from the temporal scaling transformation equation and the 24-hour A parameter have been calculated as shown in Table 16. From this result, it is evident that for all rainfall durations of all three radar, errors in extreme radar rainfall of the scaling case are less than the 24-hour case. The 24-hour A parameter gives higher errors, especially at high rainfall intensities, and at low temporal resolutions. Using the scaling Z-R relationship can reduce error in extreme radar rainfall especially at the finer temporal resolution. However, the improvement in radar rainfall estimates when considering all radar data excluding zero values are not significant if the scaling Z-R relationship has been used.

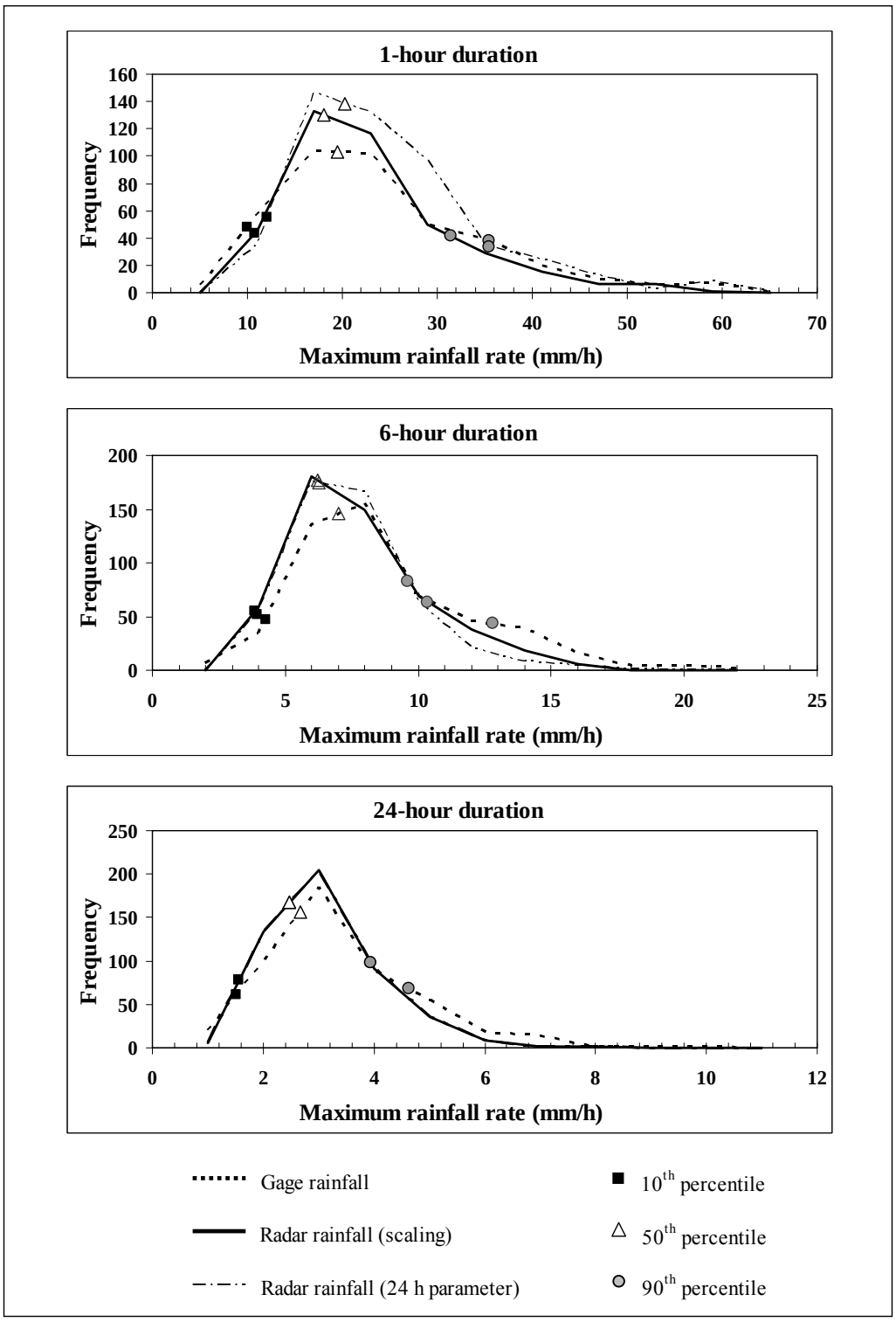

Figure 34 Frequency of maximum gauge rainfall and the scaling transformation based estimated radar rainfall for 1-, 6-, and 24-hour durations for Sydney dataset.

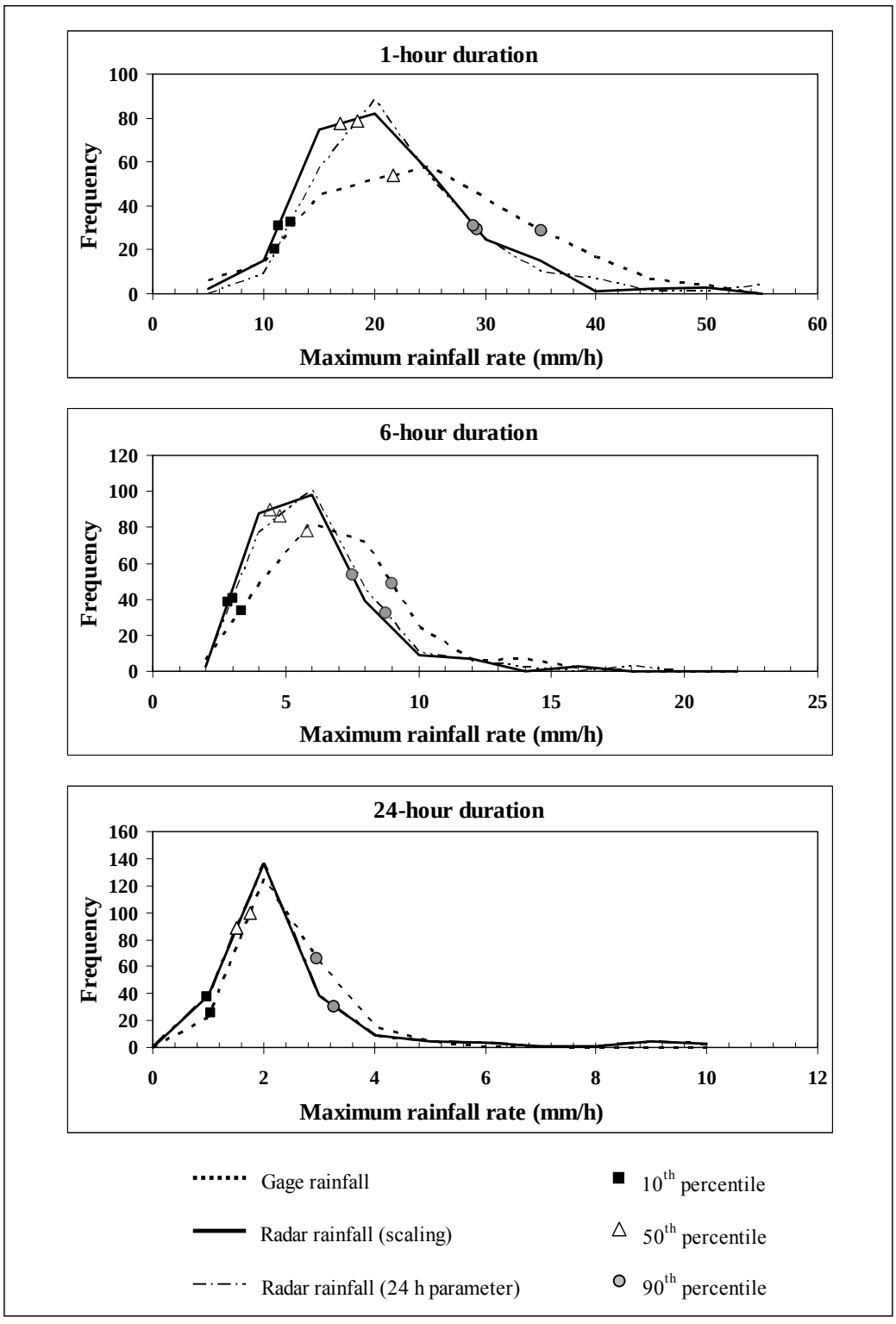

Figure 35 Frequency of maximum gauge rainfall and the scaling transformation based estimated radar rainfall for 1-, 6-, and 24-hour durations for Brisbane dataset.

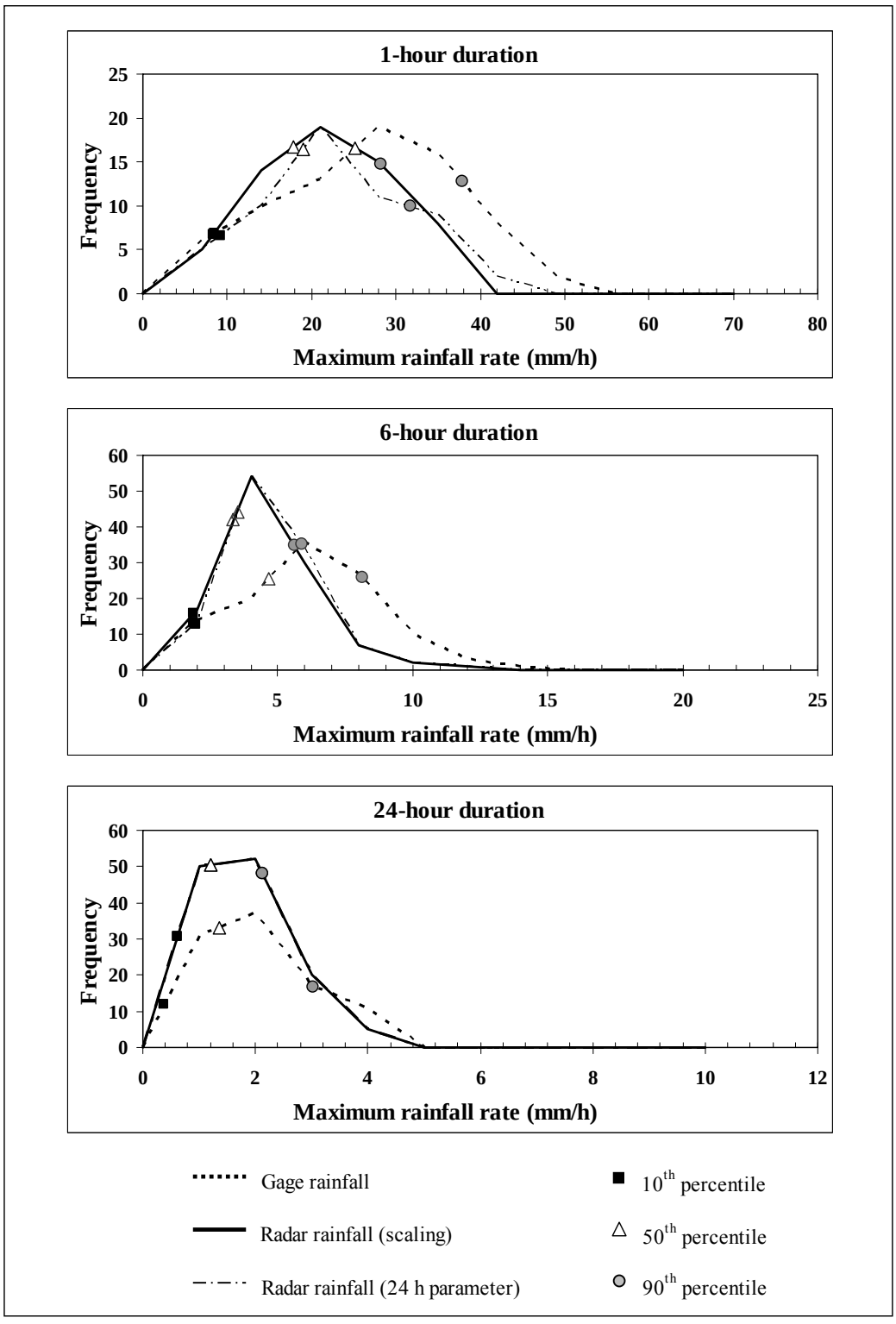

Figure 36 Frequency of maximum gauge rainfall and the scaling transformation based estimated radar rainfall for 1-, 6-, and 24hours durations for Bangkok dataset.

Table 16 Effectiveness of the scaling function for estimation of radar rainfall at varying temporal resolutions.

a) Sydney data

Mean Square Error (MSE) $(mm\ hr^{-1})^2$	Time Resolution					
	1 h	2 h	4 h	6 h	12 h	24 h
MRR – optimal (1)	296.82	107.45	45.57	24.36	12.49	5.08
MRR – scaling (2)	307.37	107.99	45.65	24.37	12.49	5.08
(% Error between (2) and (1))	(3.55%)	(0.50%)	(0.18%)	(0.04%)	(0.01%)	(0.00%)
MRR – 24 h parameter (3)	386.37	121.69	46.34	24.52	12.54	5.08
(% Error between (3) and (1))	(30.17%)	(13.25%)	(1.68%)	(0.66%)	(0.39%)	(0.00%)
RR – optimal (4)	11.58	5.07	2.05	1.36	0.78	0.48
RR – scaling (5)	11.59	5.08	2.06	1.36	0.78	0.48
(% Error between (5) and (4))	(0.05%)	(0.03%)	(0.03%)	(0.10%)	(0.02%)	(0.00%)
RR – 24 h parameter (6)	11.71	5.11	2.07	1.36	0.78	0.48
(% Error between (6) and (4))	(1.08%)	(0.71%)	(0.77%)	(0.34%)	(0.28%)	(0.00%)

Note: MRR – optimal = maximum radar rainfall (optimal), MRR - scaling = maximum radar rainfall (scaling), MRR - 24 h parameter = maximum radar rainfall (24 hour parameter), RR – optimal = radar rainfall excluding zeroes (optimal), RR - scaling = radar rainfall excluding zeroes (scaling), and RR - 24 h parameter = radar rainfall excluding zeroes (24 hour parameter).

Table 16 (Continued)

b) Brisbane data

Mean Square Error (MSE) $(mm\ hr^{-1})^2$	Time Resolution					
	1 h	2 h	4 h	6 h	12 h	24 h
MRR – optimal (1)	167.69	89.51	19.22	7.96	5.31	1.50
MRR – scaling (2)	167.95	90.33	19.36	7.96	5.35	1.50
(% Error between (2) and (1))	(0.15%)	(0.92%)	(0.71%)	(0.00%)	(0.78%)	(0.00%)
MRR – 24 h parameter (3)	180.26	96.68	20.23	8.01	5.40	1.50
(% Error between (3) and (1))	(7.49%)	(8.01%)	(5.24%)	(0.57%)	(1.72%)	(0.00%)
RR – optimal (4)	0.77	0.59	6.32	0.99	0.57	0.24
RR – scaling (5)	0.77	0.59	6.32	0.99	0.57	0.24
(% Error between (5) and (4))	(0.01%)	(0.00%)	(0.01%)	(0.00%)	(0.26%)	(0.00%)
RR – 24 h parameter (6)	0.78	0.59	6.33	1.00	0.58	0.24
(% Error between (6) and (4))	(0.62%)	(0.24%)	(0.15%)	(0.75%)	(0.74%)	(0.00%)

Note: MRR – optimal = maximum radar rainfall (optimal), MRR - scaling = maximum radar rainfall (scaling), MRR - 24 h parameter = maximum radar rainfall (24 hour parameter), RR – optimal = radar rainfall excluding zeroes (optimal), RR - scaling = radar rainfall excluding zeroes (scaling), and RR - 24 h parameter = radar rainfall excluding zeroes (24 hour parameter).

Table 16 (Continued)

c) Bangkok data

Mean Square Error (MSE) $(mm\ hr^{-1})^2$	Time Resolution					
	1 h	2 h	4 h	6 h	12 h	24 h
MRR – optimal (1)	376.74	104.93	24.50	22.22	6.48	2.41
MRR – scaling (2)	376.90	105.03	24.53	22.24	6.49	2.41
(% Error between (2) and (1))	(0.04%)	(0.10%)	(0.12%)	(0.09%)	(0.15%)	(0.00%)
MRR – 24 h parameter (3)	387.54	107.05	25.19	22.89	6.50	2.41
(% Error between (3) and (1))	(2.87%)	(2.02%)	(2.82%)	(3.02%)	(0.31%)	(0.00%)
RR – optimal (4)	95.47	28.61	8.66	3.31	1.38	0.35
RR – scaling (5)	95.49	28.61	8.66	3.31	1.38	0.35
(% Error between (5) and (4))	(0.02%)	(0.00%)	(0.00%)	(0.00%)	(0.00%)	(0.00%)
RR – 24 h parameter (6)	95.78	28.64	8.68	3.32	1.38	0.35
(% Error between (6) and (4))	(0.32%)	(0.10%)	(0.23%)	(0.30%)	(0.00%)	(0.00%)

Note: MRR – optimal = maximum radar rainfall (optimal), MRR - scaling = maximum radar rainfall (scaling), MRR - 24 h parameter = maximum radar rainfall (24 hour parameter), RR – optimal = radar rainfall excluding zeroes (optimal), RR - scaling = radar rainfall excluding zeroes (scaling), and RR - 24 h parameter = radar rainfall excluding zeroes (24 hour parameter).

5. Improvement in runoff estimation accuracy using radar

The results of the climatological Z-R relationship for the upper Ping river basin ($Z = 74R^{1.6}$) and the uniform scaling exponent ($\eta = 0.055$) as described in section 3 and 4, respectively, were used for the analysis in this section. The relationship $Z = 74R^{1.6}$ was first used to estimate daily radar rainfall, and the 24-A parameter (A=74) was later substituted into Equation (89) for hourly radar rainfall without scaling logic. Finally, the proposed scaling exponent ($\eta = 0.055$) and the calculated A_{24new} was substituted into Equation (90) for hourly radar rainfall with scaling logic. Results of the URBS model calibration and verification, comparison of

model performance using four different rainfall datasets, and investigation of impact of sub-daily rainfall variability on the accuracy of runoff estimation are presented as follows.

5.1 Results of model calibration and verification

Control parameters of each runoff station are different for each rainfall type and they are presented in Table 17. By using these parameters for the model calibration and verification, the average statistical values within 3 flow periods (2003-2005) are summarized in Table 18. It shows that the URBS model can reasonably simulate the hydrographs at these 6 runoff stations with the average r and EI values of around 0.74 and 62.56 %, respectively, while the average RMSE and RMSEpeak are within a reasonable range. However the statistical values for each station vary depending on the rainfall types. The daily radar rainfall (DRR) seems to produce flow hydrograph closer to the observed data than those produced by the daily rain gauge rainfall (DGR) data. The hourly radar rainfall both without (HRR) and with scaling logic (HRRS) can further improve the accuracy of flow hydrographs over the daily radar rainfall, respectively. Time series plot between the observed and calculated flow hydrographs using different rainfall datasets for the 6 runoff stations are shown in Figures 37 to 42. Further discussion on the comparison of model performance using four different rainfall datasets for each flow period is described in the next section.

Table 17 Model parameters of the 6 runoff stations with different rainfall types.

Runoff Station	Type of rainfall	Control parameters of the URBS model				
		α	β	IL	PR	IF
P.21	DGR	0.20	7	20	0.10	800
	DRR	0.20	7	10	0.10	1,000
	HRR	0.40	7	50	0.10	900
	HRRS	0.40	7	10	0.12	900
P.71	DGR	0.30	8	0	0.05	900
	DRR	0.30	8	0	0.08	1,100
	HRR	0.30	8	0	0.08	1,000
	HRRS	0.30	8	0	0.10	1,000
P.77	DGR	0.20	8	80	0.07	1,000
	DRR	0.10	7	50	0.05	1,500
	HRR	0.10	8	100	0.05	1,500
	HRRS	0.10	8	50	0.06	1,500
P.24A	DGR	0.30	7	10	0.10	800
	DRR	0.30	7	10	0.04	1,100
	HRR	0.30	6	60	0.03	1,100
	HRRS	0.30	6	20	0.04	1,000
P.73	DGR	0.45	8	10	0.17	800
	DRR	0.40	7	10	0.17	800
	HRR	0.40	8	25	0.17	1,000
	HRRS	0.40	7	10	0.18	800
P.14	DGR	0.10	8	50	0.05	800
	DRR	0.10	8	50	0.05	800
	HRR	0.10	7	20	0.08	900
	HRRS	0.10	7	20	0.10	900

Table 18 Average statistical measures for each rainfall type at 6 runoff stations.

Station name	Type of rainfall	Average statistical values			
		r	EI (%)	RMSE	$RMSE_{peak}$
P.21	DGR	0.684	46.744	4.418	7.040
	DRR	0.766	65.781	3.545	5.612
	HRR	0.787	60.813	3.728	4.770
	HRRS	0.787	67.819	3.446	4.969
P.71	DGR	0.649	53.272	10.173	14.019
	DRR	0.779	61.907	8.179	8.839
	HRR	0.787	58.085	8.205	8.752
	HRRS	0.790	57.951	7.816	7.747
P.77	DGR	0.684	39.473	3.024	7.141
	DRR	0.726	46.932	3.520	6.577
	HRR	0.731	45.512	3.411	6.738
	HRRS	0.732	52.728	3.288	6.585
P.24A	DGR	0.637	53.746	3.190	7.407
	DRR	0.679	60.040	3.001	6.138
	HRR	0.697	66.679	2.674	6.552
	HRRS	0.700	67.337	2.665	6.493
P.73	DGR	0.927	87.186	48.594	71.697
	DRR	0.930	89.346	45.006	60.450
	HRR	0.929	90.244	43.882	61.310
	HRRS	0.932	91.682	42.957	61.428
P.14	DGR	0.654	25.195	27.970	47.558
	DRR	0.586	70.821	20.074	45.555
	HRR	0.632	64.812	21.279	37.743
	HRRS	0.629	72.047	19.172	40.434

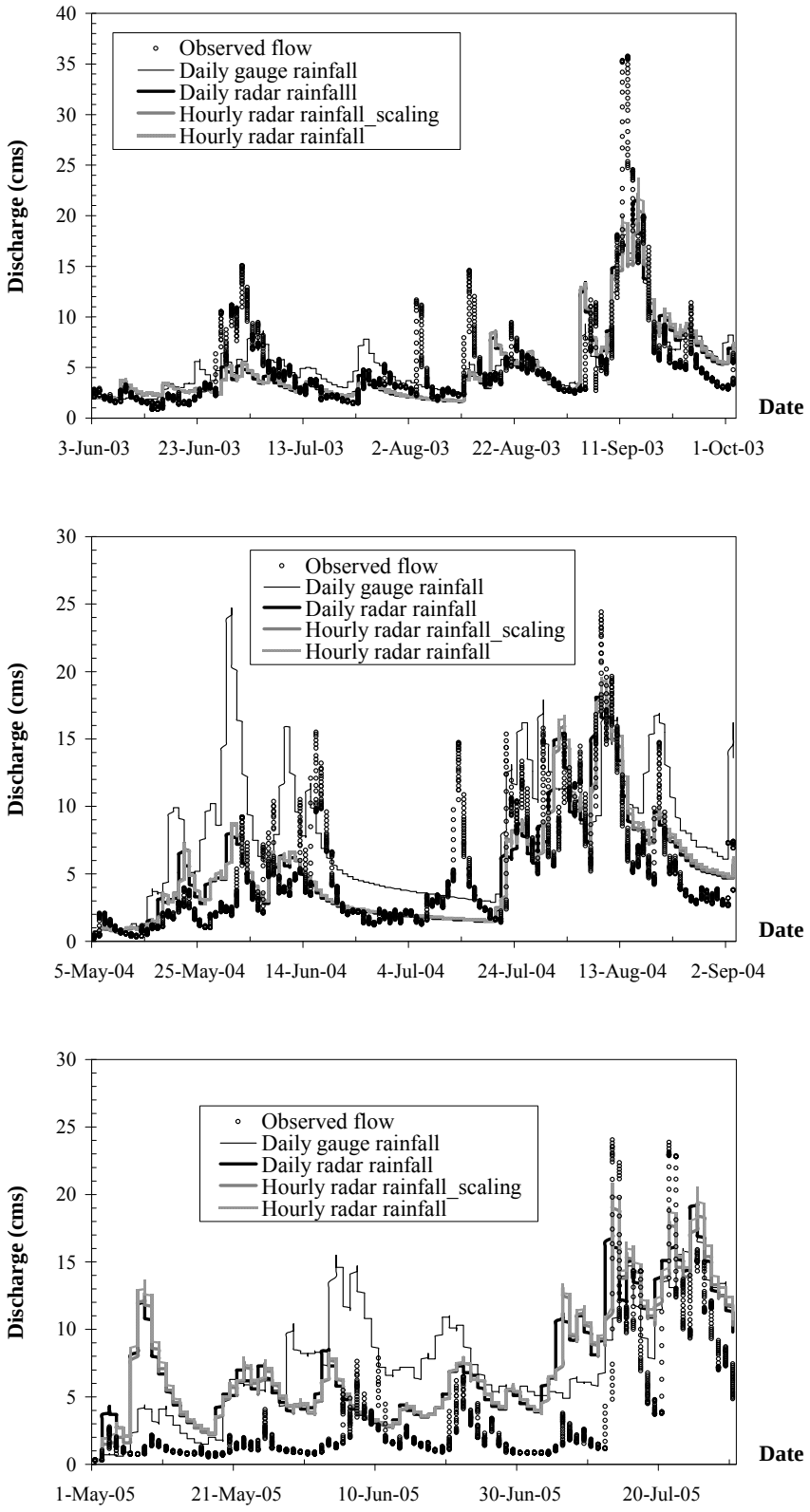

Figure 37 Observed and calculated flow hydrographs at the runoff station P.21.

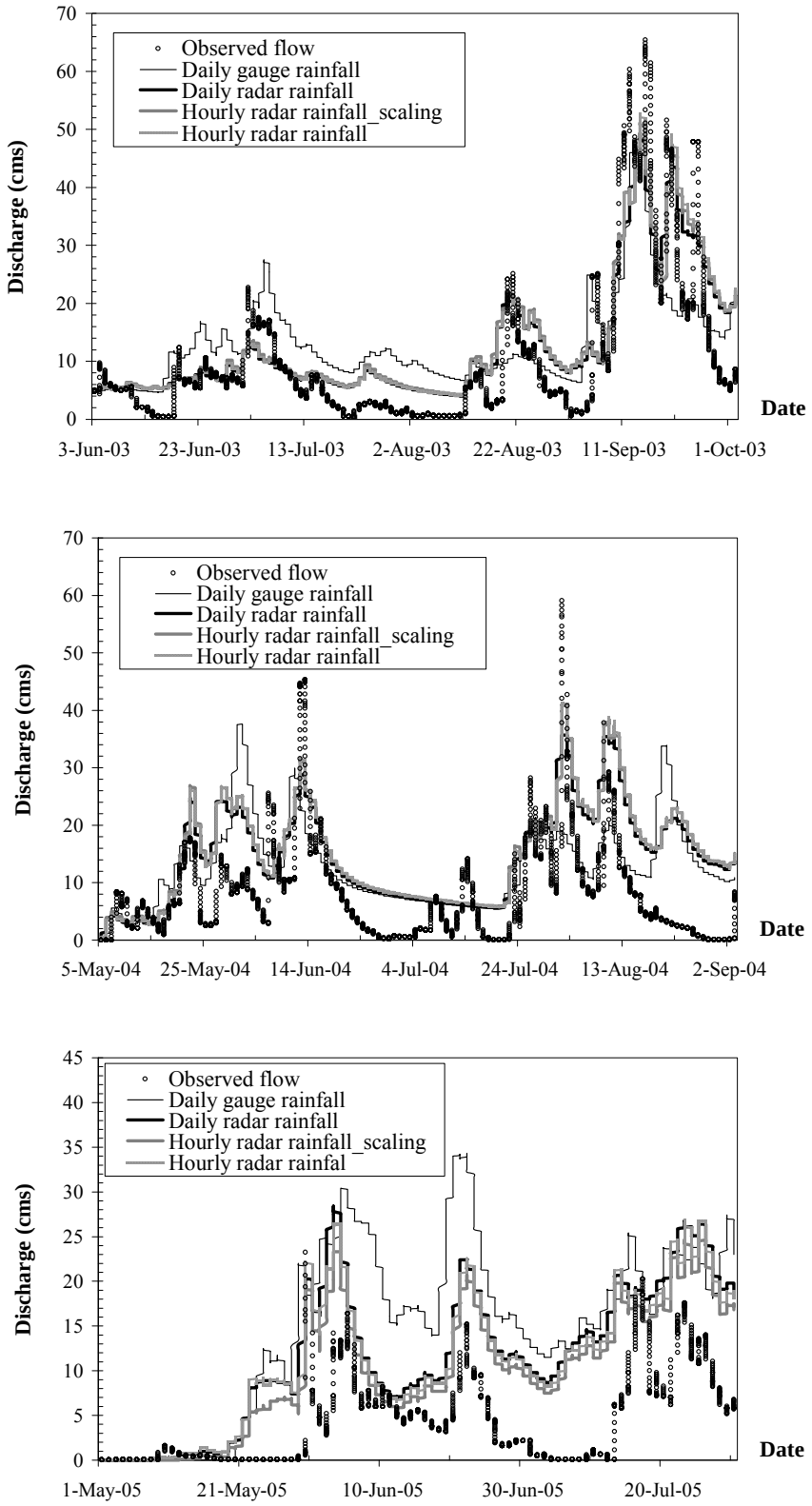

Figure 38 Observed and calculated flow hydrographs at the runoff station P.71.

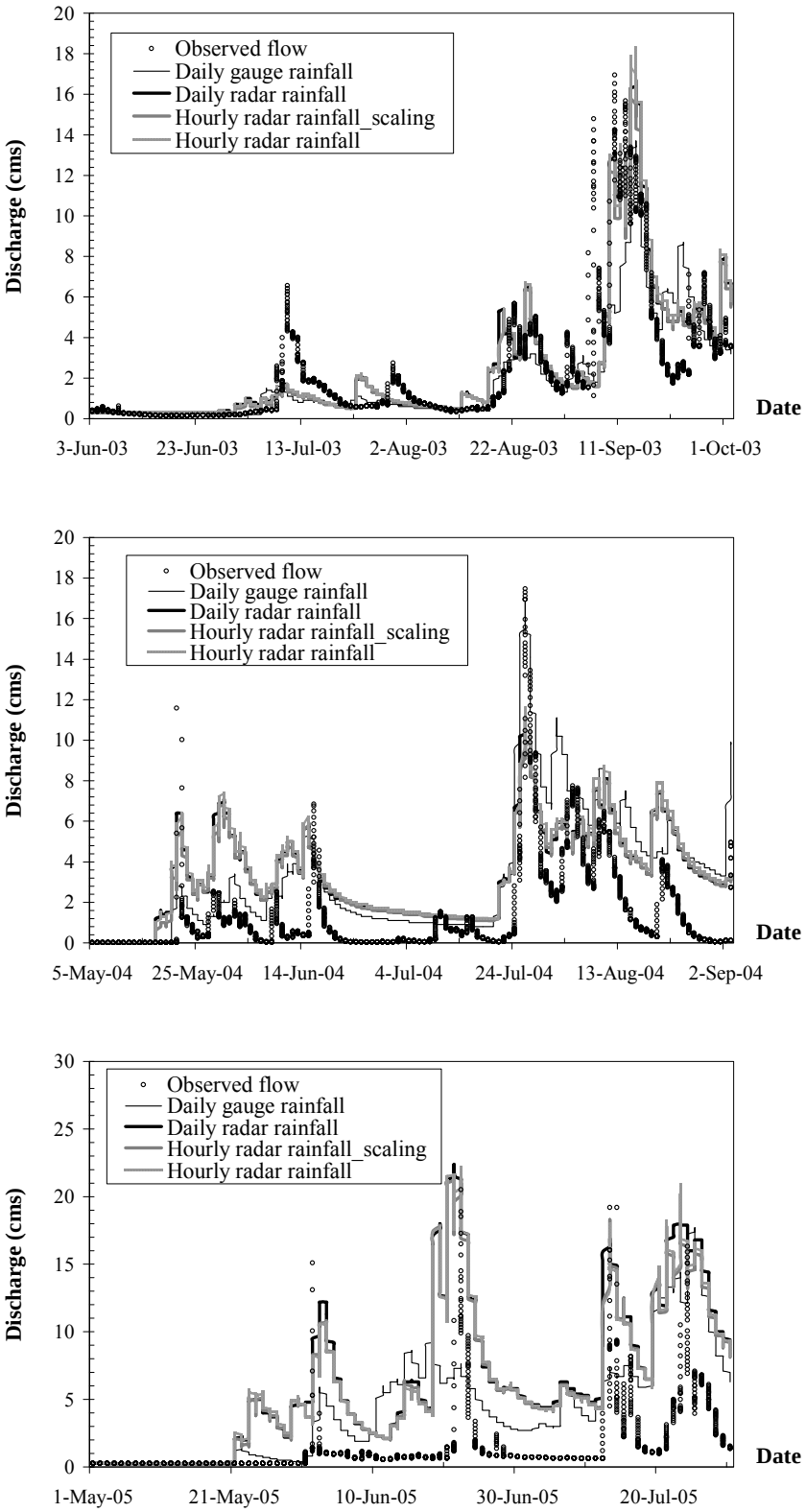

Figure 39 Observed and calculated flow hydrographs at the runoff station P.77.

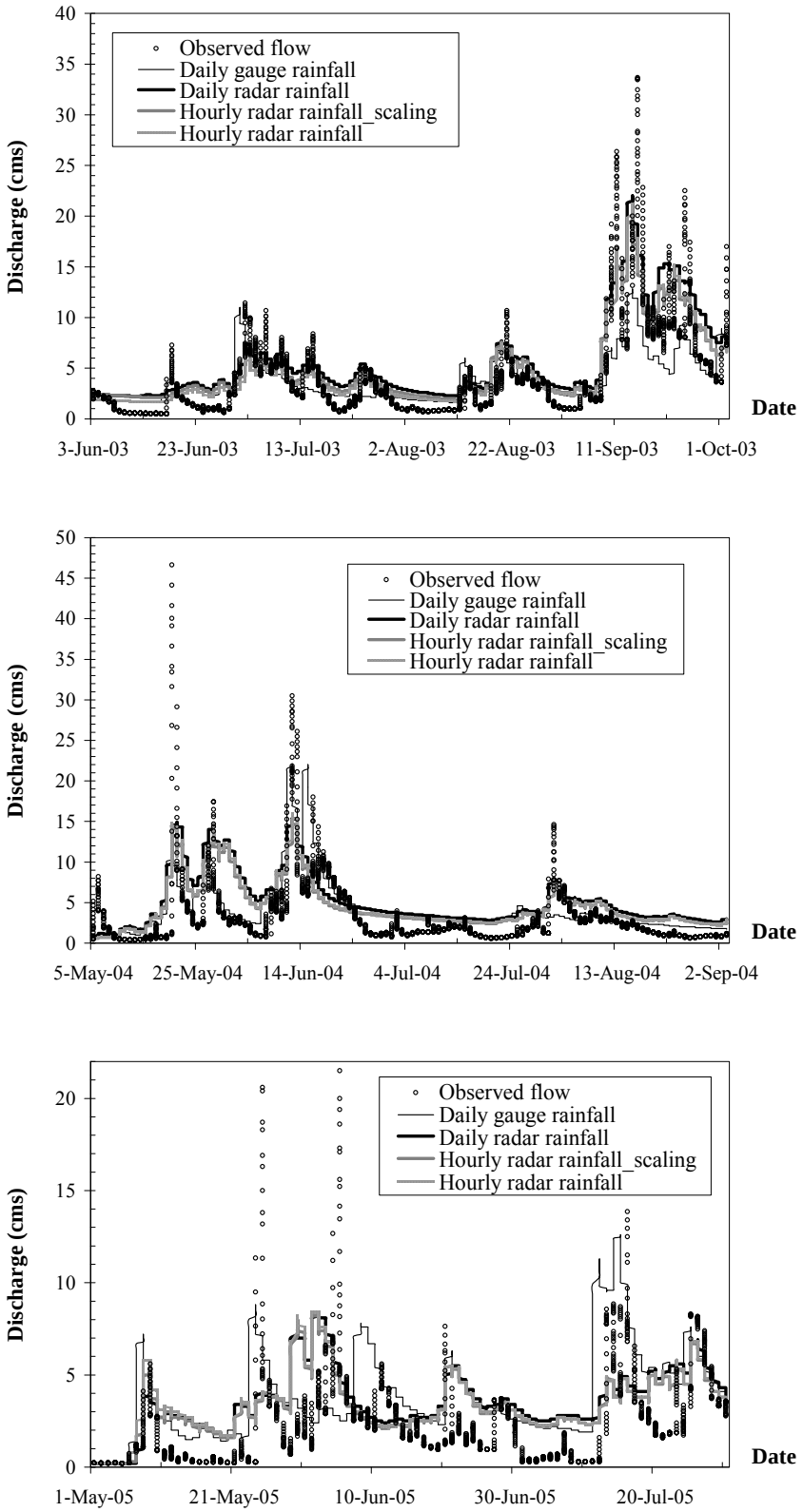

Figure 40 Observed and calculated flow hydrographs at the runoff station P.24A.

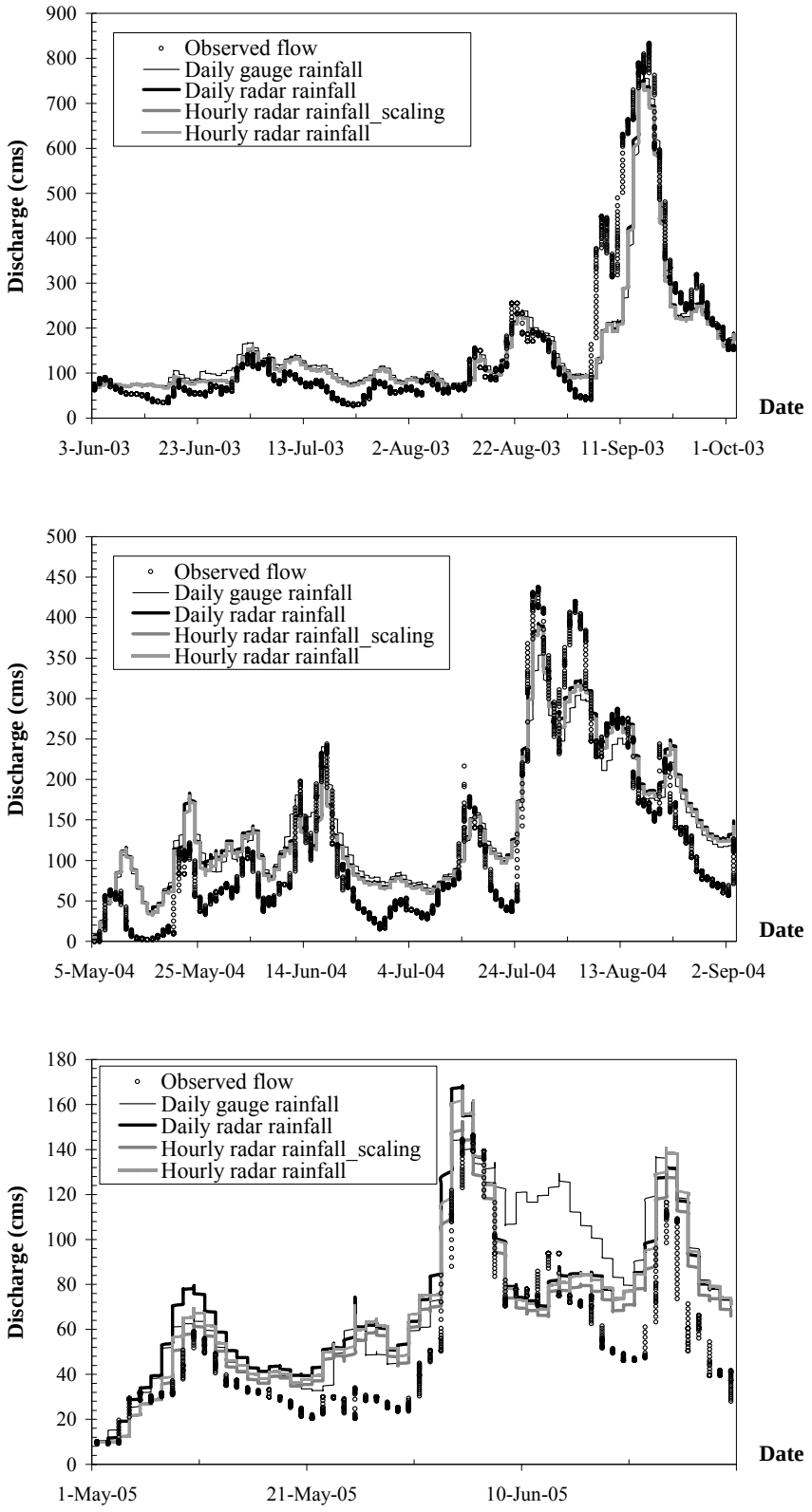

Figure 41 Observed and calculated flow hydrographs at the runoff station P.73.

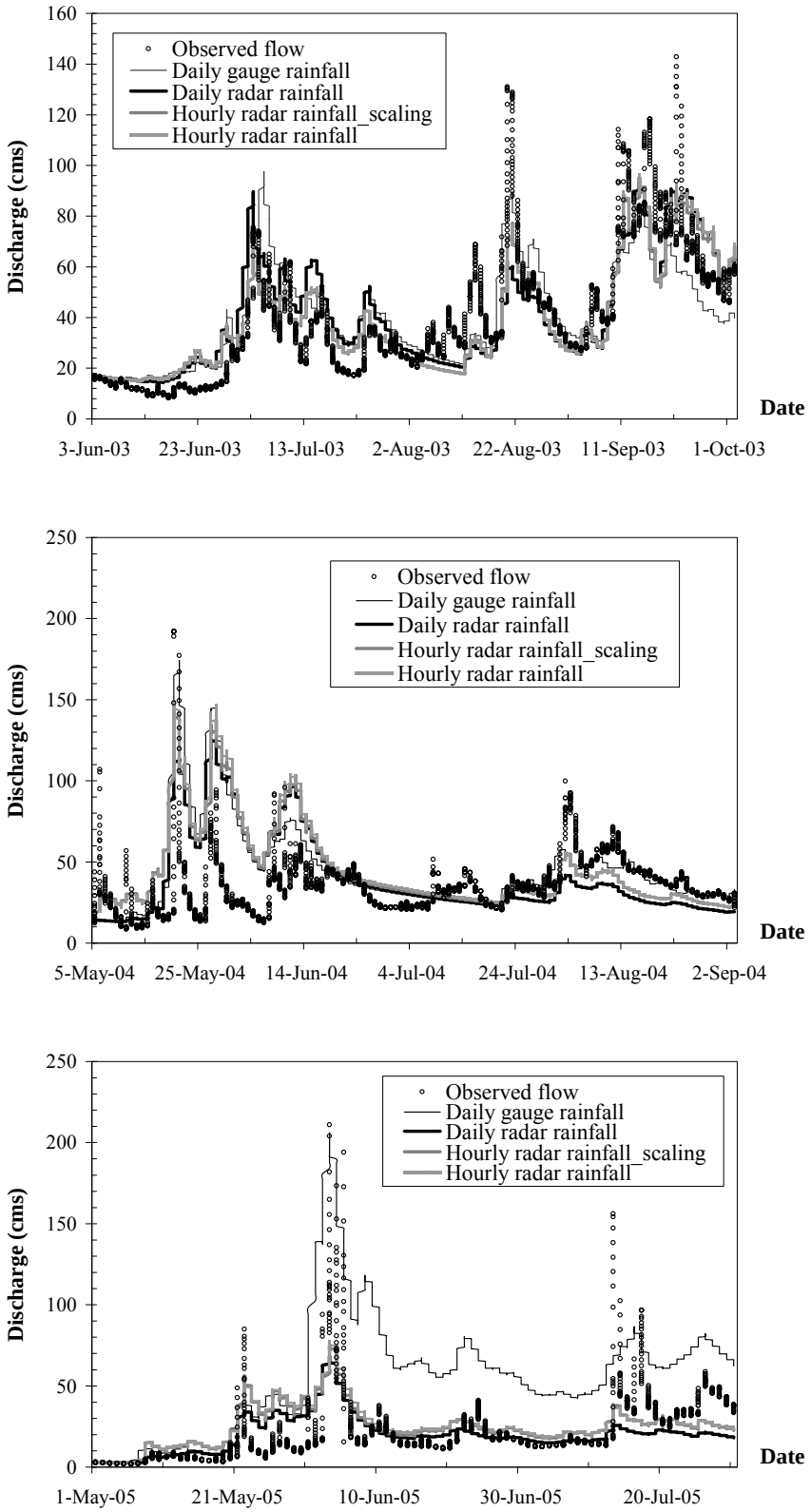

Figure 42 Observed and calculated flow hydrographs at the runoff station P.14.

5.2 Comparison of model performance using four different rainfall datasets

RMSE and $RMSE_{peak}$ were selected as the indicators to further evaluate the URBS model performance in runoff estimation using four different rainfall datasets as the input data. Table 19 shows the percent improvement in the accuracy of runoff estimation using each rainfall type compared with other types. It shows that $RMSE_{peak}$ calculated using the three types of radar rainfall are much lower than using the daily gauge rainfall (DGR) data at all runoff stations. The average value of percent improvement in $RMSE_{peak}$ for all events at all stations varies between 4.21% and 44.74% with the average of around 19.45%. Average values of percent improvement in $RMSE_{peak}$ of using DRR, HRR, and HRRS instead of DGR for all 6 stations are around 17.16%, 20.49%, and 20.73%, respectively. RMSE calculated using three types of radar rainfall are also lower than using DGR for 5 stations except for P.77. The average value of percent improvement in RMSE within 5 stations varies between 5.91% and 31.46% with the average of around 18.02%. Average values of percent improvement in RMSE of using DRR, HRR, and HRRS instead of DGR for 5 stations are around 16.18%, 16.95%, and 20.93%, respectively. These results confirm that all radar rainfall data (DRR, HRR, and HRRS) tends to produce more accurate runoff hydrographs (both overall hydrograph and peak flow) than the DGR. Moreover the HRRS and HRR also seem to provide a little more realistic results than the DRR, respectively.

The comparison between DRR and HRRS can be seen by the average values of percent improvement in RMSE of using HRRS instead of DRR for all 6 stations varying between 2.78% and 11.19% with the average of around 5.68%. However, $RMSE_{peak}$ of using HRRS instead of DRR improved only at stations P.21, P.71, and P.14 with the percent improvement of around 11.45%, 12.36%, and 11.24%, respectively, but reduced at stations P.77, P.24A, and P.73 with the percent reduction of around 0.13%, 5.79%, and 1.62%, respectively. The HRRS compared to the DRR therefore tends to improve the accuracy of the overall hydrograph better than the peak flow. On the other hand, the HRR does not have any consistency in improving the accuracy of both the overall hydrograph and peak flow compared to the

DRR, because there are both the percent improvement and reduction for RMSE and $RMSE_{peak}$ within those 6 stations. It can be concluded that we rather use DRR instead of HRR and use HRRS instead of DRR for runoff estimation.

The comparison between HRR and HRRS can be seen by the average values of percent improvement in RMSE of using HRRS instead of HRR for all 6 stations varying between 0.33% and 9.91% with the average of around 4.71%. On the other hand, the HRRS does not have any consistency in improving the accuracy of peak flow compared to the HRR, because there are both the percent improvement and percent reduction of $RMSE_{peak}$ within those 6 stations. The results confirm that using HRRS instead of using the HRR can improve the accuracy in overall hydrograph more consistency than the peak flow. The scaling logic is therefore an effective algorithm to be useful for preparing the HRRS and can be applied for improving the accuracy of the overall hydrograph better than the peak flow.

Table 19 Improvement of the hourly flow hydrograph estimates using daily gauge rainfall (DGR), daily radar rainfall (DRR), hourly radar rainfall without scaling logic (HRR), and hourly radar rainfall with scaling logic (HRRS) at varying runoff periods.

a) Runoff stations P.21

Overall root mean square error (RMSE – m^3/s)	2003	2004	2005	Average
DGR (1)	2.82	5.15	5.28	4.42
DRR (2)	3.12	2.82	4.69	3.54
(% improvement between (2) and (1))	(-10.66%)	(45.31%)	(11.11%)	(19.77%)
HRR (3)	3.15	2.86	5.18	3.73
(% improvement between (3) and (1))	(-11.49%)	(44.53%)	(1.93%)	(15.63%)
(% improvement between (3) and (2))	(-0.75%)	(-1.42%)	(-10.33%)	(-5.16%)
HRRS (4)	3.13	2.67	4.53	3.45
(% improvement between (4) and (1))	(-11%)	(48.08%)	(14.19%)	(22%)
(% improvement between (4) and (2))	(-0.31%)	(5.06%)	(3.46%)	(2.78%)
(% improvement between (4) and (3))	(0.44%)	(6.39%)	(12.5%)	(7.55%)
Average root mean square error of peak flow event ($RMSE_{peak}$ - m^3/s)	2003	2004	2005	Average
DGR (1)	8.62	5.45	7.06	7.04
DRR (2)	9.20	2.98	4.65	5.61
(% improvement between (2) and (1))	(-6.83%)	(45.25%)	(34.13%)	(20.29%)
HRR (3)	8.87	1.92	3.51	4.77
(% improvement between (3) and (1))	(-3%)	(64.66%)	(50.25%)	(32.24%)
(% improvement between (3) and (2))	(3.59%)	(35.44%)	(24.48%)	(15%)
HRRS (4)	8.96	2.31	3.63	4.97
(% improvement between (4) and (1))	(-4.01%)	(57.53%)	(48.52%)	(29.41%)
(% improvement between (4) and (2))	(2.64%)	(22.44%)	(21.85%)	(11.45%)
(% improvement between (4) and (3))	(-0.98%)	(-20.15%)	(-3.49%)	(-4.17%)

Table 19 (Continued)

b) Runoff stations P.71

Overall root mean square error (RMSE - m^3/s)	2003	2004	2005	Average
DGR (1)	8.33	9.69	12.50	10.17
DRR (2)	6.43	9.18	8.92	8.18
(% improvement between (2) and (1))	(22.75%)	(5.3%)	(28.6%)	(19.6%)
HRR (3)	6.59	9.69	8.34	8.21
(% improvement between (3) and (1))	(20.86%)	(0.1%)	(33.27%)	(19.35%)
(% improvement between (3) and (2))	(-2.44%)	(-5.5%)	(6.54%)	(-0.32%)
HRRS (4)	6.63	9.69	7.13	7.82
(% improvement between (4) and (1))	(20.36%)	(0.05%)	(42.99%)	(23.17%)
(% improvement between (4) and (2))	(-3.09%)	(-5.55%)	(20.15%)	(4.44%)
(% improvement between (4) and (3))	(-0.63%)	(-0.05%)	(14.56%)	(4.75%)
Average root mean square error of peak flow event ($RMSE_{peak}$ - m^3/s)	2003	2004	2005	Average
DGR (1)	19.87	13.37	8.82	14.02
DRR (2)	11.50	9.45	5.57	8.84
(% improvement between (2) and (1))	(42.13%)	(29.33%)	(36.83%)	(36.95%)
HRR (3)	10.07	9.06	7.13	8.75
(% improvement between (3) and (1))	(49.32%)	(32.23%)	(19.2%)	(37.57%)
(% improvement between (3) and (2))	(12.42%)	(4.1%)	(-27.91%)	(0.99%)
HRRS (4)	10.32	8.85	4.07	7.75
(% improvement between (4) and (1))	(48.07%)	(33.8%)	(53.83%)	(44.74%)
(% improvement between (4) and (2))	(10.26%)	(6.32%)	(26.91%)	(12.36%)
(% improvement between (4) and (3))	(-2.47%)	(2.31%)	(42.86%)	(11.48%)

Table 19 (Continued)

c) Runoff stations P.77

Overall root mean square error (RMSE - m^3/s)	2003	2004	2005	Average
DGR (1)	1.87	2.67	4.53	3.02
DRR (2)	1.63	2.54	6.39	3.52
(% improvement between (2) and (1))	(12.96%)	(4.73%)	(-40.99%)	(-16.4%)
HRR (3)	1.70	2.56	5.98	3.41
(% improvement between (3) and (1))	(9.47%)	(4.02%)	(-31.92%)	(-12.8%)
(% improvement between (3) and (2))	(-4.01%)	(-0.74%)	(6.44%)	(3.09%)
HRRS (4)	1.59	2.38	5.89	3.29
(% improvement between (4) and (1))	(15%)	(10.77%)	(-30.01%)	(-8.72%)
(% improvement between (4) and (2))	(2.35%)	(6.34%)	(7.79%)	(6.6%)
(% improvement between (4) and (3))	(6.11%)	(7.03%)	(1.44%)	(3.62%)
Average root mean square error of peak flow event ($RMSE_{peak}$ - m^3/s)	2003	2004	2005	Average
DGR (1)	5.03	3.80	12.59	7.14
DRR (2)	4.64	3.01	12.08	6.58
(% improvement between (2) and (1))	(7.77%)	(20.84%)	(4.04%)	(7.89%)
HRR (3)	5.07	3.03	12.11	6.74
(% improvement between (3) and (1))	(-0.74%)	(20.28%)	(3.77%)	(5.64%)
(% improvement between (3) and (2))	(-9.23%)	(-0.71%)	(-0.27%)	(-2.45%)
HRRS (4)	4.61	3.23	11.92	6.59
(% improvement between (4) and (1))	(8.42%)	(15.05%)	(5.32%)	(7.77%)
(% improvement between (4) and (2))	(0.7%)	(-7.31%)	(1.34%)	(-0.13%)
(% improvement between (4) and (3))	(9.09%)	(-6.55%)	(1.6%)	(2.26%)

Table 19 (Continued)

d) Runoff stations P.24A

Overall root mean square error (RMSE - m^3/s)	2003	2004	2005	Average
DGR (1)	3.21	3.40	2.96	3.19
DRR (2)	2.83	3.64	2.54	3.00
(% improvement between (2) and (1))	(11.93%)	(-7.06%)	(14.29%)	(5.91%)
HRR (3)	2.34	3.22	2.46	2.67
(% improvement between (3) and (1))	(26.97%)	(5.3%)	(16.93%)	(16.17%)
(% improvement between (3) and (2))	(17.07%)	(11.55%)	(3.08%)	(10.9%)
HRRS (4)	2.40	3.19	2.41	2.67
(% improvement between (4) and (1))	(25.27%)	(6.24%)	(18.59%)	(16.44%)
(% improvement between (4) and (2))	(15.15%)	(12.42%)	(5.02%)	(11.19%)
(% improvement between (4) and (3))	(-2.32%)	(0.98%)	(2%)	(0.33%)
Average root mean square error of peak flow event ($RMSE_{peak}$ - m^3/s)	2003	2004	2005	Average
DGR (1)	7.52	10.14	4.56	7.41
DRR (2)	4.18	8.67	5.56	6.14
(% improvement between (2) and (1))	(44.4%)	(14.51%)	(-22.01%)	(17.14%)
HRR (3)	5.23	8.75	5.68	6.55
(% improvement between (3) and (1))	(30.54%)	(13.66%)	(-24.53%)	(11.54%)
(% improvement between (3) and (2))	(-24.94%)	(-1%)	(-2.06%)	(-6.76%)
HRRS (4)	4.73	9.04	5.71	6.49
(% improvement between (4) and (1))	(37.2%)	(10.85%)	(-25.36%)	(12.34%)
(% improvement between (4) and (2))	(-12.96%)	(-4.28%)	(-2.74%)	(-5.79%)
(% improvement between (4) and (3))	(9.59%)	(-3.25%)	(-0.66%)	(0.91%)

Table 19 (Continued)

e) Runoff stations P.73

Overall root mean square error (RMSE - m^3/s)	2003	2004	2005	Average
DGR (1)	71.76	46.72	27.30	48.59
DRR (2)	66.95	43.76	24.32	45.01
(% improvement between (2) and (1))	(6.71%)	(6.34%)	(10.95%)	(7.38%)
HRR (3)	66.51	42.54	22.60	43.88
(% improvement between (3) and (1))	(7.32%)	(8.93%)	(17.24%)	(9.7%)
(% improvement between (3) and (2))	(0.66%)	(2.77%)	(7.07%)	(2.5%)
HRRS (4)	68.05	42.47	18.35	42.96
(% improvement between (4) and (1))	(5.17%)	(9.09%)	(32.79%)	(11.6%)
(% improvement between (4) and (2))	(-1.65%)	(2.94%)	(24.53%)	(4.55%)
(% improvement between (4) and (3))	(-2.33%)	(0.18%)	(18.79%)	(2.11%)
Average root mean square error of peak flow event ($RMSE_{peak}$ - m^3/s)	2003	2004	2005	Average
DGR (1)	112.27	94.06	10.76	72.36
DRR (2)	98.74	63.07	19.54	60.45
(% improvement between (2) and (1))	(12.05%)	(32.95%)	(-81.64%)	(16.46%)
HRR (3)	96.67	68.65	18.61	61.31
(% improvement between (3) and (1))	(13.9%)	(27.01%)	(-72.97%)	(15.28%)
(% improvement between (3) and (2))	(2.1%)	(-8.86%)	(4.77%)	(-1.42%)
HRRS (4)	102.23	68.85	13.21	61.43
(% improvement between (4) and (1))	(8.95%)	(26.8%)	(-22.73%)	(15.11%)
(% improvement between (4) and (2))	(-3.53%)	(-9.17%)	(32.43%)	(-1.62%)
(% improvement between (4) and (3))	(-5.75%)	(-0.29%)	(29.05%)	(-0.19%)

Table 19 (Continued)

f) Runoff stations P.14

Overall root mean square error (RMSE - m^3/s)	2003	2004	2005	Average
DGR (1)	15.12	26.97	41.81	27.97
DRR (2)	15.18	26.54	18.51	20.07
(% improvement between (2) and (1))	(-0.37%)	(1.62%)	(55.74%)	(28.23%)
HRR (3)	13.16	31.86	18.81	21.28
(% improvement between (3) and (1))	(12.96%)	(-18.13%)	(55.01%)	(23.92%)
(% improvement between (3) and (2))	(13.28%)	(-20.08%)	(-1.64%)	(-6%)
HRRS (4)	12.58	26.85	18.09	19.17
(% improvement between (4) and (1))	(16.85%)	(0.46%)	(56.74%)	(31.46%)
(% improvement between (4) and (2))	(17.15%)	(-1.18%)	(2.26%)	(4.5%)
(% improvement between (4) and (3))	(4.46%)	(15.74%)	(3.84%)	(9.91%)
Average root mean square error of peak flow event ($RMSE_{peak}$ - m^3/s)	2003	2004	2005	Average
DGR (1)	39.29	49.25	54.14	47.56
DRR (2)	38.77	42.40	55.50	45.56
(% improvement between (2) and (1))	(1.33%)	(13.9%)	(-2.51%)	(4.21%)
HRR (3)	23.67	48.08	41.48	37.74
(% improvement between (3) and (1))	(39.76%)	(2.37%)	(23.38%)	(20.64%)
(% improvement between (3) and (2))	(38.94%)	(-13.39%)	(25.25%)	(17.15%)
HRRS (4)	33.55	40.66	47.09	40.43
(% improvement between (4) and (1))	(14.61%)	(17.43%)	(13.02%)	(14.98%)
(% improvement between (4) and (2))	(13.45%)	(4.1%)	(15.15%)	(11.24%)
(% improvement between (4) and (3))	(-41.75%)	(15.43%)	(-13.52%)	(-7.13%)

CONCLUSION AND RECOMMENDATIONS

The conclusion and recommendation for the study on "Applications of rain gauge and radar rainfall to a hydrological model for flood estimation" are described as in the followings.

1. Hydrological model selection

The first objective of this study is to select the most suitable hydrologic model for flood estimation among four well known hydrological models namely NAM, HEC-HMS, URBS, and SWAT models. The selection criteria were set and the scores were given to each criterion and model. The results show that the URBS model obtains the highest total score but it is not much higher than the other three models. However, a special training opportunity given by the experts on the URBS model application at the Water Resources Department encouraged the author to finally choose the URBS model for further study.

2. Testing the URBS model performance and extending its application to the ungauged catchments

After the URBS model was chosen for flood estimation, it was applied to simulate flood hydrographs at P.20, P.4A, P.28, P.21, and P.71 stations using rain gauge rainfall as the input data. The NAM model, which has been accepted for flood estimation world wide, was also applied at these 5 stations. These two models have shown promising results of flood hydrograph estimations which are very close to the observed data. The URBS model was later applied at other 6 stations in the study basin. To be able to extend the model application on the ungauged catchments in the upper Ping rive basin, the ungauged relationships between its parameters and catchment characteristics were formulated. Since there are only 4 model parameters (α, β, PR and IF) needed for the URBS model for flood estimation, these parameters was therefore used to formulate the ungauged relationships for flood estimation of the ungauged catchments in the upper Ping river basin. Four catchment

characteristics consisting of the catchment area (A), main channel length (L), main channel length from the centroid (L_c), and channel slope (S) were recommended to be suitable for creating the relationships with the 4 parameters in this study. Four proposed relationships for estimating the URBS model parameters PR, IF, α and β for ungauged catchment in the upper Ping river basin are presented in Equations. (93) to (96), respectively. For the application of the proposed ungauged relationships for flood estimation in the upper Ping river basin, it is evident that the proposed ungauged relationships can be efficiently applied for flood estimation only for the ungauged catchments which are the sub-catchments of the 11 stations used for formulating the ungauged relationships.

It should be recommended that the form of the ungauged relationships possibly vary depending on the catchment and flood characteristics, which are used in formulating the relationships. The methodology used in formulating the ungauged relationships proposed in this study should be performed in other catchments in Thailand's river basins to find out the efficiency of the proposed method that would be a helpful tool for flood estimation of the ungauged catchments in Thailand.

3. Climatological Z-R Relationship for Radar Rainfall Estimation in the upper Ping river basin

Since most of rainfall stations located in and around the upper Ping river basin are non-automatic stations, the climatological Z-R relationship was therefore determined by uses of daily gauge rainfall at 42 stations and the reflectivity data at the Omkoi radar station. During the calibration procedure, parameter A was adjusted to minimize four statistical measures comprising the Mean Error, Mean Absolute Error, Root Mean Square Error, and Bias, whereas parameter b was set as a constant of 1.6. The results show that the climatological Z-R relationship as in the form of $Z=74R^{1.6}$ give more accurate results of mean daily radar rainfall than the conventional relationship of $Z=200R^{1.6}$ used for the Omkoi radar can provide. The climatological Z-R relationship of $Z=74R^{1.6}$ is therefore the appropriate equation for radar rainfall assessment in the upper Ping river basin. Within the calibration period (between June

and October in 2003 and 2004), this relationship produced the minimum Mean Error, Mean Absolute Error, Root Mean Square Error, and Bias of approximately -1.23, 2.30, 3.14, and 1.25 mm, respectively. Daily radar rainfall in 2003 and 2004 were then computed using this relationship and were compared to the daily gauge rainfall in the form of time series plot. Even the estimated radar rainfall tend to be a bit lower than the gauge rainfall; the overall results are acceptable with the correlation coefficient between the estimated radar and gauge rainfall of around 0.857 and 0.912, respectively.

It should be noted that this study aims to investigate the suitable Z-R relationship for daily radar rainfall estimation in the upper Ping river basin to reduce some radar rainfall errors caused by Z-R conversion. This proposed climatological relationship ($Z=74R^{1.6}$) represents the average relationship for Omkoi radar station and can also be used as an initial relationship to convert measured reflectivity into daily radar rainfall. However, the parameters A in the Z-R relationship usually change in both space and time; the applications of the proposed relationship to estimate daily rainfall at different storm events especially in real time environment possibly have a number of uncertainties. To improve the accuracy of radar rainfall, the estimated radar rainfall calculated by the proposed Z-R relationship should be adjusted by applying a mean field bias correction technique (Battan, 1973; Wilson, 1970; Brandes, 1975; Collinge, 1991; Seo and Breidenbach, 2002; Chumchean *et al*., 2006). The adjusted radar rainfall will then be used as the input data for the selected rainfall-runoff model for flood estimation in the upper Ping river basin.

4. Effect of rain-gauge temporal resolution on the specification of a Z-R relationship

To study the effect of using rain gauge data of different temporal resolutions for calibrating climatological Z-R relationships, different climatological Z-R relationships were estimated using rainfall aggregated over 1 to 24 hours. Weather radar - which has sufficient continuous tipping-bucket gauge stations located within the radar range - was selected for the analysis. This study, radar reflectivity data from

the Kurnell, the Mt Stapylton, and the Pasicharoen radars located in Sydney, Brisbane, and Bangkok, respectively, and corresponding rain gauges data in the three cities, were used in the analysis. From the results, it can be concluded that the A parameters of the Z-R relationship of Sydney, Brisbane, and Bangkok radar stations tend to decrease with a decrease in the rainfall temporal resolution. The decrease in the A parameters can be described through a simple scaling law and a scaling transformation function derived. The scaling exponents for five datasets representing three locations (Sydney, Brisbane, and Bangkok) are lie in the vicinity of 0.055. Hence a climatological scaling law with exponent equal to 0.055 is proposed.

Since the Sydney and Bangkok radars are the C-band radars - which attenuation is considered to be a severe problem for measurement of high-intensity rainfall - the impact of attenuation on the temporal scaling relationship was therefore investigated. The results can be concluded that attenuation might have some effects on the climatological scaling component for C-band radar at far range from the radar site; however, scaling hypothesis appears to be valid for the S-band radar.

For the verification of the proposed scaling transformation function, it found that the equation with scaling exponent 0.055 exhibits significant improvements in estimating extreme rainfall, especially at fine temporal resolutions, in contrast to the accuracy obtained when using the A parameter that is based on 24 hour rainfall. For the extreme rainfall, this accuracy decreases as one proceeds to higher resolutions.

Finally, it can be concluded that the proposed scaling relationship is consistent across multiple locations but exhibits variations with range in radars where attenuation is a significant issue. The use of this relationship is promising especially in locations with limited short-duration rain gauge measurements and attenuation corrected radar measurements.

5. Improvement in runoff estimation accuracy using radar

The highlight of this research for improving an accuracy of flood estimation using radar rainfall approximation at selected runoff stations (P.21, P.71, P.77, P.24A, P.73, and P.14) in the upper Ping river basin is explained in this item. An investigation was carried out by using the daily gauge rainfall, and the daily and hourly radar rainfall as the input data for the URBS model. The areal daily gauge rainfall (DGR) for each sub-catchment was approximated using the Thiessen polygon technique. The daily radar rainfall (DRR) was calculated using the proposed Z-R relationship at the Omkoi radar ($Z=74R^{1.6}$) and the mean field bias correction method. The hourly radar rainfall without scaling logic (HRR) was estimated using the update daily Z-R relationship which was changed with day depending upon the mean field bias used for correcting daily radar rainfall. Finally, the scaling transformation equation ($A_t = (t/24)^{-0.055} A_{24}$) was applied to the update daily Z-R relationship for hourly radar rainfall (HRRS) estimation.

Results of flood estimates using the 4 rainfall types show that the accuracy of overall hydrograph and peak flow estimated using all radar rainfall data (DRR, HRR, and HRRS) are generally higher than that of estimated using the DGR data, respectively. The results have therefore confirmed an ability of the weather radar rainfall to be used to as the input data for improving the accuracy of runoff estimation in the upper Ping river basin, where continuous gage rainfall measurement is unavailable and the available daily rain gages are sparsely distributed. Additionally, the use of HRR cannot produce better results of runoff hydrograph than the use of DRR. On the other hand, the HRRS has already proved its ability to be used to improve the accuracy of runoff estimates, especially the overall hydrographs. The scaling logic is therefore necessary to be applied to prepare the HRRS for the situation like the upper Ping river basin, where daily Z-R relationship is only available.

LITERATURE CITED

Anagnostou, E. N., W. F. Krajewski, D.-J. Seo, and E. R. Johnson, 1998. Mean-field radar rainfall bias studies for WSR-88D, **ASCE J. Hydrol. Eng.**, 3(3), 149–159.

Andrieu, H. and J.D. Creutin. 1995. Identification of vertical profiles of radar reflectivity for hydrological applications using an inverse method. Part I: Formulation. **J. Appl. Meteorol.** 34: 225-239.

Atlas, D. 1964. **Advances in radar meteorology**. Advances in geophysics, Ed. Atlas, D., Academic press, New York, U.S.A., pp 318-478.

Atlas, D. and C.W. Ulbrich. 1977. Path- and area-integrated rainfall measurement by microwave attenuation in the 1-3 cm band. **J. Appl. Meteorol.** 16: 1322–1331.

Arcelus, E.A. 2000. Coupling Two Hydrological Models to Compute Runoff in Ungauged Basins. **Journal of Hydrology** 101: 301-309.

ASCE. 1996. **Handbook of hydrology**, ASCE Manual and Rep. on Engineering Practice No. 28, New York.

Austin, P. 1987. Relation between measured radar reflectivity and surface rainfall. Mon. **Weather Rev.** 115: 1053-1071.

Battan, L.J. 1973. **Radar Observation of the Atmosphere.** University of Chicago Press, Chicago, 324 pp.

Bennett, T.H. 1998. **Development and application of a continuous soil moisture accounting algorithm for the Hydrologic Engineering Center Hydrologic Modeling System (HEC-HMS)**. MS thesis, Dept. of Civil and Environmental Engineering, University of California, Davis.

Bevan, K.J. and G.M. Hornberger. 1982. Assessing the effect of spatial pattern of precipitation in modelling stream flow hydrograph. **Water Resour. Bull** 18: 823-829.

Borga, M., E.N. Anagnostou and F. Enrico. 2000. On the use of realtime radar rainfall estimates for flood prediction in mountainous basins. **J. Geophys. Res.** 105 (D2), 2269–2280.

Boughton, W.B. 1993. A hydrograph based model for estimating the water yield of ungauged catchments. **Hydrology & Water Resources Symposium**, Newcastle.

Boyd, M.J., M.C. Bufill and R.M. Knee. 1993. Pervious and impervious runoff in urban catchments. **Hydrological Services Journal** 38, 6, Dec. 1993.

Boyd, M.J. 1987. **WBNM: A general runoff routing model – programs and user manual**. University of NSW, Water Resources Laboratory, Report No. 170.

Brandes, E.A. 1975. Optimising rainfall estimates with the aid of radar. **J. Appl. Meteorol** 14: 1339-1345.

Breit, G. and M.A. Tuve. 1926. A test for the existence of the conducting layer. **Phys. Rev.** 28: 554-575.

Burrows, D.R. and S.S. Attwood. 1949. **Radio Wave Propagation**. Academic Press, 219 pp.

Carroll. D.G. 2004. **URBS a Rainfall Runoff Routing Model for flood forecasting & design**. version 4.00. 168 p.

Collier, C. G. 1996. **Applications of Weather Radar System: A Guide to Uses of Radar in Meteorology and Hydrology**. John Wiley & Sons, Newyork, 383 pp.

Collinge, V.K. and C. Kirby. 1987. **Weather radar and flood forecasting**, John Wiley & Sons, Great Britain, England.

Chapra, S.C. and R. P. Canale. 2002. **Numerical Methods for Engineers**. McGraw-Hill Book Company, New York.

Chaudhry, H.C. 1993. **Open-channel hydraulics**. Prentice Hall, NJ.

Chow, V.T. 1959. **Open channel flow**. McGraw-Hill, New York, NY.

Chow, V.T., D.R. Maidment and L.W. Mays. 1988. **Handbook of Applied Hydrology**. McGraw-Hill, New York.

Chumchean, S. 2004. **Improved Estimation of Radar Rainfall for Use in Hydrological Modelling**. Ph.D Thesis. University of New South Wales, Sydney, Australia.

——, A. Sharma and A.W. Seed. 2003. Radar rainfall error variance and its impact on radar rainfall calibration. **J. Phys. Chem. Earth** 28: 27-39.

——, A. Seed and A. Sharma. 2004. Application of scaling in radar reflectivity for correcting range dependent bias in climatological radar rainfall estimates. **J. Atmos. Oceanic Technol**. 21: 1545–1555.

Chumchean, S., A. Seed and A. Sharma. 2006a. Correcting of real-time radar rainfall bias using a Kalman filtering approach. **J. Hydrology.** 317: 123–137.

——, A. Sharma and A. Seed. 2006b. An Integrated Approach to Error Correction for Real-Time Radar-Rainfall Estimation. **J. Atmos. Oceanic Technol.** 23: 67–79.

——, A. Sharma and A. Seed. 2008. An operational approach for classifying storms in real time radar rainfall estimates. **J. Hydrology**. 363: 1-17

Clift, G.A. 1985. **Use of radar in meteorology**. WMO Technical Note No. 181, World Meteorological Organisation, Geneva, 90 pp.

Collier, C.G. 1996. **Applications of Weather Radar System**. A Guide to Uses of Radar in Meteorology and Hydrology, John Wiley & Sons, Newyork, 383 pp.

Collinge, V.K. 1991. **Weather radar calibration in real time**: Prospects for improvement. In: Hydrology Applications of Weather Radar, Eds. Cluckie, I. D. and Collier, C. G., Ellis Horwood, Chinchester. U.K., pp 25-42.

Collinge, V. K. and C. Kirby. 1987. **Weather radar and flood forecasting**. John Wiley & Sons, Great Britain, England.

Danish Hydraulic Institute (DHI). 1990. **NAM documentation and user's guide**. 70 p.

Delrieu, G., H. Andrieu and J.D. Creutin. 2000. Quantification of path-integrated attenuation for X- and C-band weather radar systems operating in Mediterranean heavy rainfall. **J. Appl. Meteorol.** 39: 840-850.

Doviak, R.J. and D.S. Zrnic. 1992. **Doppler Radar and Weather Observations**. Acadamic Press Inc., Orlando, Florida, U.S.A., 545 pp.

Doelling, I.G., J. Joss and J. Riedl. 1998. Systematic variations of Z-R relationships from drop size distributions measured in northern Germany during seven years. **Atmos. Res.** 47-48: 635-649.

Fabry, F., A. Bellon, M.R. Duncan and G.L. Austin. 1994. High resolution rainfall measurements by radar for very small basins: the sampling problem reexamined. **J. Hydrol.** 116: 415-428.

——, G. L. Austin and D. Tees. 1992. The accuracy of rainfall estimates by radar as a function of range. Q.J.R. **Meteorol. Soc** 118: 435-453.

——, F and I. Zawadzki. 1995. Long-term radar observations of the melting layer of precipitation and their interpretation. **J. Atmos. Sci** 52: 838-861.

Fields, G., A. Seed, B. Yu and T. Malone. 2004. Calibration of Weather Radar in South East Queensland. **Sixth International Symposium on Hydrological Applications of Weather Radar**, Melbourne, Australia

Fulton, R.A., J.P. Breidenbach, D.J. Seo, D.A. Miller and T. O'Brannon. 1998. The WSD-88D rainfall algorithm. **Wea. Forecasting** 13: 377–395.

Gabella, M. and G. Perona. 1998. Simulation of the orographic influence on weather radar using geometric-optics approach. **J. Atmos. Oceanic Technol**. 15: 1485-1494.

Goovaerts, P. 2000. Geostatistical approaches for incorporating elevation into the spatial interpolation of rainfall. **J. Hydrol.**, 228, 113–129.

Green, W.H. and G.A. Ampt. 1911. The flow of air and water through soils. **Journal of Agricultural Sciences** 4:11-24.

Gupta, V.K. and E.C. Waymire. 1990. Multiscaling properties of spatial rainfall and river flow distribution. **J. Geophys. Res.** 95: 1999–2009.

Hamlin, M.J. 1983. The significance of rainfall in the study of hydrological processes at basin scale. **J. Hydrol**. 65: 73-94.

Hagen, M. and S.E. Yuter. 2003. Relations between radar reflectivity, liquid water content, and rainfall rate during the MAPSOP. **Quarterly J. Royal Meteorol. Soc**. 128: 477-494.

Hildebrand, P.H. 1978. Iterative correction for attenuation of 5 cm radar in rain. **J. Appl. Meteor.** 17: 508–514.

Hitschfeld, W.F. 1986. The invention of radar meteorology. **Bull. Am. Meteorol. Soc.** 67, No. 1, 33-37.

Hitchfeld, W. and J. Bordan. 1954. Errors inherent in the radar measurement of rainfall at attenuating wavelengths. **J. Appl. Meteorol.** 11: 58-67.

Horton, R.E. 1919. Rainfall interception. **Monthly Weather Rev** 147: 603–623.

——. 1933. The role of infiltration in the hydrologic cycle. **Trans., Am. Geophys. Union** 145: 446–460.

——. 1935. **Surface runoff phenomena, Part 1—Analysis of hydrograph**. Horton Hydrology Laboratory Publication No. 101, Voorheesville, N.Y.

——. 1939. Analysis of runoff plot experiments with varying infiltration capacities. **Trans., Am. Geophys. Union** 20 (IV): 683–694.

Hursh, C. R. 1936. Storm water and absorption. **Trans., Am. Geophys. Union** 17 (II): 301–302.

Hursh, C.R., and E.F. Brater. 1944. Separating hydrographs into surface- and subsurface-flow. **Trans., Am. Geophys. Union** 25: 863–867.

Hydrologic Engineering Center (HEC). 2000. **Hydrologic modeling system HEC-HMS user's manual, version 2**. Engineering, U.S. Army Corps of Engineers, Davis, Calif.

Jordan, P., A. Seed, P. May and T. Keenan. 2004. Evaluation of dual polarization radar for rainfall runoff modeling-A case study in Sydney, Australia. **6th International symposium on hydrological applications of weather radar**, Melbourne, Australia.

Joss, J. and A. Waldvogel. 1970. A method to improve the accuracy of radar measured amounts of precipitation. **Preprints, 14th Radar Meteorology Conf**., Tucson, AZ, Amer. Meteor. Soc., 237–238.

Keulegan, G. H. 1944. Spatially variable discharge over a sloping plane. **Trans., Am. Geophys.** Union 25 (VI): 959–965.

Kitchen, M., R. Brown and A.G. Davies. 1994. Real-time correction of weather radar for the effects of bright band, range and orographic growth in widespread precipitation. **Q.J.R. Meteorol. Soc** 120: 1231-1254.

Klaassen, W. 1988. Radar observations and simulations of the melting layer of precipitation. **J. Atmos. Sci** 45: 3741-3753.

Klazura, G. E. 1981. Differences between some radar-rainfall estimation procedures in a high rain rate gradient storm. **J. Appl. Meteor**. 20: 1376–1380.

Knudsen, J., A. Thomsen and J.C. Refsgaard. 1986. WATBAL, a semi-distributed, physically-based hydrological modelling system. **Nordic Hydrol.** 17: 347-362.

Krajewski, W. F. and J. A. Smith. 2002. Radar hydrology: Rainfall estimation. **Adv. Water Resour.** 25: 1387–1394.

Krause, P., D.P. Boyle and F. Base. 2005. Comparison of different efficiency criteria for hydrological model Assessment. **Advances in Geosciences**. 5: 89–97.

Kwanyuen, B. and C. Poowarakulchai. 2003. Comparison of HEC-HMS Models and TOP Model for runoff prediction in Lampachi Basin. **Kamphaengsaen Acad. J**. 1 (1): 49-55.

Laurenson, E.M. and R.G. Mein. 1990. **RORB - Version 4 Runoff Routing Program User Manual**. Monash University, Dept of Civil Engineering.

Linsley, R.K., M.A. Kohler and J.L.H. Paulhus. 1982. **Hydrology for engineers**. McGraw-Hill, New York, NY.

Lowdermilk, W.C. 1934. Forests and streamflow: A discussion of Hoyt-Trozell report. **J. Forestry** 21: 296–307.

Madsen, H. 2000. Automatic Calibration and Uncertainty Assessment in Rainfall-Runoff Modelling. **Joint Conference on Water Resources Engineering and Water Resources Planning & Management**, 1-10.

Malone, T. 1999. Flood Forecasting in North Queensland. **International Workshop on Flood Forecasting for Tropical Regions**, Malaysia.

Malone, T. 2000. **Streamflow Routing Techniques in Large Rivers in Queensland**. In WMO project: Intercomparison of Forecast Models for Streamflow Routing in Large Rivers.

——, A. Johnston, J. Perkins and S. Sooriyakumaran. 2003. Australian Bureau of Meteorology, HYMODEL – A Real-time Flood Forecasting System. **International Hydrology and Water Resources Symposium**, The Instituation of Engineers, Australia.

—— and I. Cordery. 1989. An Assessment of Network Models in Flood Forecasting. **New Directions in Surface Water Modelling**, IAHS Publ. No. 181.

Manley, R.E. 1974. **Catchment models for river management**. MSc Thesis, University of Birmingham.

Marshall, J.S. and W.M. Palmer. 1948. The distribution of raindrops with size. **J. Meteorol.** 5: 165-166.

Marshall, J.S. 1969. Power-law relations in radar meteorology. **J. Appl. Meteorol**. 8: 171-172.

Mandelbrot, B. B. 1982. **The Fractal Geometry of Nature**. W. H. Freeman, 460 pp.

Markar, S. 2001. **Person communication recovering initial loss model**.

Menabde, M., A. Seed, and G. Pegram. 1999. A simple scaling model for extreme rainfall. **Water Resour. Res**. 35: 335–339.

Nash J.E. and J.V. Sutcliffe. 1970. River flow forecasting through conceptual models, part 1 – A discussion of principles. **J. Hydrol** 10: 282-290.

Neitsch, S.L., J.G. Arnold, J.R. Kiniry, R. Srinivasan and J.R. Williams. 2002. **Soil and Water Assessment Tool User's Manual**, Version 2000.

Neitsch, S.L., J.G. Arnold, J.R. Kiniry, R. Srinivasan and J.R. Williams. 2002. **Soil and Water Assessment Tool Reference's Manual**, Version 2000.

Nielsen, S.A. and E. Hansen. 1973. Numerical simulaton of the rainfall-runoff process on a daily Basic. **Nordic Hydrology** 4: 171-190.

Paiva, J. 1993. **Finniss River floodplain mapping**. Report 21/93 of Power and Water Authority, Water Resources Division, Australia. 22pp.

Pawattana, C., N.K. Tripathi and S. Weesakul. 2007. Floodwater retention planning using GIS and hydrodynamic model: a case study for the Chi River Basin, Thailand. **Environmental Informatics Archives** 5: 548-556

Pengel, B., T. Malone, S. Tes, P. Katry, S. Pich and M. Hartman. 2007. Towards a new flood forecasting system for the lower Makong river basin. **3rd South-East Asia Water Forum**, Malaysia.

Pessoa, M.L., L.B. Rafael and R.W. Earle. 1993. Use of weather radar for flood forecasting in the Sieve river basin: a sensitivity analysis. **J. Appl. Meteorol.** 32, 462–475.

Peters, J. and D. Easton. 1996. Runoff simulation using radar rainfall data. **Water Resources Bulletin, AWRA**. 32(4): 753-760.

Poomthaisong, A. 1997. **Flood control investigation of upper Nam river Yot and Yao tributaries**. Thesis, Asian Institute of Technology, Bangkok, Thailand.

Probert-Jones, J. R. 1962. The radar equation in meteorology. **Q.J.R. Meteorol. Soc**. 88: 23-36.

Rawls, W.J. and D.L. Brakensiek. 1982. Estimating soil water retention from soil properties. **Journal of the Irrigation and Drainage Division, ASCE**. 108(IR2): 166-171.

Rayleigh, L. 1871. On the scattering of light by small particles. **Phil. Mag**. 41: 447-452.

Refsgaard, J.C. and J. Knudsen. 1996. Operational validation and intercomparison of different types of hydrological models. **Water Resour. Res**. 32 (7): 2189-2202.

Rinehart, R.E. 1991. **Radar for Meteorologist, Univ. of North Dakota Press**. Grand Forks, North Dakota, U.S.A., 333 pp.

Russo, F., F. Napolitano and E. Gorgucci. 2005. Rainfall monitoring systems over an urban area: the city of Rome. **Hydrological Processes** 19: 1007–1019.

Seed, A. and G. L. Austin. 1990. Sampling errors for rain gauge derived mean-areal daily and monthly rainfall. **J. Hydrol** 118: 163-173.

——, A. W., L. Sirivardena, X. Sun, P. Jordan and J. Elliott. 2002. **On the Calibration of Australian Weather Radars**. Cooperative Research Centre for Catchment Hydrology, Technical Report 02/7, Melbourne, Australia, 40 pp.

——, A. W., J. Nicol, G. L. Austin, C, D. S. and S. G. Bradley. 1996. The impact of radar and raingauge sampling errors when calibrating a weather radar. **Meteorol. Appl** 3: 43-52.

Segond, M., H.S. Wheater, C. Onof. 2007. The significance of spatial rainfall representation for flood runoff estimation: a numerical evaluation based on the Lee catchment, UK. **Journal of Hydrology** 347, 116–131.

Seo, D.J. and J. P. Breidenbach. 2002. Real time correction of spatially nonuniform bias in radar rainfall data using raingauge measurements. **J. Hydrometeorol** 3: 93-111.

Silverman, B.A. and W. Sukarnjanaset. 2000. Results of the Thailand warm-cloud hygroscopic particle seeding experiment. **J. Appl. Meteorol** 39: 1160 – 1175.

Singh, Vijay P. and A. David. 2002. Mathematical modeling of watershed hydrology. **Journal of hydrologic engineering**.

Sivakumar, B. and A. Sharma. 2007. A cascade approach to continuous rainfall generation at point locations. **Stochastic Environmental Research and Risk Assessment (SERRA)** (DOI 10.1007/s00477-007-0145-y): 1-9.

Smith, P. D. E. Cain and A. S. Dennis. 1975. Derivation of an R–Z relationship by computer optimization and its use in measuring daily areal rainfall. Preprints, 16th Radar Meteorology Conf., Houston, TX. **Amer. Meteor. Soc**. 461–466.

Smith, J.A. and W.F. Krajewski. 1993. A modeling study of rainfall rate–reflectivity relationships. **Water Resour. Res**. 29: 2505–2514.

Stewart, R.E., J.D. Marwitz and J.C. Pace. 1984. Characteristics through the melting layer of stratiform clouds. **J. Atmos. Sci** 41: 3227-3237.

Stiener, M. and J. A. Smith. 2000. Reflectivity, rain rate, and kinetic energy flux relationships based on raidrop spectra. **J. Appl. Meteorol**. 39: 1923-1940.

——, R. A. Houze and S. E. Yuter. 1995. Climatological characterization of three-dimensional storm structure from operational radar and rain gauge data. **J. Appl. Meteor**. 34, 1978–2007.

Stiener, M., J. Smith, S.J. Burges, C.V. Alonso and R.W. Darden. 1999. Effect of bias adjustment and raingauge data quality control on radar rainfall estimation. **Water Resour. Res**. 35: 2487-2503.

Shallcross, W. 1987. **Flood Estimation by Runoff Routing - Program WT42**, Queensland Water Resources Commission.

Soil Conservation Service (SCS). 1956. Supplement A, Section 4, Chapter 10, Hydrology. **National engineering handbook**, USDA, Washington, D.C.

——. 1971. **Hydrology in national engineering handbook**. Section 4, USDA, Springfield, VA.

——. 1972. **Hydrology in national engineering handbook**. Section 4, USDA, Springfield, VA.

——. 1986. **Urban hydrology for small watersheds**. Technical Release 55. USDA, Springfield, VA.

Sugawara, M. 1974. **Tank Model with Snow Component**. National Research Center for Disaster Prevention, Japan.

Sun, X., R. G. Mein, T. D. Keenan and J. F. Elliott. 2000. Flood estimation using radar and raingauge Rata. **J. Hydrol**. 239: 4–18.

Tingsanchali, T. and M. R. Gautam. 2000. Application of tank, NAM, ARMA and neural network models to flood forecasting. **Hydrological processes**. 14: 2473-2487.

Uijlenhoet, R. 2001. Raindrop size distributions and radar reflectivity-rain rate relationships for radar hydrology. **Hydrol. Earth System Sci**. 5: 615-627.

Uijlenhoet, R. and J.N.M. Stricker. 1999. A consistent rainfall parameterisation based on the exponential raindrop size distribution. **J. Hydrol**. 218: 101–127.

Ulbrich, C.W. 1983. Natural variations in the analytical form of the raindrop size distribution. **J. Climate Appl. Meteor**. 22: 1764–1775.

US Army Corps of Engineers (USACE). 1998. **HEC-1 flood hydrograph package user's manual**. Hydrologic Engineering Center, Davis, CA.

——. 2000. **HEC-HMS hydrologic modeling system user's manual**. Hydrologic Engineering Center, Davis, CA.

——. 2000. **HEC-HMS technical reference manual**. Hydrologic Engineering Center, Davis, CA.

Vieux, B. E. 2003. **Combined use of radar and gauge measurements for flood forecasting using a physics-based distributed hydrologic model**. Vieux & Associates, Inc., Norman, Oklahoma, USA.

Vignal, B. and H. Andrieu. 1999. Identification of vertical profiles of reflectivity from volume scan radar. **J. Appl. Meteorol** 38: 1214-1228.

—— and W. F. Krajewski. 2001. Large-sample evaluation of two methods to correct range-dependent error for WSR-88D rainfall estimates. **J. Hydrometeorol 2**: 490-504.

Vleck, V., J.H. 1947a. The absorbtion of microwaves by uncondensed water vapor. **Phys. Rev**. 71: 425-433.

——, J.H. 1947b. Absorption of microwaves by oxygen. **Phys. Rev** 71: 413-424.

Williams, C. R. and W. L. Ecklund. 1995. Classification of precipitation clouds in the tropics using 915-MHz wind profiles. **J. Appl. Meteorol** 12: 996-1012.

Wilson, C. B., J. B. Valdes and I. Rodriguez-Iturbe. 1979. On the influence of thespatial distribution of rainfall on storm runoff. **Water Resour. Res** 15: 321-328.

Wilson, E.M. 1983. **Handbook of Engineering Hydrology**. English Language Book Society, Administration of the British Government.

Wilson, J. W. 1970. Integration of radar and raingauge data for improved rainfall measurement. **J. Appl. Meteorol** 9: 489-497.

Wilson, J. W., and E. A. Brandes. 1979. Radar measurement of rainfall-A summary. **Bull. Amer. Meteor. Soc**. 60: 1048–1058.

Wyss, J., E.R. Williams and R.L. Bras. 1990. Hydrologic modelling of New England river basins using radar rainfall data. **J. Geophys. Res.** 95 (D3), 2143–2152.

Yang, D., T. Koike and H. Tanizawa. 2004. Application of a distributed hydrological model and weather radar observations for flood management in the upper Tone River of Japan. **Hydrological Processes** 18, 3119–3132.

CURRICULUM VITE

NAME : Mrs. Punpim Puttaraksa Mapiam

BIRTH DATE : January 23, 1977

BIRTH PLACE: Chonburi, Thailand

EDUCATION :	**YEAR**	**INSTITUTION**	**DEGREE/DIPLOMA**
	1999	Kasetsart University	B.Eng (Water Resources Engineering)
	2004	Kasetsart University	M.Eng (Water Resources Engineering)

SCHOLARSHIP/AWARDS : Thailand Research Fund 2004-2009